Republic of Iraq
Ministry of Higher Education and Scientific Research
University of Misan/College of Engineering
The Department of Civil Engineering

NUMERICAL INVESTIGATION OF REINFORCED CONCRETE BEAMS WITH TAPERED FLANGES

By
Ghufran Jabbar Raheem
B.Sc. in Civil Engineering, 2019

A thesis
submitted in partial fulfillment of the
requirements for the Master of Science
degree in Civil Engineering
University of Misan

July 2022
Thesis Supervisors: Prof. Dr. Sa’ad Fahad Resan

بِسۡمِ ٱللَّهِ ٱلرَّحۡمَٰنِ ٱلرَّحِيمِ

’’يَرْفَعِ اللَّهُ الَّذِينَ آمَنُوا مِنْكُمْ وَالَّذِينَ أُوتُوا الْعِلْمَ دَرَجَاتٍ وَاللَّهُ بِمَا تَعْمَلُونَ خَبِيرٌ‘‘

سورة المجادلة آية 11

صَدَق اللَّه الْعَظِيْم

DEDICATION

I dedicate this work to whom stood beside me and took care of me over the years, to my

Parents,

sisters,

Brother,

and close friend

To all those who supported and helped me, made the difficult easy, present my effort to them with all of my respect and appreciation.

ACKNOWLEDGEMENTS

In the Name of Allah.

all my thanks for Allah who led me during my way to complete this work.

I would like to express my cordial thanks and deepest gratitude to my supervisor **Prof. Dr. Saad Fahad Resan** whom I had the honor of being under his supervision, for his advice, help, and encouragement during the course of this study.

I would like to extend my thanks to Professor **Dr. Abbas O. Dawood Dean** of the college of engineering and Assistant Professor **Dr. Samir Mohammed Chasib;** head of Civil Engineering Department and to all my teachers in my college.

Special thanks go to **my father** for her great efforts. Also, thanks go to **my mother** ,**sisters** and **my close friend.**

ABSTRACT

Reinforced concrete beam type T-section is an optimal beam and has special importance while the tapered configuration is a specific mechanism could be utilized in structural engineering to get optimum materials investment. This study is introduced to verify the structural confidence of the recently developed flanged beam of new trend in plane tapered flanges using a numerical analysis by ANSYS package which included a wide spectrum of variables that relate to various structural aspects.

This work is divided into six phases .The verification process was carried out on non-prismatic for 9 beams analyzed by nonlinear finite element method by ANSYS to ascertain the accuracy and validity of FE procedure. These validated beams were provided by experimental study conducted in 2020. The results of the validation showed a well matching between the finite element models and the experimental test involving the strength rating, load-deflection curves and crack pattern. Besides, a parametric study that related to the developed reinforced concrete beams, is concerned with many structural parameters. Which as uniformity of mid length within tapered length, orient variation of Tapered flange(α), boundary conditions, steel reinforcement strength, concrete compressive strength, provided steel ratio. It also included a study shear span effect, serviceability investigation, flange effective width and continues beam and moment redistribution.

The result depicts that the middle region uniformity within the tapered domain assigned a slightly effect on the ultimate strength when increased from 0 to 52 cm, while the best flexural ductility and the best energy dissipation are predicted in a certain uniformity length (26 cm) which is indicated as an optimum uniformity length that corresponding to ductility improving rate of 1.49 and an energy dissipation enhancement rate of 1.53. Besides, the ultimate strength gets improving with reinforcement steel strength, reinforcement steel ratio increases and the over increment turns the section to be over reinforcement section within certain limits. On the other hand, when the value of (α) is increased from 3.27° to 5.44°, a slight difference in strength occurs. The reliability of the tapered flange section was checked for a spectrum range of flange width (65,75,85 cm) and the analysis was compared with the corresponding specimens of uniform flanges. The rates of strength, ductility and energy dissipation are approximately the same in both uniform and tapered section. Moreover, the tapered flange mode is compatible with varying section moment of inertia along the beam. Hence, the serviceability limit in the scope of deflection could be effected. Full scale specimens are introduced to check acceptance of getting deformation to be with ACI limitations and comparative analysis is achieved by considering T-section specimens of the uniform flange. Additionally, the continuity of the tapered flange beam and the redistribution of the moment were investigated. The reduction of reinforcement in the negative region which is companied with enchainment provided reinforcement in mid span, tends to upgrade strength capacity by 1.19 while the over design that introduced in C_{ove} specimens turns the behavior to brittleness response without moment redistribution. While the significant moment redistribution in specimen C_{w1} is assigned the change of p from 0.0063 to 0.0094 companies by strength improving due to moment redistribution of (β= 0.889). Finally, the changing of shear span that correspond to turn stress distribution modes, compatible with failure mode turning to flexural, flexural-shear, and shear failure mode respectively as a/d have varying range 1.5,2.5,3.5 respectively.

TABLE OF CONTENTS

LIST OF FIGURES

LIST OF TABLES

LIST OF SYMBOLES

Symbol	Description	Unit
b_w	Beam web width	mm
b_e	Beam flange width	mm
$\mathrm{d_f}$	Effective flange depth	mm
E	Modulus of elasticity	MPa
Ec	Modulus of elasticity of concrete	MPa
Es	Modulus of elasticity of reinforcing bars	MPa
E_T	Strain hardening modulus	
F	Function of principal state $(\sigma_{xp}, \sigma_{yp}, \sigma_{zp})$	
f_t	Ultimate uniaxial tensile strength of concrete	MPa
f_r	Modulus of rupture of concrete	MPa
fcb	Ultimate biaxial compressive strength	MPa
f_1	Ultimate compressive strength for a state of biaxial compression superimposed on hydrostatic stress state	MPa
fc'	Compressive strength of concrete cylinder	MPa
fy	Yielding stress of steel reinforcement	MPa
f_2	Ultimate compressive strength for a state of uniaxial compression superimposed on hydrostatic stress state	MPa

$f'c$	Concrete ultimate uniaxial compressive strength	MPa
f_t	Concrete strength in tension	MPa
f_u	Steel ultimate tensile strength	MPa
f_{cr}, ε_{cr}	Cracking stress and strain	MPa
ψ	Energy dissipation	
$D.I$	Ductility index	
Rs	Strength rating	
I_1	First stress invariant	
J_2	Second deviatoric stress invariant	
L	Span length of the beam	mm
L_f	Middle uniform region	mm
P and V	Any applied force on the structure	kN
Me	Elastic moment strength	Mpa
Mu	Ultimate moment strength	Mpa
P_u	Ultimate load	kN
u,v,w	Displacement components in x,y and z coordinates	mm
W_{ext} ,W_{int}	External and internal work	
x,y,z	Global coordinate	
α	Haunch angle with horizontal line	Degree
β	Shear transfer coefficient	
B_t , β_c	Opened and closed shear transfer coefficient	
γ,	Shear strain	
ε	Normal strain	mm/mm
ε_o	Strain at ultimate compressive stress $f'c$	
ε_u	Ultimate strain	

ζ , η	Local coordinates	
(σ)	Normal stress	MPa
σ_h^a	Ambient hydrostatic stress state	MPa
σxp	Principal stress in the x – direction.	MPa
σyp	Principal stress in the y – direction.	MPa
σzp	Principal stress in the z – direction.	MPa
σh	Hydrostatic stress	MPa
τ	Shear stress	MPa
ν	Poisson's ratio	
$[A]^\mathrm{T}$	Transpose of matrix [A]	
$[B]$	Strain-displacement matrix	
$[D]$	Constitutive matrix	
$[J]$	Jacobian matrix	
$[K]$	Overall stiffness matrix	
$[K]_\mathrm{e}$	Element stiffness matrix	
$[L]$	Differential operator matrix	
$[N]$	Matrix of shape functions	
$[T]$	Transformation matrix	
$\{a\}$	Nodal displacement vector	
F^a	Vector of applied loads	
$\{f\}$	Load vector	
$\{U\}$	Displacement vector	
$\{\varepsilon\}$	Strain vector	
$\{\sigma\}$	Stress vector	

ABBRIVATION

RC	Reinforced Concrete
N.A	Neutral Axis
SWNTs	Single-Walled Nanotube
WSD	Working Stress Design
RCC	Reinforced Cement Concrete
ACI	American Concrete Institute
EC2	Euro Code2
CFRP	Carbon Fiber Reinforced Polymer
SCC	Self-Compacting Concrete
FRPRC	Fiber-Reinforced polymer Reinforced Concrete
FRP	Fiber-Reinforced polymer
GFRP	Glass Fiber Reinforced Polymer
FE	Finite Element
NLFEA	Non Linear Finite Element Analysis
RCHBs	Reinforced Concrete Hunched Beams
FEA	Finite Element Analysis

CHAPTER ONE:INTRODUCTION

1.1 General

Reinforced concrete beams of flanged section are an excellent option and have a specific importance in reinforced beam design approaches for their importance in structural fields to maximize concrete beam strength capacity. Developing flanged section considers as an interesting subject for researchers and designers due to its important in structural fields.Various techniques had been considered in previous studies to improve the structural characteristics of flanged beams. Flanged section is a traditional section used for long-span RC beams to improve the structural efficiency, while the RC beams in which the depth of cross section varies along the axis (tapered beams), which are characteristics by reduced cross-sectional dimensions could be utilized in build portal frame, cantilever member and bridge pier construction. Hence, the proposed cross section is introduced to utilize flange section benefits besides tapering benefits to upgrade structural characteristic of RC T- beams and could be used in the same situations where beams of flanged section or tapered alignment are utilized.

1.2 Reinforcement Concrete Beam of Special Section Shape

1.2.1 General

Smart section area distribution and optimal strength selection are powerful variables in design philosophy for the creation of economic structural members. Durability, economy, and decreased construction time, in addition to complexity factors, are the main elements influencing building success considered these characteristics for each part of a project ultimately leads to a decrease in the cost of build construction, as well as time savings. Concrete members are among the most significant aspects of most construction projects, and so improving their characteristics, increasing their strength, and using additives to allow for more uncomplicated construction methods all contribute effectively to a project's success [1]. RC Beams are used as links in the transfer of loads from slabs to columns or walls, and as such, there are several types of cross-sections of beams to meet their required functions, taking into account the requirements of construction and architecture. The most common cross-sections are rectangular and T-section, but other cross-sections can be used, such as trapezoidal, tapered, circular, triangular beam and others [2].

Reinforced concrete (RC) beams with circular cross sections are frequently used in civil engineering structures, such as laterally loaded bridge piers, because they are simple to construct have a pleasing appearance, and provide equal strength characteristics in all directions under wind and seismic loads [3]. In addition, RC circular cross-section beams are often used in infrastructure works such as retaining structures for excavations and shallow tunnels [4]. While trapezoidal section beams are used to reduce cost and increase efficiency, where the trapezoid shape is proportional to the required compressive and tensile strength, which increases the compressive area and thus increase the compressive strength and vice versa for the tensile region where the strength of the rebar can distribute tensile stresses [5].

1.3 Flanged Reinforcement Concrete Beam of Tee-Section

In the field of civil engineering, flanged reinforced concrete beams have been widely used in many of its engineering applications .this type of structural members has been analyzed and experimentally discussed [6].T-beams are the most common flanged sections used in conventional construction and moment-resisting frames. Because slabs are cast monolithically with the beam's web, the slab's involvement adds stiffness or strength to the rectangular beam section [7], In addition, T-beams are widely used in bridge decks, as well as in floor or roof simply supported slabs on load bearing walls or girders. This building approach is extensively utilized and ideal for residential, commercial, prefabrication, and industrial buildings, particularly those with long spans [8] as shown in Figure 1-1. These beams are formed by two rectangular sections: the vertical web section and the horizontal flange. They are most efficient when, compression exists in the flange section because a large area in the flange is available for compression [9].

Figure 1-1 Applications of T-beam member [8].

1.3.1 Classification of Flanged Reinforcement Concrete Beam of Tee-section

Based on the location of their neutral axis, T-beams can be classified into two groups: rectangular beam behavior if the NA were in the flange or T-beam behavior if the N.A. were in the web. According to the location of the NA, T-beams are categorized in Figure 1-2 [10] .

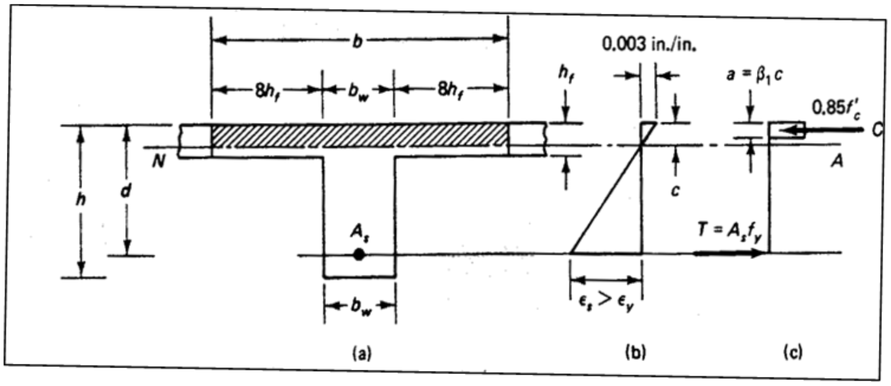

Figure 1-2a Classification of T-beam systems (Rectangular section) [11]

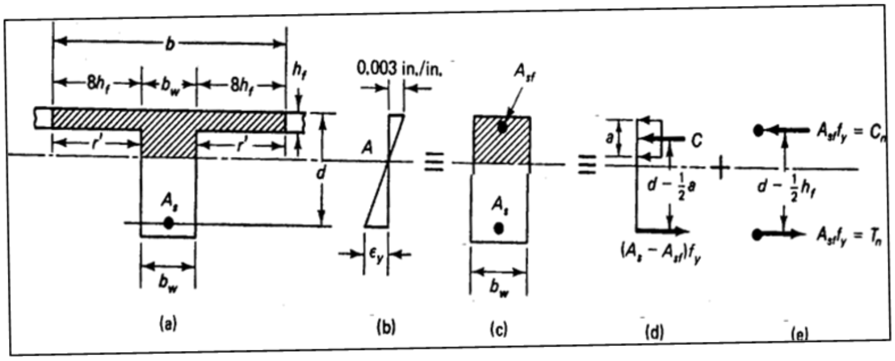

Figure 1-2b Classification of T-beam systems (T-section) [11]

1.3.2 Structural Behavior of Flanged Reinforcement Concrete Beam of Tee-section

The compression force generated by the bending moment is distributed along the effective width of the compression flange, which is more than the web width, resulting in a lower compression block depth and a larger lever arm z than in a rectangular section with width. Additionally, the weight of the section is reduced in comparison to a rectangular beam with the same top width.

The flexural and shear resistant mechanisms are frequently separated in current codes [12]. The forces C (the compression at the concrete part) and the forces T (the tension at the longitudinal reinforcement) are taken when bending. While the shear is taken by the web through the use of a truss mechanism as shown in Figure 1-3. Therefore, they do not consider any contribution of the flanges to the shear strength[13].

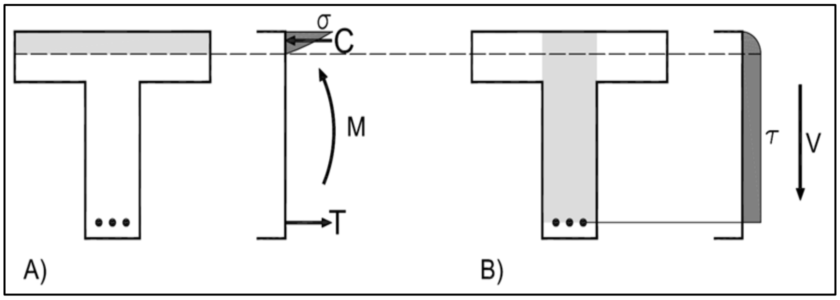

Figure 1-3 Internal force resistant mechanisms (a) Flexure, (b) Shear [13]

As the load increases, the inclined cracks open and the contributions to the shear strength of the frictional forces along the crack length and that of the residual tensile stresses remaining. Shear stresses along the critical crack reduce and concentrate in the cracks' nearest top section and the compression chord of the beam, particularly after stirrups yield. Additionally, when the load increases, the compression force (C) and the normal stresses due to bending at the uncracked concrete chord increase, increased to the concrete compression chord's capacity to resist shear stresses. Thence, near the ultimate limit state the shear resisted by the concrete compression the chord becomes very relevant [14].

This effect is particularly pronounced in members with T-shaped sections for two reasons. (1) A T-shaped section's neutral axis depth is closer to the top compressed fiber. As a result, for a given ratio M/Mcr > 1 and the aggregate interlock is lower in a T-shaped section beam than in a rectangular beam of the same web width because the crack opening is greater in a T-shaped section beam as shown in Figure 1-4. (2) When the shear stresses are concentrated on the concrete edge of the T section, the contribution to the shear strength of the concrete chord is higher than that of the rectangular section [13].

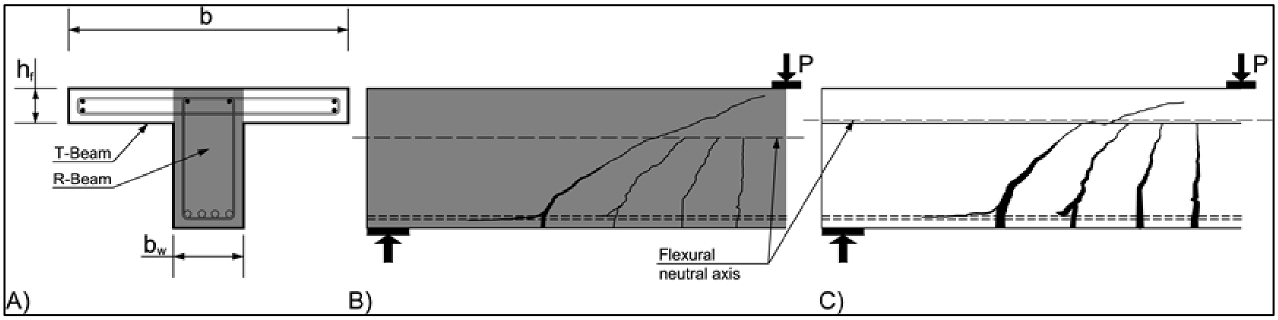

Figure 1-4 Comparison between T-shaped section beam and rectangular beam. (A) Sections. (B) Crack pattern scheme of a rectangular beam. (C) Crack pattern scheme of a T- beam [13].

1.4 Reinforcement Concrete Beam of Non-prismatic Section

Engineers should design structures in such a way that structural systems execute their jobs satisfactorily while also being cost effective. This aids in the selection of the appropriate type of sections that are both economical and safe for construction. Beams are a common medium for carrying and transferring loads. A meticulous approach to design may result in good serviceability and cost optimization of the structure. Prismatic beams are often utilized for medium span and bending forces. Bending moments and shear forces at the center of the span and over the supports grow significantly as the span lengthens. So, prismatic beams may become uneconomical in such instances.Furthermore,with the increased depth there is considerable decrease in headroom. As a result, in such cases, non-prismatic beams are an appealing choice [15].

The non-prismatic reinforced concrete (RC) beam is a unique case in structural engineering because it has variable depth throughout the beam section and lacks sufficient information in structural codes. this can put structural engineers in a challenge to predict how this beam will react under specific types of loads or with different geometrical variables and strengthening existence [16].

Non-prismatic beams can be classified based on the variation of height [17]:

1. Tapered beams or Haunched beams: beams that have a linear variation in cross-section along their length. Tapered beams have greater depth near the support, sufficient to resist the applied shear forces, and less depth at the center, sufficient to resist the applied bending moment. The depth in the center may increase if the load applied is large or the amount of reinforcement used is insufficient.
2. Curved beams: beams with a parabolic or curvilinear cross-section that varies along the length. This change could occur in either the horizontal or vertical

plane. These beams have the structural advantage of being able to carry torsional moments.

3. Twisted beams: beams with varying cross-sections along the length of the beam, such that the cross-section rotates around the centroid axis.

1.4.1 Advantage and Disadvantage of Reinforcement Concrete Beam of Non-prismatic section

The Reinforced concrete beam of the tapered section provides the following advantages compared with prismatic beams [18]**:**

1. Reducing construction weight for a given lateral stiffness.
2. More efficient use of concrete and steel reinforcement.
3. Eased placement of various facilities or equipment types (electrical, sewage, air conditioning etc.)
4. Aesthetic reason.

Despite the wide spread at the present time of this type of beams and some advantages that engineers can obtain, there are some difficulties that occur in the modeling of non-prismatic beams, Which can lead to inaccurate predictions and thus performing optimization operation, On the other hand , the high construction costs, such as a high-quality worker in construction and special molds, caused unfavorable in a common structural solution in building,[19] Also, there are some code available such as ACI318-14 [20]and BS-5400-1[21] not covering this type of beams. the designers in this field must rely on some experience and provision [19].

1.4.2 Applications of Reinforcement Concrete Beam of Non-prismatic Section

Non- prismatic beams are an important issue in structural engineering, not only for their versatile application in engineering structures, also because of their unique ability to simulate different types of material or geometrical variations, such as crack formation or plasticity spreading along the beam [22]. Also, can be utilized to form the members according to the internal stress distribution. These sorts of members can provide the required strength and use the minimum weight and material, as well as satisfy architectural or functional requirements. Non-prismatic members with constant, linear, and parabolic height or width variations are commonly used in industrial structures, bridges, and high-rise buildings [23]. Non-prismatic beams are used also in simply supported or continuous bridges worldwide and buildings as shown in Figure 1-5 and in mid-rise framed structures constructions from the early half of the twentieth century. where a structure built recently is shown in Figure 1-6 [18].

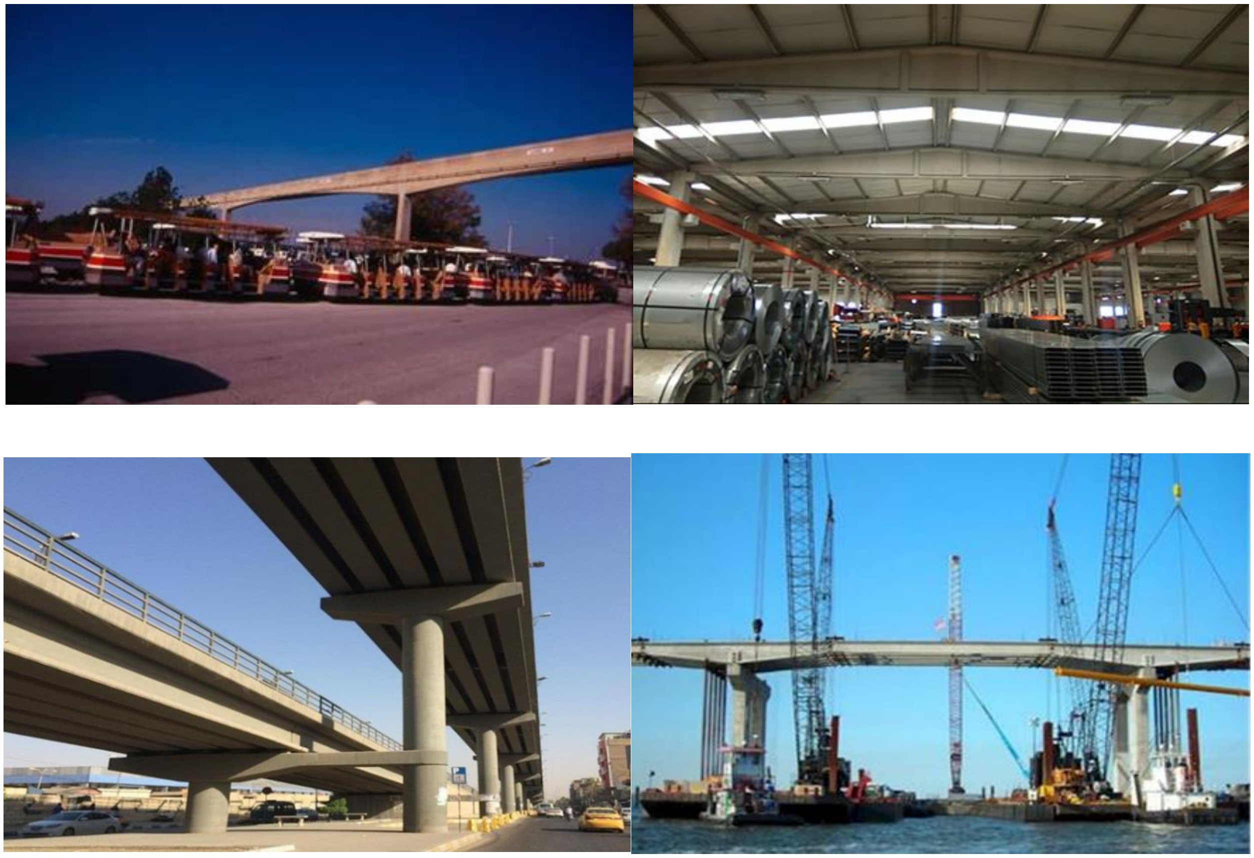

Figure 1-5 Typical non-prismatic member in building and bridge [18].

Figure 1-6: RC buildings with haunched beams recently constructed in Mexico City [18]

Generally, non-prismatic beams can be used for many instances for example, in modern buildings, where utility ducts and pipes are accommodated under the floor beams in the space above the false ceiling, A non-prismatic beam with a recess would allow these ducts to pass through the beam, avoiding a considerable amount of dead space. This would minimize the height of each floor, resulting in significant material and construction cost savings as shown in Figure 1-7a. it could also be employed as ground beams Figure 1-7b in residential renovation projects where existing utility lines frequently hinder the building of tie beams that join newly erected columns to existing ones. The use of non-prismatic tie beams allows construction to continue without the requirement for these pipes to be relocated. A non-prismatic beam in the form of a stepped beam can also be used to support a split-level floor Figure 1-7c. For aesthetic reasons, this application is typically found in theaters and private dwellings. Finally, non-prismatic sills are used in building renovations. There may be a requirement to add new service channels, which is frequently difficult due to limited height. In this situation, a break in the existing package can be established to allow the new service channels as shown in Figure 1-7d [24].

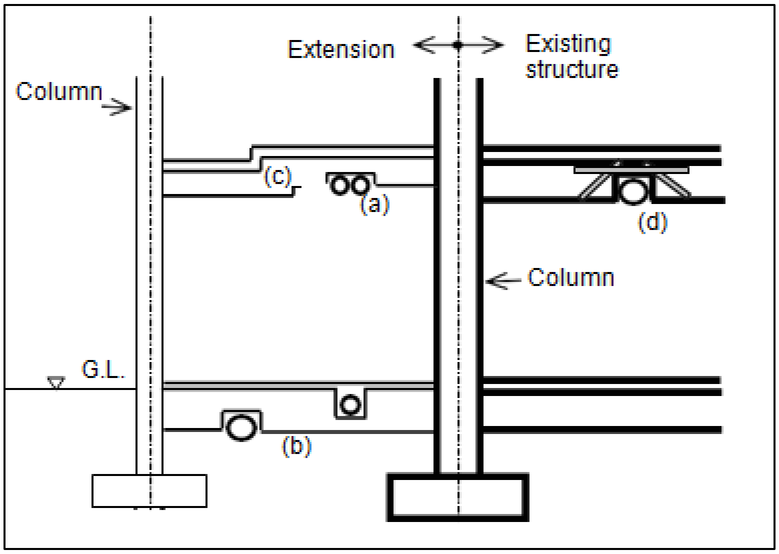

Figure 1-7 Examples of Recess Beams: (a) Floor Beams; (b) Ground Beam; (c) Stepped Beam; (d) Retrofitted Beam [24] .

1.4.3 Structural Behavior Reinforcement Concrete Beam of Non-prismatic Section

The general behavior of non-prismatic members is different from that of prismatic members to these cases [25-26].

1. In a tapered beam, the main internal tension or compression is inclined, providing a vertical component that may be capable of resisting shear.
2. The varying in cross section towards the supports is unlikely.
3. The discontinuity of the centroidal axis in tapered beam causes a strong coupling between bending moment, shear and axial forces.

The cracking of these beams begins with small flexural cracks. With increased load, these flexural cracks transform into flexural shear cracks, with more shear cracks developing. Flexural-shear cracks increase in length and size until they reach the e soffit of the flange. By increasing the load, shear stress failure occurs for beams with large hunch, while instability failure occurs for beams with a small hunch.

The change in angle of haunch inclination affects the behavior at failure, thus bringing about two distinct types;

(a) Beam of small depth in Support, failure of this type of beams occurs due to the instability of the failure as a result a large crack has occurred above the line connecting the loading point with support which leads to the creation of a weak arch in the top and the beam failure.

(b) Beam with large depth in support, failure of this type of beam occurs due to shear compression as a result a large crack has occurred a below the line connecting the loading point with support which leads to the creation of a stronger arch in the top. A greater shear load is transferred from the arch to support and this results in more resistance to rotation about the load point, until it occur crushed in concrete [27].

1.4.4 Shear Behavior Reinforcement Concrete Beam of Non-prismatic Section

The shear behavior of tapered concrete buildings has received limited attention. It is obvious that a suitably inclined force in compression or tension may give some resistance to shear [28] Park and Paulay [29] propose that Equation (1.1) should be used to calculate the effective shear force in haunched beams without shear reinforcing (derived by considering the equilibrium of a tapered beam) .

$$V_{eff} = V - (M/z)(\tan\theta') \qquad 1.1$$

Where:

V_{eff} = the effective shear force on a section.

V= the shear force on the section from the applied loads.

M= the bending moment at a section, z is the lever arm between centers of tension and compression.

θ'= angle of beam slope from the horizontal, this value is positive in sections where the member depth increases in the direction of increasing moment .
When the principal tensile stress in the concrete exceeds its tensile capacity, cracks occur in the steel reinforced section and as the applied loads are increased, inclined cracks often spread from the member's tension face towards the neutral axis. It is imaginable that in sections that taper towards their supports, the interaction of these diagonal cracks with the course of the compression force that reaches the supports may be more crucial along with the factors that contribute to a reinforced concrete beam's ability to resist shear, as shown in Figure1-8 [28].

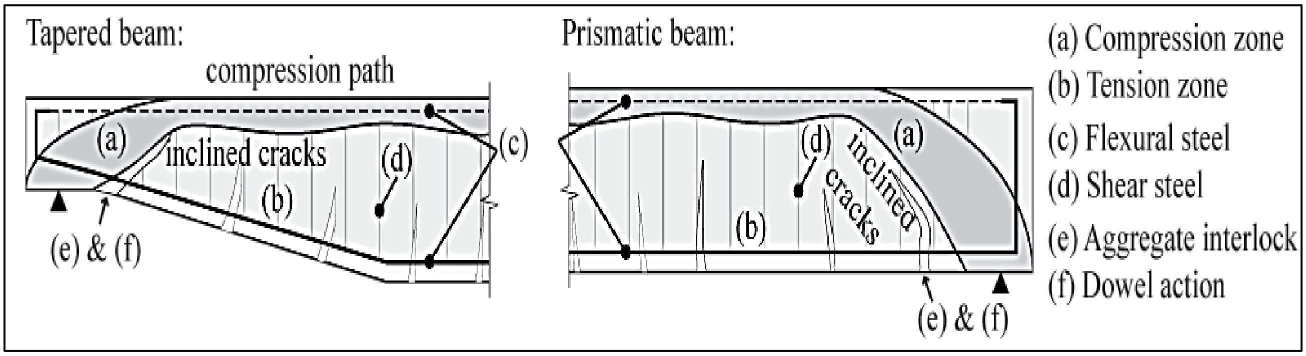

Figure 1-8 Contributing factors to shear resistance in tapered and prismatic section [28].

1.5 Aim of Study

The main aim of this study is to verify the structural confidence of the recently developed flanged beams of tapered flanges using a numerical analysis by using ANSYS 15.0 [30] program, besides;

1. Studying of many materials-specific variables such as the effect of concrete compressive strength, strength and amount of steel reinforcement.
2. Studying of the effects of geometric beam change such as the sectional dimensions and boundary condition of beams.

3. Studying of the serviceability aspects beams and comparing the results with the serviceability limit.
4. Studying of non-prismatic beam behavior within the slab system.
5. Studying of continues non-prismatic beams with moment redistribution assessment.
6. Studying the shear span effect of non-prismatic beams.

1.6 Layout of the Thesis

This thesis is divided into five chapters which can be clarified as follows:

1. **Chapter one:** It is the introduction that includes the introduction and general description of related issues.
2. **Chapter Two**: It concerns with the literature review of the flanged section and related topics.
3. **Chapter Three:** It is the numerical formulation of developed models.
4. **Chapter Four:** It deals with the obtained results and the related discussions, besides; the comparative analysis.
5. **Chapter Five:** It is the conclusions and recommendations that summarized the overall outcome of the study as well as suggested recommendations for the future work.

CHAPTER TWO:LITERATURE REVIEW

2.1 General

The available studies in the literature related to the current work are presented in this chapter. The studies are divided into three parts. The first part presented beam of special section shape. The second part presented the available studies conducted on of RC beam of Tee-section. The third part provides an overview of the experimental and analytical studies that dealt with the behavior of non-prismatic beams.

2.2 Reinforcement Concrete Beam of Special Section Shape

In 2006, Vodenitcharova and Zhang [31] explained the pure bending and torsion induced by the local bending of a nano composite beam reinforced with a single-walled carbon nanotube using the airy stress function method that was used to analyze the matrix deformation.The SWNT's cross-sectional change during bending was taken into consideration. The effect of the SWNT's radial flexibility on strain/stress states and buckling was given special attention. The result shown that, A two-dimensional deformation issue for the matrix has been addressed, taking the ovalisation of the SWNT cross section into account. A particular emphasis has been put on the phenomenon, of local buckling of the SWNT as a possible failure mode of the nanocomposite beam. Although adding a matrix to a SWNT increases its load carrying capability, it also increases its radial deformation at the same bending angle. As a result, thickly-coated SWNTs buckle preferentially at lower beam curvature and longitudinal strains and stresses. The higher the strain/stress levels in thicker matrix layers in the plane of the beam, the higher the degree of flattening of the SWNT.

In 2011, Mahzuz [32] studied the Performance evaluation of triangular singly reinforced concrete beam . The major aim of the study were ; The development of relevant mathematical equations for design. and the essential comparison with rectangular section equations is made. The bending moment and the shear force are both compared. The entire study was carried out using the working stress design method (WSD) using a single-reinforced beam. The results exhibited that the triangular RCC sections better than rectangular ones in terms of higher moment and shear taking ability. It uses less steel and has a lower concrete volume; therefore the triangular section assures both less dead load and economic safety.

In 2015, Al-Ansari. [33] presented study about reliability and flexural behavior of triangular and T- section of reinforced concrete beams. Three reinforced concrete beams were experimentally tested and analytically studied using the finite element method. The dependability index method was also used to examine their reliability. The results revealed that the finite element vertical displacements matched those measured experimentally quite well. They also demonstrated that the finite element method produced higher vertical displacements than the experimental method. This is strong evidence that the finite element solutions were conservative and reliable. The results showed that triangular beams had higher ductility at failure than T-beams. The triangular beams had higher plastic deformations upon failure than the T-beam. This is a significant evidence of the triangular beams' greater ductility when compared to the T-beam. For equivalent areas of steel and concrete, triangular beams had smaller cracks than T-beams. The design moment strengths Mc obtained using the American Concrete Institute (ACI) design formulation were safe and close to those computed using testing results. The experimental results verified the reliability study results, which showed that triangular beams are more reliable than T-beams for equal steel and concrete areas. Figure 2-1 shows the crack pattern and shape of triangular and T-beams after collapse.

Figure 2-1 Crack pattern and shape of triangular and T-beams after collapse [33]

In 2017, Khalil et al. [34] investigate the shear behavior of trapezoidal beam. The main aim of this research was validate and improves the current analytical and design methodologies for shear analysis of normal reinforced concrete beams. As well as evaluates the shear resistance of trapezoidal beams with variable width beams. the test was done for eight direct models of RC beam. The specimens with 2300 mm long and clear spans of 2000 mm and that the cross section dimensions were (175 Avg.) x 300 mm . all the tested specimens had the same longitudinal reinforcement, the bottom reinforcement of all specimens was 4Φ18 and the stirrups were 8Φ6 for B5, B6, B7, B8 and there is no stirrups for B1, B2, B3, B4. the experimental results show that , The standard beams "B1 & B5" have the highest gross moment of inertia, resulting in the lowest deflection value when compared to the other specimens (B2, B3, B4, B6, B7, & B8) until the first crack develops, at which point the section behavior is determined by the cracked moment of inertia. The standard beams "B1 and B5" have the lowest cracked moment of inertia when compared to the other specimens (B2, B3, B4, B6, B7, and B8), resulting in the maximum deflection value once the first crack occurs till failure.in addition, The shear behavior of beams is determined by the average cross section area (the average width) in resisting shear force.

In 2018, Geevar et al. [35] performed an experimental and numerical assessment of deflections in circular reinforced concrete beams as shown in Figure2-2.

Approaches for determining deflections (at service loads) in codes such EC2 [36] and ACI 318 [20] are mostly based on semi-empirical methods that have been tested for rectangular cross sections of beams. The application of these methods to circular cross-section beams is demonstrated in this work through experimental studies on eight circular beams with various concrete grades and reinforcing steel percentages. Similar beams with square cross sections were also tested for comparison, and it was discovered that the code estimates for square and circular beams have almost the same degree of conservatism. The effects of the proportion of reinforcing steel and axial compression on load-deflection behavior have also been investigated using the proposed approach. This research reveals that as the proportion of reinforcing steel increases, post cracking stiffness increases and ductility declines. Due to variances in steel rebar distribution, circular beams are found to have less strength and ductility than square beams (with the same area of cross section).

(a) Typical failure of square beam (b) Typical failure of circular beam

Figure 2-2 patterns observed in experiments[35].

In 2018, Hussnawi [37] showed the effect of trapezoidal cross-section dimensions on the behaviors of CFRP SCC beams. The beams were divided into two groups based on their cross-sections; each group had five beams; the first group (T20) had trapezoidal cross-sections with dimensions of length 1,600 x height 260x width 200 mm at the top and 160 mm at the bottom, The second group (T24) included those with trapezoidal cross-sections measuring 1,600 mm in length, 260 mm in height, 160 mm in width at the bottom, and 240 mm in width at the top. The experimental program included investigating the effects of top width on the flexural behavior of trapezoidal cross-section beams, as well as the impact of reinforcing those beams with varying numbers, locations, and methods of CFRP strip placement. The results showed that trapezoidal cross-sections with 240 mm top width had 4 to 11.54 % higher ultimate load capacity and lower deflection than trapezoidal cross-sections with 200 mm top width. In addition, strengthening beams with CFRP strips increases the ultimate load capacity of trapezoidal cross-section beams by 4 to 24 percent while decreasing deflection. finally When compared to beams strengthened with strips applied along the beam, applying CFRP strips to the maximum moment region increased the ultimate load capacity by an average of 4.17 to 7.7 %.

In 2019, Al-Ansari and Afzal [38] presented a Simplified Irregular Beam Analysis and Design. The selected irregular beam shaped parts in this study are classified into three groups: beams with straight edges, beams with slanted edges, and circular beams. Each group contains the beam shaped portions that are most typically utilized in that category. In this study, the selected irregular beam shaped sections are divided mainly into three groups, beams with straight edges, beams with sloped edges and circular beams. Based on section geometry and the ACI [20] building code of design, flexural beam formulas for three types of reinforced concrete beams are derived. In addition to analyzing numerical examples for some of the sections in each group category utilizing the proposed simplified method to calculate the strength design of the irregular beams. The result show that ,the simplified approach results for all three groups are compared to the finite element. The percentage difference between the simplified approach and finite element software is between 5% and 10%. As a result, the simplified technique for irregularly shaped beam sections appears to be quite promising.

In 2019, Mousa et al. [39] presented the deflection prediction methodology for circular concrete members reinforced with fiber-reinforced polymer bars. The main objective of study was to use available design equations to evaluate the deflection predictions of eight full-scale circular FRPRC flexural members with dimension 500 mm in diameter and 6000 mm in length under four-point bending load. The type of FRP reinforcing bars used and the reinforcement ratio were among the test variables. Glass FRP (GFRP) bars were used to strengthen three specimens, carbon FRP (CFRP) bars were used to reinforce three specimens, and basalt FRP (BFRP) bars were used to reinforce two specimens based on the test results analysis, a new equation was constructed to precisely estimate the deflection of the tested circular specimens. Furthermore, an analytical model was created utilizing a layer-by-layer curvature analysis method based on cross-sectional analysis that satisfied strain compatibility and equilibrium conditions. The load-deflection relationship for circular FRPRC flexural members can be constructed using an incremental strain technique to calculate curvature. The model's capacity to reproduce the experimental load-deflection responses of the tested circular specimens is demonstrated by comparisons with experimental results. Figure 2-3 show the deflected shape and failure modes of test specimens.

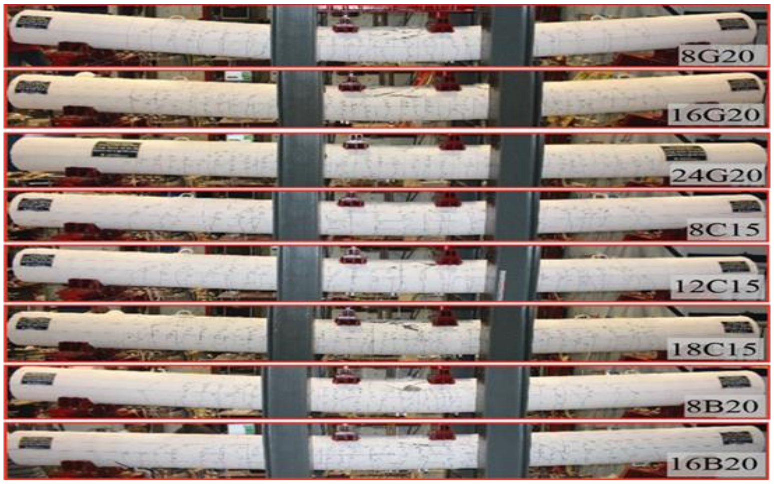

Figure 2-3 Failure modes of test specimens[39].

In 2021, Sada and Resan [5] outlined experimental investigation on hybrid -trapezoidal reinforced concrete section. The study presented an experimental study of 10 simply supported reinforced concrete beams subjected to four -point load. Two groups, each group contain five beams and had equal cross -sectional area were investigated. The first group is used to test the flexural behavior and the second group is used to test the behavior of the shear. The variables used in experiment are the compressive strength where value used (25 and 50) Mpa and using a trapezoidal section with different side angle (75^o,80^o,85^o). The results of the experiment showed that the trapezoidal section showed high deflection results as the rates of increase in the flexural failure mode were from 20% to 57% and in the mode of shear failure of 22% to 60% and it was concluded that the trapezoidal section has a significant effect on improving the section capacity compared to the rectangular section, in addition to an increase in the failure load in proportion to 6.77% when bending failure and in proportion 3.66% to failure of shear compare with the rectangular section. on other hand, the effect of the area distribution within the section (section shape sides orientation) is clear on the load of the first cracks as the highest value of the crack load related to angle of 80^o.

2.3 Reinforcement Concrete Beam of T- section

In 1981, Johnson and Oehlers [40] studied the longitudinal shear in composite T-beams. The main target of this research was to find a reasonable basis for existing knowledge and practice in composite T-beam push tests and studs. The process included testing four composite T-beams and of 125 push tests were analyzed statistically, and 101 new push tests. Based on four different failure patterns, results were extracted that included, methods for forecasting the shank failure load, which is influenced by the size of the weld collar, and the splitting strength of a composite T-reinforced beam's concrete slab were devised. It is decided that design static loads for stud connectors with weld collars of a specified minimum size may be up to 20% greater than those required in BS 5400[21].

In 2000, Khalifa and Nanni [41] presented study improving shear capacity of existing RC T-section beams using CFRP composites. The experiential proceedings included carrying out six full-scale, simply supported beams. One beam was used as a reference, and five beams were strengthened using various CFRP. The main parameters were CFRP amount, wrapping schemes, and CFRP end anchorage. The result exhibited that the externally bonded CFRP can greatly improve the beam's shear capability. Additionally, the U-wrap with end anchorage was proved to be most effective configuration. To forecast the capacity of referenced members, design techniques in ACI [42] Code and Euro[43] code formats are proposed. The findings demonstrated that the proposed design approach is conservative and acceptable.

In 2003, Deniaud and Roger Cheng [44] investigation the reinforced concrete T-beams strengthened for shear with fiber reinforced polymer sheets. The study presented an experimental study of four T-section reinforced concrete beams subjected to four –point load as shown in Figure 2-4. The beams were subjected to eight tests. Each end of each beam was tested separately. The major parameters were the three types of FRP, triaxial glass fiber, uniaxial glass fiber, and uniaxial carbon fiber. Externally, FRP was used to reinforce the web of the T-beams, while some ends were left without FRP. The experimental results show that, FRP reinforcement increases the maximum shear strength by 15.4 to 42.2 %when compared to non-glass fiber reinforced girders. The ductile failure of the triaxial glass fiber reinforced beam was more than that of the other FRP reinforced beams.

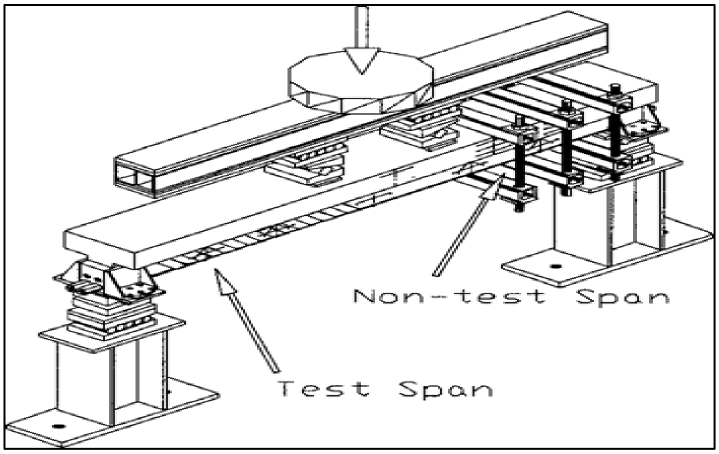

Figure 2-4 Isometric view of the test setup[44]

In 2004, Kwan and Au [45] presented study about flexural strength ductility performance of flanged beam section cast of high strength concrete for three beam sections (A, B,C)with same overall dimensions, (B = 1200mm, D = 1500 mm). Section A is a T-shaped section with B_w = 400 mm web breadth and D_f = 400 mm flange depth, respectively, Whereas section B is a T-shaped section with Bw = 800 mm web breadth and D_f = 400 mm flange depth, respectively by using numerical analysis as shown in Figure 2-5. The post-peak flexural behavior of flanged sections is investigated in this study using an analytical method that takes into account strain reversal of the tension reinforcement and uses the actual stress-strain curves of the materials. The numerical result show that, The flexural strength-ductility performance of flanged sections is explored by plotting the strength and ductility that can be attained simultaneously as design graphs. It was discovered that, a flanged section has lower strength-ductility performance than a rectangular section with the same overall dimensions and a flanged section has lower flexural ductility than a rectangular section with the same overall size and amount of reinforcement. Finally, a flanged section offers higher strength-ductility performance than a rectangular section across the same sectional area.

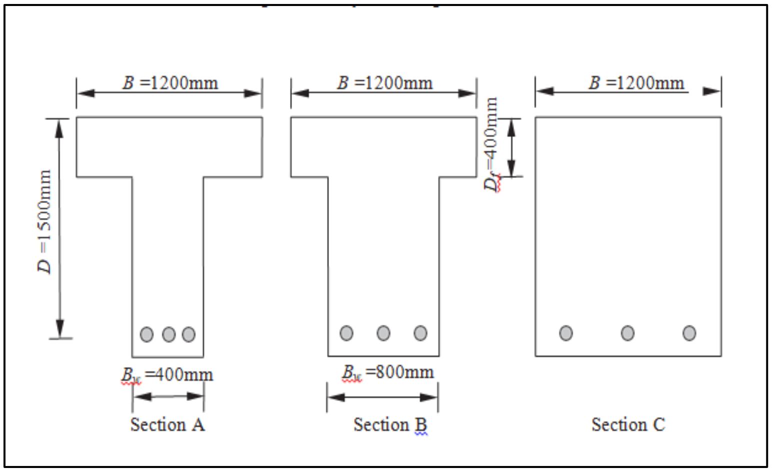

Figure 2-5Dimensions of specimens[45]

In 2012, Hawileh et al. [46] They studied nonlinear response of RC shear deficient T-beam subjected to cyclic load by finite element. The main comparison between experimental and FE results is made based on cracking load, failure loads, crack patterns and response hysteresis envelopes. The results indicate that the pattern of finite element model for the direction of the cracks, distribution and response envelope is close to the experimental test while the stiffness is higher compared to the experimental test this results in less deflection. The finite element model predicts its value of maximum free and deflection is 1.7 mm its less than of that of the tested experimental results, this depend on the stiffness of concrete material used in the model. Through the results, it was that the model with linear results can be used to predict the load capacity, load-displacement relation and failure mode of RC beams. At the end displacement of T-beam and on shear strain the value of shear transfer coefficients will have a different effect. Finally, when both shear transfer coefficients are equal 0.2 the FE result gave the best correlate to the experimental results.

In 2013, Santos et al. [47] achieved experimental and numerical investigations about the ductility and moment redistribution capacity of multi-span T-section concrete beams reinforced with GFRP by using finite element. The main parameters were the confinement level in critical zone of the beams and GFRP reinforcement ratio numerical investigation were carried out to develop non-linear models for all beams T-section and compare it with test data and after proving the validity of the test and calibrating it using was conducted to evaluate the cross section geometry, the span and longitudinal GFRP reinforcement ratio on the moment redistribution capacity. The results of the experimental and numerical investigations show that elastic analyses are considerably conservative and that moment redistribution occurs in critical section concrete insulation may be a good solution to enhance the moment redistribution in GFRP reinforced concrete beams and plastic hinge ductility.

In 2016, Demir et al.[48] implemented nonlinear finite element study on the improvement of shear capacity in reinforced concrete T-beams by alternative diagonal shear reinforcement by using ABAQUS[49] program. The main objective of the study is to improve the ductility and shear capacity of shear critical reinforced concrete (RC) beams under monotonic and cyclic loadings. First, a study is conducted for numerical nonlinear finite element by two tested beams with shear and flexural failure modes then diagonal shear reinforced is included to see how efficient it is when it is included. The numerical result that when the PRS system was included it was found that there was a significant increase in the capacity of the shear and ductility, in addition to the improvement of the shearing capacity further and the failure to it turns from failure of shear to failure of flexural.

In 2017, Subramani et al. [50] performed analytical study of T-beam using finite element analysis by using ANSYS programs investigate to failure effect on various T-beam behaviors under static loading and developed to simulate beam deflection behavior. The results appeared that the result of model predicted that the system is slightly softer after the post-cracking of the load - deflection response of T-beam, the reason for this difference is due to the difference in the bond - slip model of reinforcement used in the analysis when compared with that present in the experiment, on the other hand, it was observed that the predicted load in T-beams is consistent with the test data. Predictions of the diagonal tension failure and shear compression when using the Ansys model is correct when compared with the results observed in the experiment.

In 2018, Panggabean and Pakpahan [51] searched the experimental analysis of T-beam reinforced concrete with holes. The experimental proceedings included carrying out three specimens for checked collapse model. The first specimen was consisting of one hole in middle and this specimen was used as a model for flexural failure. The second and third specimen contain two and three holes between the load and used as models to study the failure of shearing. The conclusions indicate that the Load collapse of first model at 18.36 Ton when it was subjected to a load measured 19Ton in the laboratory. and for the second model, the load collapsed at a point of magnitude 19.5 Ton when subjected to a load measured 20 Ton in the laboratory, while the third model was discontinued load while it was subject to a load of 14 Ton. on other hand, The results show that the type of failure for the three models when they were subjected to different values of the load, as they showed that the type of failure in the first material is the bending failure that occurs in the pure flexible loading region, second material is the shear failure that occurs in the holes under a centralized load, and finally the third material that suffers from the failure of the shear that occurs in the maximum shear area.

In 2018, Ghaziyani [52] performed an analytical study of bending behavior for concrete beams with T-shaped cross section using composite and steel bars by using ABAQUS finite element software. The numerical stud y consisted of 12 reinforced concrete T-shape beams divided into two groups, The first series was consisting of six executed as a T-shape with three reinforced with FRP rebar's and three reinforced with steel rebar's. As the same, as first six beams, property, other, six beams defined by rectangular performance. The nonlinear static approach was employed for analysis, and a load-displacement diagram was used to compare the results. The result exhibited that, the stiffness of a T-shape beam is substantially higher than that of rectangular beams. Furthermore, when comparing FRP and steel rebar, the use of FRP bars resulted in lower stiffness and higher load capacity.

In 2018, Fang [53] searched the horizontal shear behaviors of normal weight and light weight concrete composite T-Beams. The experimental study involved testing 12 beams with T- cross section and. necessary control cylinders with varied parameters such clamping stress and lightweight slab concrete strength. Based on the experimental results, the interface shear transfer strength of composite concrete T-beams was predicted using a more precise equation. By comparing the published experimental findings of previous beam tests and shear-friction push-off tests for various types of concrete with both rough and smooth interfaces, the proposed formula has been found to be reliable in estimating the horizontal shear strength of concrete composite T-beams.

In 2019 Al-Rousan and Abo-Msamh [54] studied the bending and torsion behavior of CFRP strengthened RC beams by Finite Element Analysis (NLFEA). Twenty-six simply support models of T-section beams divided equally into six groups. Variable parameters in this study were: effect of clear span to depth ratio, CFRP strip spacing, CFRP length, and CFRP depth. The results observed that; Increases in the clear span to depth ratio and length of CFRP result in a decrease in ultimate load and an increment in ductility. Models with zero spacing CFRP strips (Fully) had a greater significant effect than models with strips wrapping. Additionally, this improvement was greatest in group six, which contains the models with the greatest CFRP depth. Figure 2-6 shows the crack pattern at failure.

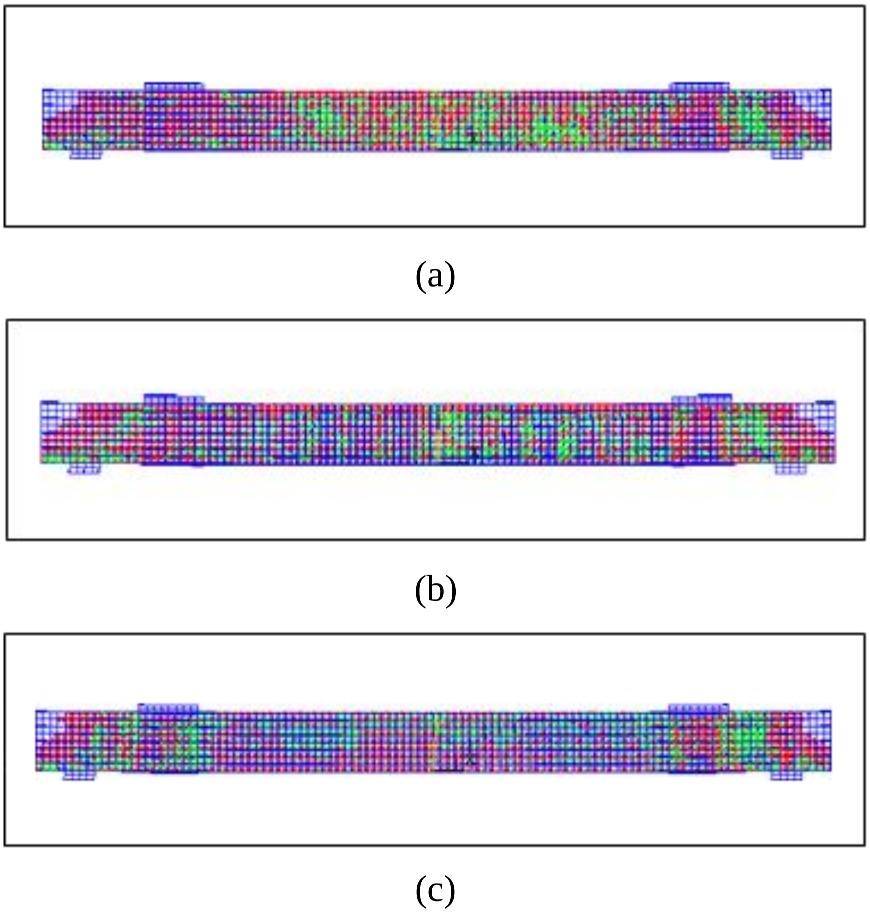
(a)

(b)

(c)

Figure 2-6: Crack pattern at failure: (a) control beam, (b) strengthened beams using FRP strips, and (c) strengthened beam using fully FRP U-wrap[54].

2.4 Reinforcement Concrete Beam of Tapered Section

In 1981,To [55] described a linearly tapered beam finite element incorporating shear deformation and rotary inertia for vibration analysis. Two sets of eigenvalue solutions were taken. One of them was carried out with various tapering ratios in order to compare with the classical cases. The effect of aspect ratio on the eigenvalues of thin-walled cantilever beam installations tapered with others was studied. The results show that, the eigenvalues of the structure are reduced as a result of shear deformation and rotating inertia. the reduction in eigenvalues becomes quite pronounced when the aspect ratio I/dv decreases. Finally, it enables comparisons with other explicit solutions without the need for numerical examples.

In 1983, Stefanou [26] investigated the shear resistance of reinforced concrete beams with non-prismatic sections of varying depth, and the way in which they fail in shear and compared with prismatic beams. A series of 24 beams were tested under the same loading conditions. The main parameters were the slope of the beams, main longitudinal reinforcement, presence of stirrups, depth of beams at supports .Based on the results of parametric studies and British Code of Practice [56], the American A.C.I Code and the Russian Code of Practice [57];The effect of a slope on the top surface is less than that of a slope on the bottom surface when compared to rectangular beams and beam with stirrups, the effect of either slope is higher than in one without And The predictions for beams without stirrups are safer than those for beams with stirrups. Also using trial sections to define Soviet Code forecasts is unsafe, especially for beams with a bottom slope. Finally the proposed method for applying the British Code [56] predicts strengths that are reasonably consistent with the test results.

In 2001, Balkaya (58) investigation the behavior and modeling of non-prismatic members having T-section based on a 3D finite-element as shown in Figure 2-7 Based on the findings of parametric investigations, a simple realistic 2D beam model with an effective length concept is given for the analysis of non-prismatic T-section members. In the proposed model, the effective length of the 2D beam element representing the haunch evolves to be 75% of its actual length. The variance in results from the results of the finite-element analysis is found to be within 15%. In addition, utilizing the proposed 2D beam representation, several modeling approaches in the study of frames with non-prismatic members are studied.

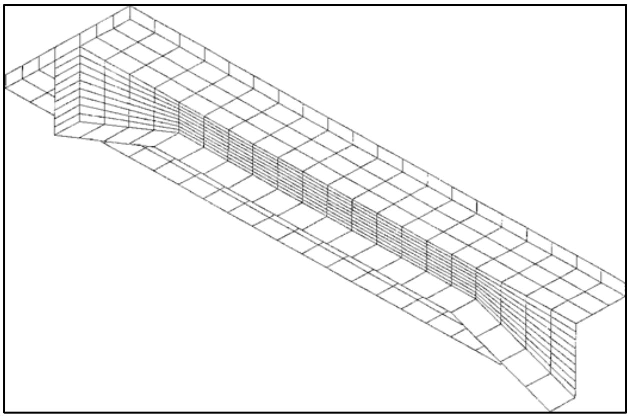

Figure 2-7; 3D finite-element model [58]

In 2007, Tena-Colunga et al. [59] devoted an inclusive experimental study to the cyclic shear behavior of reinforced concrete hunched beams. Five RCHBs with no shear reinforcement under the cyclic load are shown in Figure2-8 the parameters included the haunch angle, the shear reinforcement, the concrete compressive strength and the negative contribution of the inclined longitudinal reinforcement. The investigation outcomes exhibited that haunched beams behave differently in terms of cyclic shear than prismatic beams. Because non-prismatic beams favor an arching action in the haunched length as the principal resisting mechanism, they have higher deformation and energy dissipation capacities.

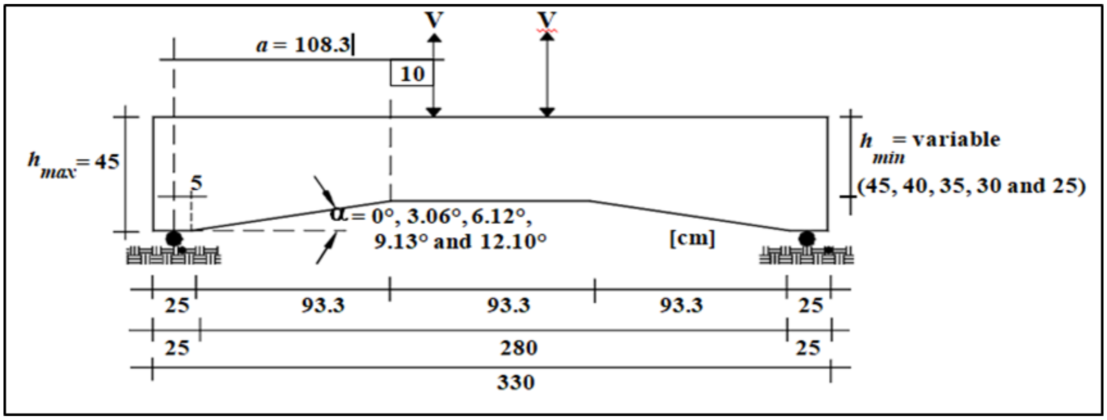

Figure 2-8 Geometry and loading condition for the test specimens [59]

In 2008, Tena-Colunga et al. [18] performed an experimental study on the behavior of reinforced concrete haunched beams under static loading 10 simply supported reinforced concrete beams (eight haunched and two prismatic) divided in two groups were tested experimentally. The first group involved four haunches and one prismatic without shear reinforcement. The second group involved four haunches and one prismatic with shear reinforcement. The Different parameters were considered in this research such as haunch angle (varied from 3° to 12°), amount of shear reinforcement, and compressive strength. The result of the experimental study show that, The shear behavior of RCHBs differs from that of prismatic beams. In comparison to prismatic members, RCHBs demonstrated higher deformation and energy dissipation capacities. As the haunch angle increases, the angle of inclination of the main shear crack decreases. Crack propagation was higher in RCHBs than in prismatic beams. Before the primary diagonal crack forms, RCHBs create an arch mechanism that permits the damage to be spread along the haunched length.

In 2013, Al-Maliki [60] studied the experimental behavior of non-prismatic hollow reinforced concrete beams modified with CFRP panels was studied. The study conducted by testing five reinforced concrete non-prismatic beams hollows section under two point loads. All specimens have same dimensions (length 1170 x height 260 x width 150mm). Different parameters were considered in this research such as hollow opening filling (shapes and materials), the effect of section (solid or hollow), and the effect of retrofitting with CFRP. Four of the models were retrofitted with CFRP strips. The results show that, when compared to a solid beam, the presence of irregularity in the beam depth resulted in a loss in stiffness and an increase in beam deflection. A hollow recess in non-prismatic beams was created using (circular PVC pipe), which resulted in a decrease in load capacity and an increase in deflections and strain when compared to solid non-prismatic beams. When compared to PVC pipe, the square longitudinal aperture filled with steel hollow pipe enhanced maximum load capacity and lowered deflection by around 56% and 33%, respectively. In addition, retrofitting beams with CFRP improved load capacity and ductility, particularly when the CFRP sheet was bonded to the bottom surface of non-prismatic beams.

In 2017, Tena-Colunga et al [61] inspected the shear behavior of continuous reinforced concrete haunched beams subjected to cyclic loading as shown in Figure 2-9 The study was conducted by testing four reinforced concrete beams (three haunched and one prismatic) designed to develop a shear failure with minimum shear reinforcement. The major parameters were the angle of haunch from horizontal and its impact on the concrete strength, the contribution of the transverse steel reinforcement and the contribution of the inclined longitudinal steel reinforcement. The results show that, even when they fail under shear, reinforced concrete haunched beams are more efficient than reinforced concrete prismatic beams. Furthermore, such RCHBs are more efficient in bending than prismatic sections because the plasticity is distributed over a broader area along the haunch rather than a localized plastic hinge near the beam ends.

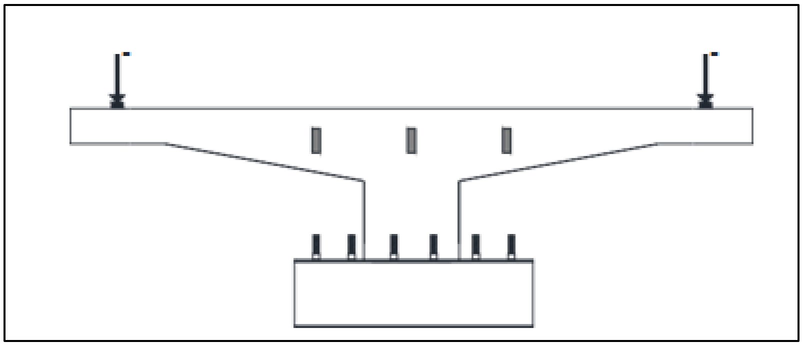

Figure 2-9 Application of cyclic load [61]

In 2017, Al-Attar et al. [62] investigated the behavior of tapered self -compacting reinforced concrete beams strengthened by CFRP. The process is included testing of 14 reinforced self-compacting concrete tapered beams with or without strengthening. The method used for strengthening is carbon fiber reinforced polymer (CFRP) to beams. Those beams have dimension (length of 200mm, a width of 150mm and a height of 250 at supports and a mid-span depth varies between 150mm and 200mm) are subject to two points loading. The major parameters were the haunch angle ,shear-span to effective depth ratio a/d and strengthening strips number and location on beams behavior . The search results show that, where decreasing haunch angle a leads to an increasing in load capacity by 56% and decreased the deflection ,while when using CFRP in the tapered beams increased the load capacity by 39% with decrease of deflection .Furthermore, decreasing the a/d ratio leads to an increment in ultimate load and decrement in deflection.

In 2018, Qissab and Salman [63] investigated the shear strength of non-prismatic steel fiber reinforced concrete beams without stirrups under monotonic loading. Fifteen non-prismatic reinforced concrete beams divided in to three groups were tested experimentally and analyzed. Based on the results of parametric studies steel fibers content, shear span to minimum depth ratio (a/d), tapering angle (a), improved the geometry of the non-prismatic concrete beams. The results of experimental tests revealed that, the compressive strength of concrete increased by 7.31% and 9.75% and the splitting tensile strength of concrete increase by 27.31% or 34.20% when the increased steel fibers ratio by 0.5% or 0.75%. The flexural strength of concrete increases by 2.1% or 6.75% with an increase in steel fiber content by 0.5% or 0.75% and the shear strength of concrete increase directly with the steel content. On other hand decrease the shear crack width and workability of concrete when addition of steel fiber increased the ductility of the beams. In addition, the increase in energy absorption of the beam in the rate of 993.18% when the addition of a steel fiber ratio of 0.75%. Finally, The shear strength had an average decrease of 56.90 when the shear span to depth ratio (a/d) increased from 1.6 to 2.8.

In 2020, Ibrahim and Rad [16] searched the numerical plastic analysis of non-prismatic reinforced concrete beams strengthened by carbon fiber reinforced polymers by using ABAQUS. The model is used for the development and exploration of shear strength for non-prismatic RC beams, in order to achieve this aim, a numerical model was calibrated according to the data obtained from laboratory tests then a series of numerical simulations and thus variables are CFRP strips and hunch angle value. The numerical results showed that, the behavior of the shear strength of the beam is greatly affected by the change in the value of the angle, as the ultimate strength value of the concrete required to resist shear failure decrease with the increase in the size of the angle and thus the beams fail at previous loads, however, increasing the value of the shear failure resistance behavior of the non-prismatic, On the other hand, the ultimate load of the beams increases which leads to more brittle and sudden failure when the CFRP is present it acts as additional support to resist shear strength and constrain the concrete section. In addition, the presence of CFRP leads to an increase in the number and intensity of cracks in the middle of the span, so most of the stresses have shifted from the shear area to the flexural area.

In 2021, Siswantoro and Pradana [64] studied the flexural behavior of non-prismatic longitudinal section reinforced concrete deep beams by using ABAQUS software. Three models are used, the first model consists of a prismatic longitudinal section and the second and third model consists of the non- prismatic longitudinal section. The numerical simulation results showed that flexural behavior such as ductility, stiffness, load-displacement relationship and mode failure is influenced by non-prismatic longitudinal section deep beam. When using non-prismatic longitudinal section a slight decrease in the maximum load occurs compared to prismatic longitudinal, the reason for this is the low height deep beam and the tensile reinforcement capacity trigger on decreasing inertia moment. In addition, the prismatic longitudinal section show good performance in terms of rigidity and flexibility compared to the non-prismatic longitudinal section. On the other hand, the failure of the shear to represent the initial crack rise from the pin support approach to center load, meanwhile, the flexural shear occurs in all three models.

In 2021, Zamel [65] investigated the flexural behavior of developed reinforced concrete beams of the non-prismatic flanges. The main target of this research was to utilize the flange section benefits besides tapering benefits to upgrade structural characteristics of the reinforced concrete T-beams such as section rotation capacity and flexural ductility as well as saving materials and reducing overall dead load without affects ultimate strength capacity. 15 non-prismatic reinforced concrete beams divided in to three groups (nine specimens of non-prismatic flanges, one specimen of rectangular section, and two specimens of uniform T- section of upper and lower tapered flange thickness of considered nine sections) were tested experimentally. Variable parameters in this study were non- prismatic flange domain and web thickness. based on the results of parametric studies up to 47% of member the weight could be saved when shape optimized concrete beams volume regards non-prismatic flanges. Moreover, the positive efficacy of considering planar non-prismatic edges within the T-section based on strength rating, and flexibility, without significant influence on the ultimate load capacity and flexural stiffness.

2.5 Concluding Remaking

1. There are limited studies related to reinforced concrete beams of untraditional section shapes.
2. In reinforced concrete beams, the flanged section presents an optimum section shape that develops satisfied structural characteristics.
3. The tapered geometry is an option to improve specific properties and reduce dead loads without scraped the strength capacity.
4. There are no theoretical or numerical studies dealing with the developed reinforced concrete beams of tapered flanges.

CHAPTER THREE: NUMERICAL FORMULATION AND MODELING

3.1 General

The finite element method (FEM) is a numerical analysis to obtain approximate solutions to a wide range of engineering problems. Recently, the focus fell on numerical methods of engineering analysis with the increasing use of high-speed electronic digital computers. A major advantage of the finite element method is that provides a solution to a variety of problems found in engineering. The basic procedure for modeling any problem using finite element analysis to provide a solution starts by dividing the structure in to elements of non - overlapping finite dimensions called finite elements. Then the original structure is considered as an assembly of these elements in a limited number of joints called nodes. The stiffness matrix is calculated for the element and the applied load vector. Besides, compiling the stiffness matrices of the current elements and constructing a general stiffness. Then, a set of the obtained linear or non-linear algebraic equations is solved to get nodal outcomes such as the values of the displacement, moment or the shear force and other significant outcomes such as stresses and strains.

3.2 Numerical Formulation

3.2.1 The Fundamental Relationships

The derivation of the stiffness matrix for the finite element is a basic stage in any finite element analysis (FEA) which relates the displacement vector (a) to the force vector (f), in order to derive this relationship, three conditions must be met;

1. Compatibility of strains and displacements (kinematic condition).

2. Equations of equilibrium (equilibrium condition).
3. Stress-strain relations (constitutive relations).

The element stiffness matrix can be determined by using the principle of virtual displacement, which states that if the work done by the external forces on a structural system is equal to the increase in strain energy of the system for any set of admissible virtual displacements, then the system is in equilibrium[66]. When a body is subjected to a series of external force, the displacement vector at any point within the element, $\{U\}_e$, is given by,

Where, [N] is a matrix for shape functions, and $\{a\}_e$ is the nodal displacements.

$$\{U\}_e = [N].\{a\}_e \qquad 3.1$$

column vector. at any point the strain calculated by differentiating Eq (3.1)[66].

[L] denotes the differential operator matrix. In its most general form, the strain vector is known as,[16]

$$\{\varepsilon\}_e = [L].\{U\}_e \qquad 3.2$$

$$\{\varepsilon\}_e = \begin{Bmatrix} \varepsilon_x \\ \varepsilon_y \\ \varepsilon_z \\ \gamma_{xy} \\ \gamma_{yz} \\ \gamma_{xz} \end{Bmatrix} = \begin{Bmatrix} \frac{\partial u}{\partial x} \\ \frac{\partial v}{\partial y} \\ \frac{\partial w}{\partial z} \\ \frac{\partial u}{\partial y} + \frac{\partial v}{\partial x} \\ \frac{\partial v}{\partial z} + \frac{\partial w}{\partial y} \\ \frac{\partial w}{\partial x} + \frac{\partial u}{\partial z} \end{Bmatrix} \qquad 3.3$$

Eq. (3.4) is obtained by substituting Eq. (3.1) for Eq. (3.2)[66].

$$\{\varepsilon\}e = [B].\{a\}e \qquad 3.4$$

where [B] is the strain-nodal displacement matrix, which is defined as[66].

$$[B]= [L].[N] \qquad 3.5$$

Once the strains within the element have been determined, the stress vector can be shown using the stress-strain relationship as follows[16];

$$\{\sigma\}_e= [D].\{\varepsilon\}_e \qquad 3.6$$

where [D] is the constitutive matrix and $\{\sigma\}_e$ is[66]:

$$\{\sigma\}_e= [\sigma_x\ \sigma_y\ \sigma_z\ \tau_{xy}\ \tau_{yz}\ \tau_{xz}]^T \qquad 3.7$$

The stress-nodal displacement relationship can be shown using Eqs. (3.4) and (3.6)[16]:

$$\{\sigma\}_e= [D].[B].\{a\}_e \qquad 3.8$$

A virtual displacement principle is used to depict the force-displacement relationship. If a random virtual nodal displacement$\{a\}_e$, is performed, the external work, W_{ext}, will be identical to the internal work, W_{int} [66].

$$W_{ext}= W_{int} \qquad 3.9$$

in which

$$W_{ext} = \{a *\}^T \cdot \{f\}_e \qquad 3.10$$

and

$$\mathrm{W_{int}} = \int_{e} \{\varepsilon^{*}\}_{e}^{T} \cdot \{\sigma\}_{\mathrm{e}} \cdot \mathrm{dv} \qquad 3.11$$

Where $\{f\}_e$ is the nodal force vector. When Eq. (3.4) is substituted for Eq. (3.11), the result is[66];

$$\mathrm{W_{int}} = \{a^{*}\}_{e}^{T} \cdot \int_{v} [B]^{T} \cdot \{\sigma\}_{\mathrm{e}} \cdot \mathrm{dv} \qquad 3.12$$

From Eq. (3.8) and (3.12),

$$\mathrm{W_{int}} = \{a^{*}\}_{e}^{T} \cdot \int_{v} [B]^{T} \cdot [\mathrm{D}] \cdot [\mathrm{B}] \cdot \mathrm{dv} \cdot \{a\}_{\mathrm{e}} \qquad 3.13$$

then Eq. (3.9) can be written as,

$$\{a^{*}\}_{e}^{T} \cdot \{f\}_{e} = \{a^{*}\}_{e}^{T} \cdot \int_{v} [B]^{T} \cdot [D] \cdot [B] \cdot dv \cdot \{a\}_{e} \qquad 3.14$$

or

$$\left\{\mathrm{f_e} = \int_{v} [B]^{T} \cdot [D] \cdot [B] \cdot dv \cdot \{a\}_{e} \right. \qquad 3.15$$

letting:

$$[K]_e = \int [B]^{T} .[D].[B].dv. \qquad 3.16$$

Then

$$\{f\}_e = [K]_e.\{a\}_e \qquad 3.17$$

Where $[K]_e$ is the element's stiffness matrix.

After translating from local to global coordinates, the comprehensive stiffness matrix, [K], can be obtained by adding the elements stiffness matrices directly[66].

$$[K]= \sum\int[B]^T .[D].[B].dv \tag{3.18}$$

$\{f\}$, the vector of total external force is then[66],

$$\{f\}= [K].\{a\} \tag{3.19}$$

Where, $\{a\}$ is the vector of unknown nodal point displacement.

3.2.2 Strain-Displacement Matrix

Eq. (3.3) relates the strain vector at any point within the brick element (8 nodes) to the nodal displacements vector, which can be written in expanded form as:

$$\begin{Bmatrix} \varepsilon_x \\ \varepsilon_y \\ \varepsilon_z \\ \gamma_{xy} \\ \gamma_{yz} \\ \gamma_{xz} \end{Bmatrix} = \sum_{i=1}^{8} \begin{Bmatrix} \frac{\partial N_i}{\partial x} & 0 & 0 \\ 0 & \frac{\partial N_i}{\partial y} & 0 \\ 0 & 0 & \frac{\partial N_i}{\partial z} \\ \frac{\partial N_i}{\partial y} & \frac{\partial N_i}{\partial x} & 0 \\ 0 & \frac{\partial N_i}{\partial z} & \frac{\partial N_i}{\partial y} \\ \frac{\partial N_i}{\partial z} & 0 & \frac{\partial N_i}{\partial x} \end{Bmatrix} \begin{Bmatrix} u_i \\ v_i \\ w_i \end{Bmatrix} \tag{3.20}$$

Where, the 6*3 matrix is the strain-displacement [B] matrix, which contains the global derivatives of the shape functions, Ni

Because shape functions are defined in terms of local coordinates, a relationship between their derivatives in the two coordinate systems must be established. The chain rule can be used to find this relationship[66].

$$\begin{aligned}\frac{\partial N_i}{\partial s} &= \frac{\partial N_i}{\partial x}\cdot\frac{\partial x}{\partial s}+\frac{\partial N_i}{\partial y}\cdot\frac{\partial y}{\partial s}+\frac{\partial N_i}{\partial z}\cdot\frac{\partial z}{\partial s}\\ \frac{\partial N_i}{\partial t} &= \frac{\partial N_i}{\partial x}\cdot\frac{\partial x}{\partial t}+\frac{\partial N_i}{\partial y}\cdot\frac{\partial y}{\partial t}+\frac{\partial N_i}{\partial z}\cdot\frac{\partial z}{\partial t}\\ \frac{\partial N_i}{\partial r} &= \frac{\partial N_i}{\partial x}\cdot\frac{\partial x}{\partial r}+\frac{\partial N_i}{\partial y}\cdot\frac{\partial y}{\partial r}+\frac{\partial N_i}{\partial z}\cdot\frac{\partial z}{\partial r}\end{aligned} \qquad 3.21$$

in matrix form, Eq. (3.21) can be written as[66],

$$\begin{Bmatrix}\frac{\partial N_i}{\partial s}\\ \frac{\partial N_i}{\partial t}\\ \frac{\partial N_i}{\partial r}\end{Bmatrix} = \begin{bmatrix}\frac{\partial x}{\partial s} & \frac{\partial y}{\partial s} & \frac{\partial z}{\partial s}\\ \frac{\partial x}{\partial t} & \frac{\partial y}{\partial t} & \frac{\partial z}{\partial t}\\ \frac{\partial x}{\partial r} & \frac{\partial y}{\partial r} & \frac{\partial z}{\partial r}\end{bmatrix}\begin{Bmatrix}\frac{\partial N_i}{\partial x}\\ \frac{\partial N_i}{\partial y}\\ \frac{\partial N_i}{\partial z}\end{Bmatrix} \qquad 3.22$$

The 3x3 matrix is called the Jacobian matrix [J], therefore[66],

$$\begin{Bmatrix}\frac{\partial N_i}{\partial s}\\ \frac{\partial N_i}{\partial t}\\ \frac{\partial N_i}{\partial r}\end{Bmatrix} = [\mathrm{J}]\begin{Bmatrix}\frac{\partial N_i}{\partial x}\\ \frac{\partial N_i}{\partial y}\\ \frac{\partial N_i}{\partial z}\end{Bmatrix} \qquad 3.23$$

For the isoperimetric element, the shape functions are also used to define the geometry of the element. Therefore, the cartesian coordinates of any point within the element are given by[66].

$$\begin{aligned}x(s,t,r) &= \sum_{i=1}^{8} N_i(s,t,r)\cdot x_i\\ y(s,t,r) &= \sum_{i=1}^{8} N_i(s,t,r)\cdot y_i\\ z(s,t,r) &= \sum_{i=1}^{8} N_i(s,t,r)\cdot z_i\end{aligned} \qquad 3.24$$

where, x_i, y_i and z_i are the global coordinates of node i. Making use of Eq. (3-24), the Jacobian matrix can be written as[66],

$$[J]=\begin{bmatrix} \sum_{i=1}^{8} \frac{\partial N_i}{\partial s}\partial x_i & \sum_{i=1}^{8} \frac{\partial N_i}{\partial s}\partial y_i & \sum_{i=1}^{8} \frac{\partial N_i}{\partial s}\partial z_i \\ \sum_{i=1}^{8} \frac{\partial N_i}{\partial t}\partial x_i & \sum_{i=1}^{8} \frac{\partial N_i}{\partial t}\partial y_i & \sum_{i=1}^{8} \frac{\partial N_i}{\partial t}\partial z_i \\ \sum_{i=1}^{8} \frac{\partial N_i}{\partial r}\partial x_i & \sum_{i=1}^{8} \frac{\partial N_i}{\partial r}\partial y_i & \sum_{i=1}^{8} \frac{\partial N_i}{\partial r}\partial z_i \end{bmatrix} \qquad 3.25$$

The global derivatives of the shape functions can be obtained by inverting the Jacobian matrix.

$$\begin{Bmatrix} \frac{\partial N_i}{\partial s} \\ \frac{\partial N_i}{\partial t} \\ \frac{\partial N_i}{\partial r} \end{Bmatrix} = [J]^{-1} \begin{Bmatrix} \frac{\partial N_i}{\partial x} \\ \frac{\partial N_i}{\partial y} \\ \frac{\partial N_i}{\partial z} \end{Bmatrix} \qquad 3.26$$

3.2.3 Element Stiffness Matrix

The stiffness matrix for an element as given in Eq. (3.16) can be written as[66]:

$$[K]_e = \iiint [B]^T.[D].[B].dv \qquad 3.27$$

where dv stands for the element's volume in global coordinates and can be written as[]:

$$dv = dx.dy.dz \qquad 3.28$$

In local coordinates it can be written as[66]:

$$dv = |J|.ds.dt.dr \qquad 3.29$$

Where, $|J|$ is the determinate of the Jacobian matrix.

The element stiffness matrix is obtained by substituting Eq. (3.28) into Eq. (3.29).

$$[K]_e = \int_{-1}^{+1}\int_{-1}^{+1}\int_{-1}^{+1} [B]^T.[D].[B].\left|J\right|.ds.dt.dr \qquad 3.30$$

3.2 ANSYS Computer Package

The computer software ANSYS[30] is a robust and intriguing engineering finite element package that can be used to solve a wide range of problems. FEM has become the most widely used method for studying deformation, stress, and other engineering parameters. ANSYS[30] can solve linear and nonlinear problems, including the effects of cracking, crushing, creep and reinforcement yielding. etc. FEM is a technique that uses complex mathematical equations to accurately approximate how a complex structure reacts to a given load or condition. To find a solution for a model, FE bundles like ANSYS [30] solve thousands or millions of these equations. It would be difficult, if not impossible, to solve all of these equations manually. ANSYS [30] is a general-purpose FE computer program that includes a variety of elements.

3.4 Finite Element Model

3.4.1 Elements and Geometry Modeling

Studying finite element models of a non-prismatic beam having various dimensions, material properties, geometric configuration, boundary conditions and loading states are discussed in Chapter 4. Figure 3-1 shows the geometry and mesh of one of the studied models. The flexural and shear steel reinforcement have some shared nodes as revealed in Figure 3-2.

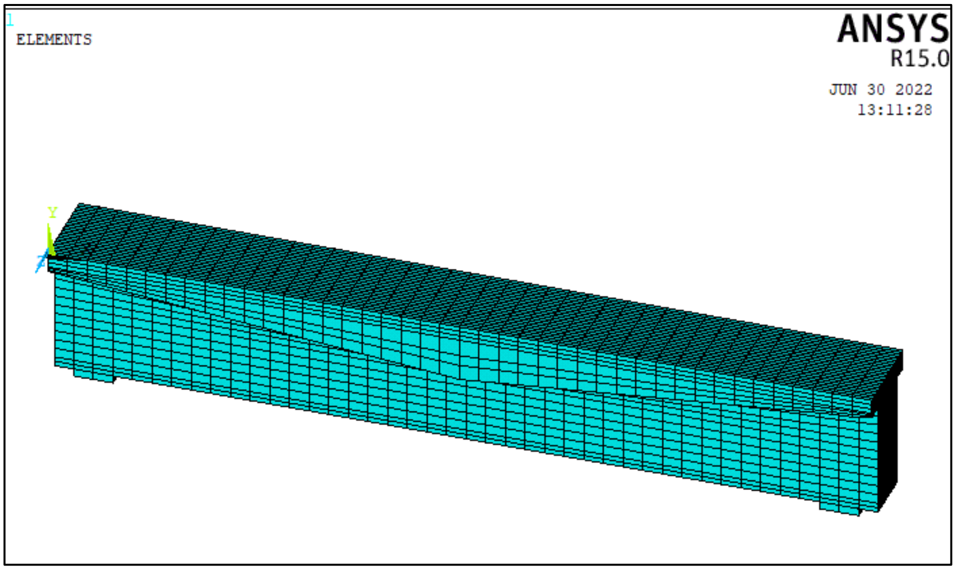

Figure 3-1: 3D Finite element isometric view of Tapered beam

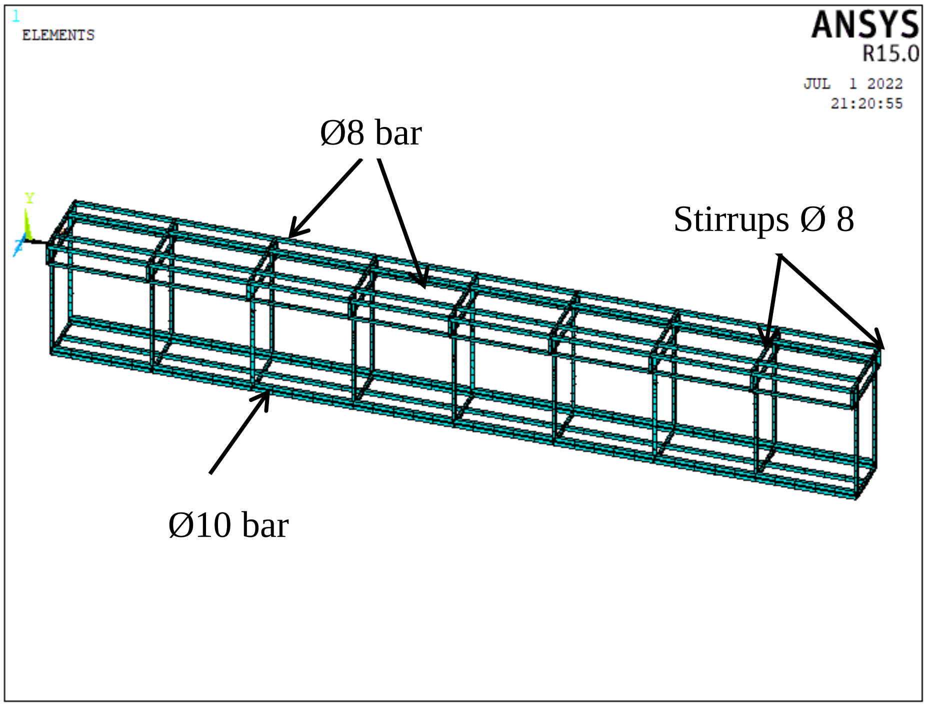

Figure 3-2 : Details of the flexural and shear reinforcement

The finite element analysis in this study is performed using ANSYS 15.0[30]. The model was developed in ANSYS MECHANICAL. To model nonlinear behavior of concrete an eight-node solid element, SOLID65 ANSYS 15.0[30] was used, The ability of solid is used to simulate the concrete material with its situation and properties. The element is formed up of eight nodes, each with three degrees of freedom and translation in the x, y, and z directions. The element can crack in tension in three orthogonal directions, crush in compression, and deform plastically. Tension and compression are possible with the rebar’s, but shear is not. They can also reveal the presence of plastic deformation. The treatment of nonlinear material properties is the most important aspect of this element.[67]. The failure surface must be defined, which is achieved by using the maximum compressive and tensile, strength. When the primary tensile stress is located in any direction outside the failure surface, the concrete element begins to crack. Following that, the ,Young modulus will decrease in value until it reaches zero in the direction of the principal tensile stress. When the principal stresses are compressive and located outside the failure surface, crushing occurs. As a result, the Young modulus is reduced to zero, and the element efficiency is lost [68] . Figure 3-3 shows the geometry, node position, and coordinate system for SOLID65.

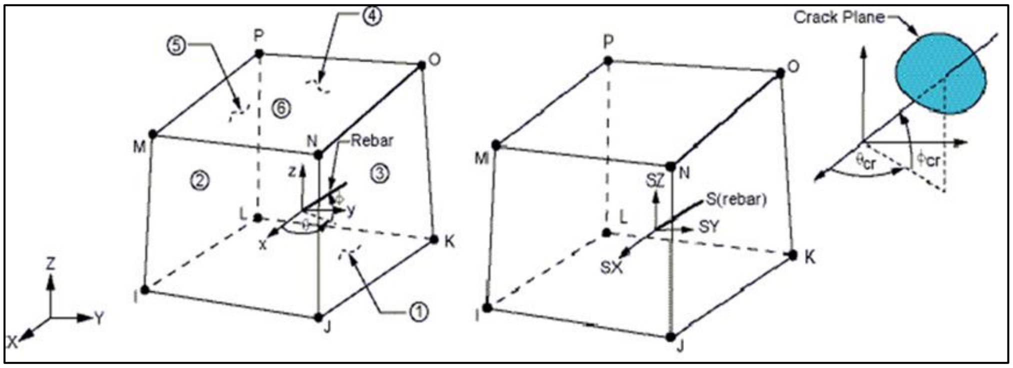

a) SOLID65 geometry b) SOLID65 stress output

Figure 3-3: SOLID65 element for representing the concrete [67]

The link element LINK180 ANSYS (15.0) [30] was used to model the discrete steel reinforcement bars as shown in Figure 3-4 This element is a tension-compression uniaxial element. There is no consideration for bending in this element, as there is a pin-jointed structure. Within, there is plasticity and stress stiffening. In this study, the element is chosen to model steel reinforcement that works as the main steel reinforcement and stirrups. The cross sectional area of the used bar, the initial strain, and the material properties are the input data for the LINK180 element. at least three different reinforcement representations were used in developing a finite element model of a reinforced concrete member [69]. as shown in Figure 3-5

1. Discrete Representation: in discrete modeling, reinforcement is provided by one-dimensional bars that are linked to concrete mesh nodes. As a result, the concrete and steel reinforcement bars will be built at the same nodes and in the same occupied regions.
2. Embedded Representation: the bar element is built in by keeping reinforcing steel displacements compatible with an adjacent concrete element.
3. Smeared (Distributed) Representation: this modeling method assumes that steel reinforcement is distributed uniformly through concrete elements within the defined region of the FE mesh .

perfect bond between the reinforcement steel and concrete is a valid assumption and was used herein. In order to provide perfect bond assumption between the concrete and steel, nodes of the LINK180 steel elements were connected to those of adjacent concrete SOLID65 elements by sharing the same nodes.

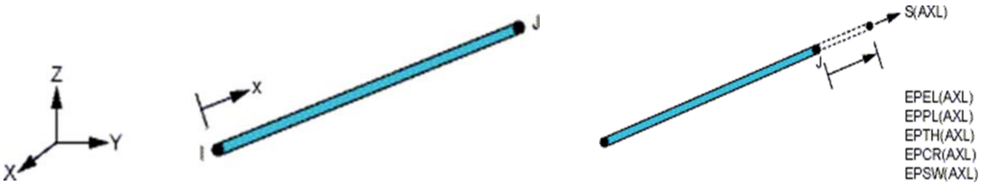

a) b)

a) LINK 180 geometry b) LINK 180 stress output

Figure 3-4: LINK180 for representing steel reinforcement[69]

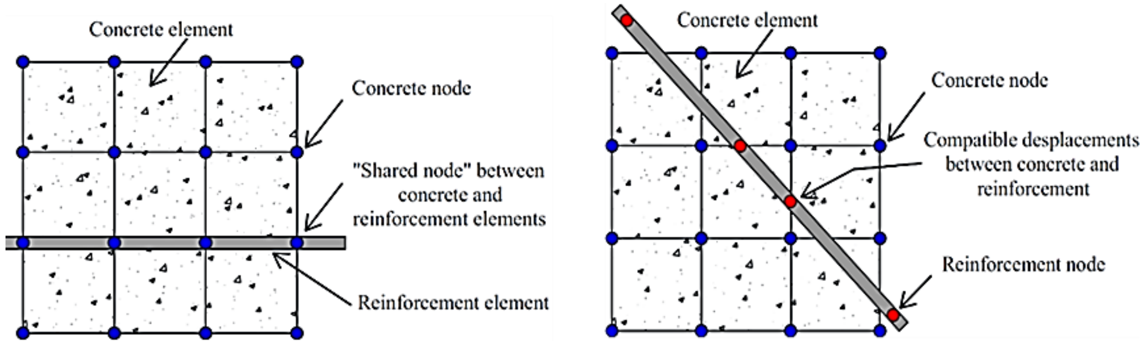

a)Discrete b) Embedded

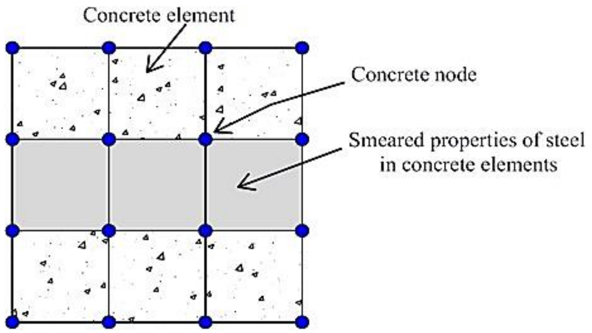

c) Smeared

Figure 3-5: Models for reinforcement in reinforcement concrete ;(a) discrete, (b) embedded and (c) smeared[69]

The solid element SOLID185 is used to model the steel plate under the applied load and at the support in the model. This element consists of eight nodes, each with three degrees of freedom. SOLID185 with translation in the x, y, and z axes. Figure 3-6 shows the geometry and node positions for this element. All beams in this work have number of element SOLID65 (13692-22764) for concrete and element LINK180 (1232-1838) for flexural and shear reinforcement.

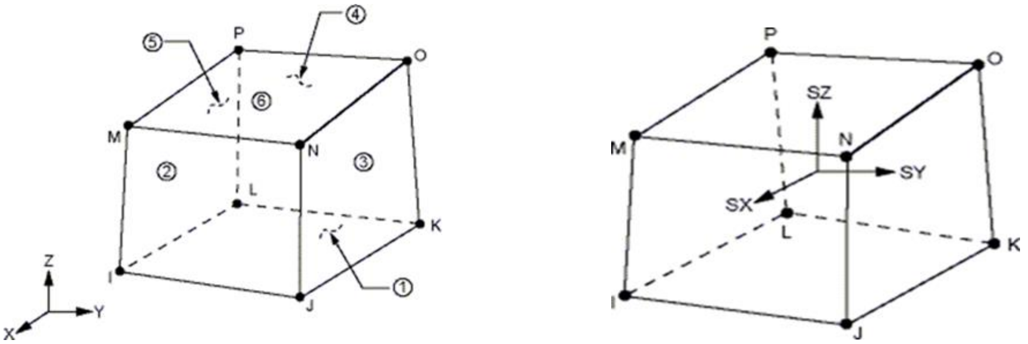

a) SOLID 185 homogeneous b) SOLID 185 homogeneous structural solid
geometry structural solid stress output

Figure 3-6: SOLID 185 used to model steel plates and supports

3.4.2 Material modeling and properties

In the finite element analysis, cracking develops in a concrete element when the principal tensile stress in any direction lies outside the failure surface. After cracking, the concrete material is considered behave as an orthotropic material and the elastic modulus of the concrete element is set to zero in the direction parallel to the principal tensile stress direction. The post cracking tensile behavior of the concrete material is adopted in the finite element model by utilizing abilinear softening stress-strain response. Crushing develops when all principal stresses are compressive and lie outside the failure surface [70]. Consequently, the elastic modulus is set to zero in all directions and the element local stiffness becomes zero resulting in large displacement and therefore divergence in the solution[46].

Defining the nonlinear material properties of reinforced concrete structures is very important for accurately simulating the behavior of the tapered beam. Basically, the nonlinear response of the RC structure is by primarily produced two major factors, concrete cracking and plasticity of the reinforcement steel. The behavior is linear up to the first concrete crack but afterwards it becomes nonlinear. The uncracked elastic stage and cracked plastic stage of the concrete had to be treated separately.

Additionally, In this study an elastic linear work hardening model is used to simulate the uniaxial stress-strain behavior of steel reinforcement as shown in Figure 3-7.

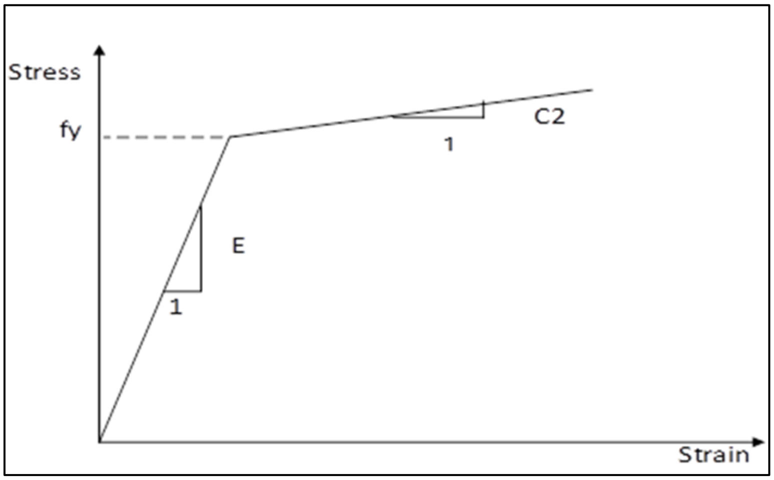

Figure 3-7: Uniaxial stress-strain curve for steel reinforcement[71]

A finite element model reflecting the beam material’s properties had to be developed. Compressive strength of concrete and tensile strength of steel reinforcement, used as ANSYS input data, was based on the tapered beams material properties obtained from experimental study [65]. Compressive and tensile strength and modulus of elasticity of concrete were taken as the measured experimental values of 35 MPa, 3.5 MPa and 27806 MPa, respectively. A Poisson's ratio of 0.3 is used. An extensive parametric study will be discussed in in chapter 4 to find the effect of material properties. Define the plastic behavior of concrete a multi-linear compressive stress-strain curve was defined according to a model that was discussed in a subsequent section. The multi-linear isotropic material uses theVon Mises failure criterion along with the William and Warnke [72] model to define the failure of the concrete.

The concrete material data table also requires additional information about the concrete material, such as the shear transfer coefficients (βt and βc). Shear transfer coefficients are typically assumed to be zero for complete loss of shear transfer, which represents a smooth crack, and 1.0 when there is no loss of shear transfer, representing rough crack ANSYS (15.0) [30]. This specification was made for both the open and the close crack presented by βt for an open crack and βc for a closed crack, respectively.

In this study, the value of βt=0.4 and βc=0.8 was adopted for the modeling of beams. The earlier mentioned bilinear softening stress-strain response has a segment that linearly ascends up to the concrete rupture stress. A tensile stiffness multiplier of 0.6 is used to simulate a sudden drop in tensile stress to 60% of the rupture stress, followed by a linearly decreasing curve to zero stress at a strain value of six times the strain corresponding to the concrete rupture stress. It was considered that the steel was elastic-plastic hardening Von Misses failure criteria were used to simulate the yielding of the reinforcing steel bars. The steel's modulus of elasticity and yield stress were taken as 204.16 GPa and 490 MPa, respectively and a Poisson's ratio of 0.2 is used.

3.4.3 Concrete Nonlinearity Modeling

Concrete is a quasi-brittle material with different compression and tension behavior; hence, developing a nonlinear material model for concrete that accurately captures all of its behavior is a difficult task. The compression part of the stress-strain curve for concrete extends linearly for up to about 30% of the maximum compressive strength. Above this point, the stress increases gradually and nonlinearly up to the maximum compressive strength. The stress-strain curve's tension part is linearly elastic up to the maximum tensile strength. After this, the concrete begins to crack and its strength gradually reduces until it is zero. Usually, the tensile strength of concrete is equivalent to 10% of its compressive strength. The tensile strength of concrete is assumed to be equal to the rupture strength of concrete fr. The tensile strengths for the tested T-beam model were calculated using Eq. (3.31) [73].

$$f_r = 0.623\sqrt{f_c'} \qquad 3.31$$

where,

f'c = ultimate concrete compressive strength, Mpa

f_r = ultimate concrete tensile strength (modulus of rupture), Mpa

In the present study, The compressive uniaxial stress-strain relationship for concrete model was obtained by using the following equations to compute the multilinear isotropic stress-strain curve for the concrete material [74].

$$f_c = \varepsilon\ E_c \text{ for } 0 \le \varepsilon \le \varepsilon_1 \qquad 3.32$$

$$f_c = \frac{\varepsilon E_c}{1 + \left(\frac{\varepsilon}{\varepsilon_0}\right)^2} \text{ for } \varepsilon_1 \le \varepsilon \le \varepsilon_0 \qquad 3.33$$

$$f_c = f_c^{'} \text{ for } \varepsilon_\circ \le \varepsilon \le \varepsilon_{cu} \qquad 3.34$$

And

$$\varepsilon_1 = \frac{0.3 f_c^{'}}{E_c} \qquad 3.35$$

$$\varepsilon_\circ = \frac{2 f_c^{'}}{E_c} \qquad 3.36$$

Where;

f'_c = stress at any strain ε, MPa

ε = strain at stress f

ε_o =strain at ultimate compressive stress f'c and,

Ec = concrete elastic modulus, MPa.

The stress-strain curve then falls until failure occurs due to concrete crushing. The

Young modulus of concrete (E_c) is a function of compressive strength (f'_c). The empirical equation found in ACI 318M-11[75] is used for normal strength concrete.

$$E_c = 4700\sqrt{f'c}\ (MPa) \qquad 3.37$$

In this study, the behavior of concrete material in compression is represented by Figure 3-8.

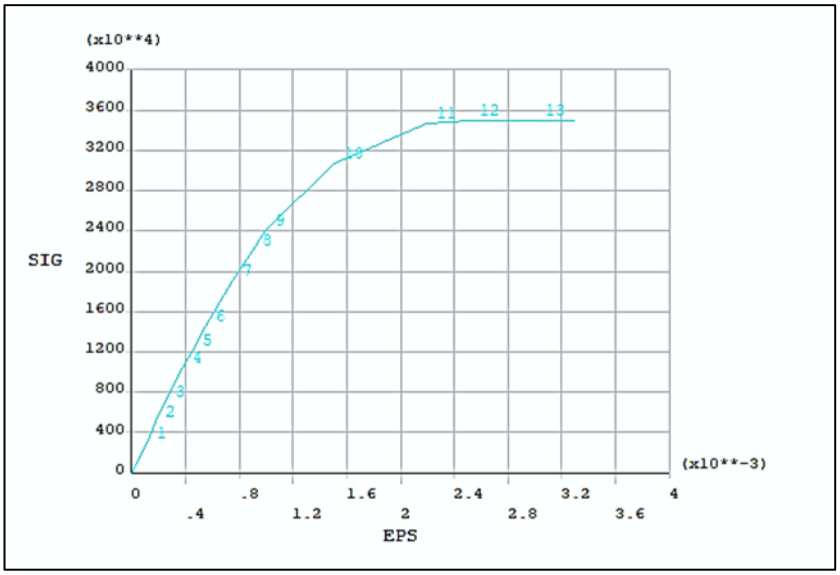

Figure 3-8: Adopted uniaxial stress-strain curve for concrete material (ANSYS v. 15.0) [30]

3.4.4 Boundary Conditions and Loading State

It has been found that the simulation of the applied load and the supports has significant effect on the results of the finite element analysis. The concrete beam was supported by pin at the bottom with a distance 100 mm wide from the edge of the beam with no displacement of the nodes in the (UY) and(UZ)direction , whereas the other support was displayed as roller by indicating the translations at the nodes (UY) equal zero value. To ensure that the model acts the same way as the experimental beam and a comprehensive parametric study will also be discussed in Chapter 4 to see the effect of different types of supports.

The force (P) at one point was placed at the top of specimen in the gravity. The applicable load was known as incremental loads. There was an adjustment for every increase in the result at certain specific load level. Figure 3-9 show that the loading and boundary condition of tapered model

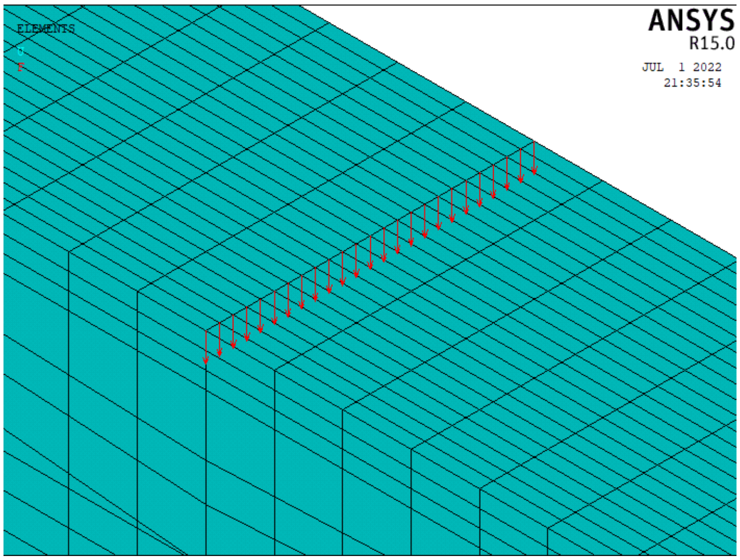

a) Loading method for Tapered model

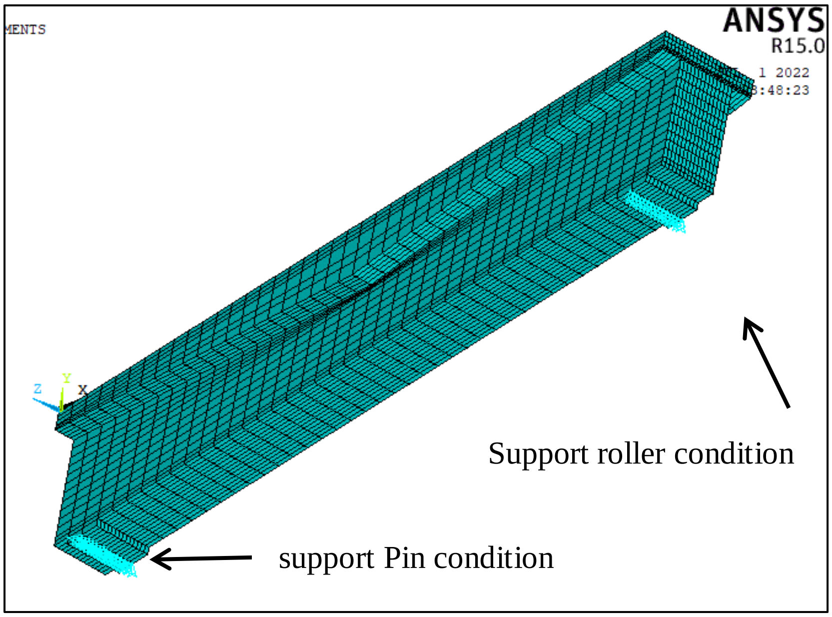

Support roller condition

support Pin condition

a)Boundary condition of Tapered model

Figure 3-9 Loading and boundary condition of Tapered model

3.4.5 Non-linear solution and convergence criteria

The applied loads were divided into load increments known as load steps and sub steps. Convergence is obtained at the end of each load increment by Newton-Raphson equilibrium iterations that are within the tolerance limits of the convergence criteria [76]. In this study, automatic time stepping option is turned on to predict and to control load step sizes. The convergence criteria were based on force and displacement, and ANSYS[30] convergence default values of 0.5% were initially selected. Due to the nonlinear behavior of the concrete element and large deflections, convergence was difficult to achieve using the default ANSYS [30] values. In order to achieve convergence of the solutions, the convergence tolerance limits were thus increased by one order of magnitude (0.05 for force and displacement checking).

CHAPTER FOUR:RESULTS AND DISCUSSIONS

4.1 General

A numerical investigation of in plane tapered flange section of the RC beam is achieved. A wide spectrum of variables that relate to various structural aspects is considered. The study topics can be divided into;

The verification with experimental results are carried out to check the validity and accuracy of the FE procedure. The results obtained by FEM are compared with the experimental results [65] in terms of ultimate strength, load-deflection curves, crack patterns, and strain distribution. The effect of the various parameters which are expected to affect the behavior of such beams is also investigated. These parameters are:

1. the extended middle uniform region within overall tapered flanged modes, the orient variation of the tapered flange, boundary condition, and material properties.
2. Serviceability limit: a study serviceability investigation of tapered section RC beams and compare the results with serviceability limit and uniform section flange.
3. Flange effective width: study of tapered RC beams behavior within the slab system.
4. Continue tapered flange RC beams and moment redistribution: Continuity of tapered flange beams are investigated with numerical modeling and the benefit of a symmetrical numerical approach.
5. Shear Span Effect: study effect of shear span section under various concentrated load.

4.2 Verification Study: Experimental - Numerical Comparative Analysis

In the current study, the structural behavior of simply supported flanged with non-prismatic beams is simulated depending on available experimental test[65]. According to that experimental work, twelve reinforced concrete beams classified into four groups under three point loading. the first one included control specimens of rectangular section and T sections (prismatic flanged section) of upper and lower adopted non-prismatic flanged thickness considered in other specimens.

Three other different groups are considered, they are of various non-prismatic trends (non-prismatic along entire beam length, along entire beam length except middle distance of d length to be prismatic, or along entire beam length except middle distance of 2d length to be prismatic), specimens of each group are of various web thickness (10,14, and 18 cm). the same flexural steel reinforcement quantity was provided (5Ø10) along the length of beams (210cm) in different of specimens, the reinforcement are distributed in manner that keep effective depth (d = 26 cm) constant, a proper shear reinforcement (8 @100 mm) are provided according to ACI-ASCE Committee 445 (1999) [77]. Only nine of non-prismatic beams were utilized in this study for the validation process. for the verification purpose in terms of load-deflection curve, ultimate load, crack patterns, and strain distribution.

Table 4-1 clearly exhibits the verification analysis, the predicted rates are varied between 0.964 to 1.08.

The experimental-numerical comparative views that relate to load-deflection responses of developed beams illustrated in Figure 4-2. The developed numerical model is succeeded to indicate beams responses numerically with highly convergence with the corresponding experimental results and the responses of various specimens exhibit approximately the same flexural stiffness behavior.

Besides, the companied failure modes that summarized the overall beams deformation under the action of applied loads till failure limit are illustrated in Figure 4-3 which shows the numerically predicated cracks patterns that clearly confirmed cracks trends in the experimental study [65]. While Figure 4-4 shows the observed failure modes in scope of the total strain distribution.

Table 4-1 Ultimate strength analysis

NO	Group	Code	$(pu)_{exp}$	$(Pu)_{FE}$	$RP_{(EXP/FE)}$
1	G1	B4	149.5	155	0.964
2		B5	143.1	147.1	0.973
3		B6	148	147.8	1.001
4	G2	B7	149.4	150	0.996
5		B8	155.6	143.1	1.087
6		B9	150.2	151.1	0.994
7	G3	B10	155.4	155.3	1.001
8		B11	158	154	1.026
9		B12	155.4	155	1.003

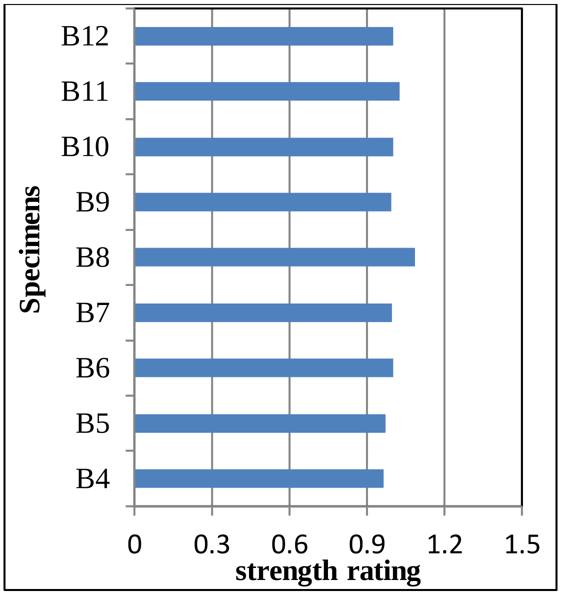

Figure 4-1 Numerical results verification; ultimate strength rating

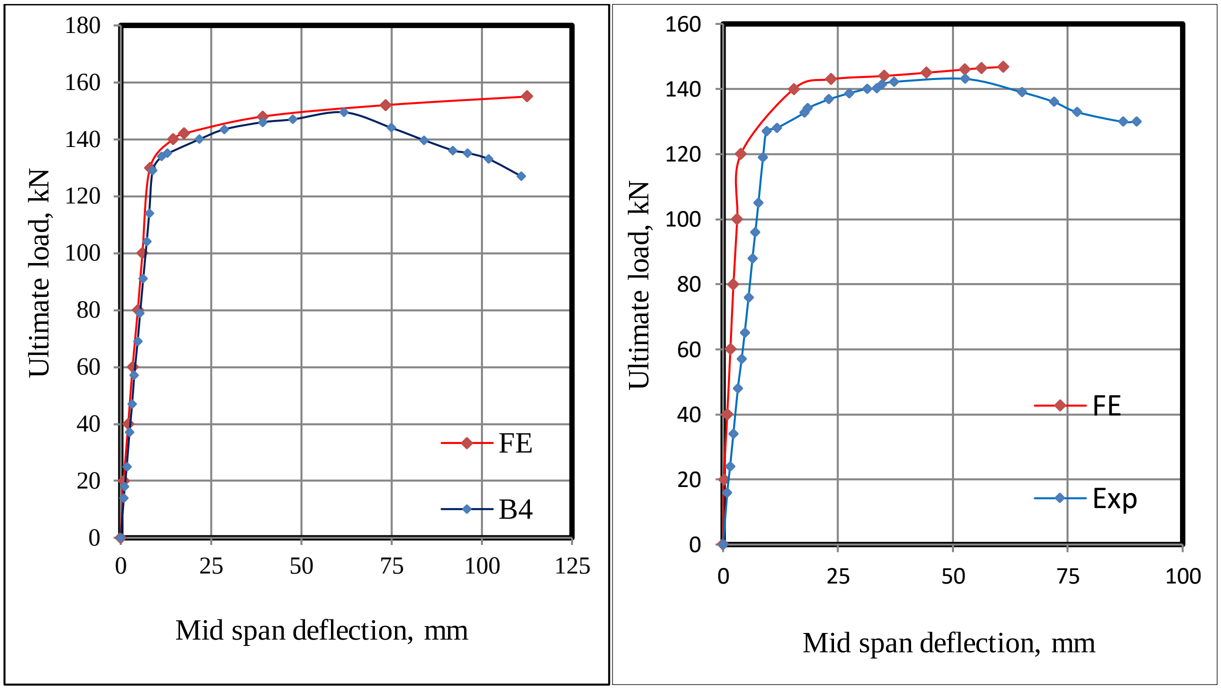

a.(B4) b.(B5)

Figure 4-2 P-Δ curves; experimental-numerical comparative views.

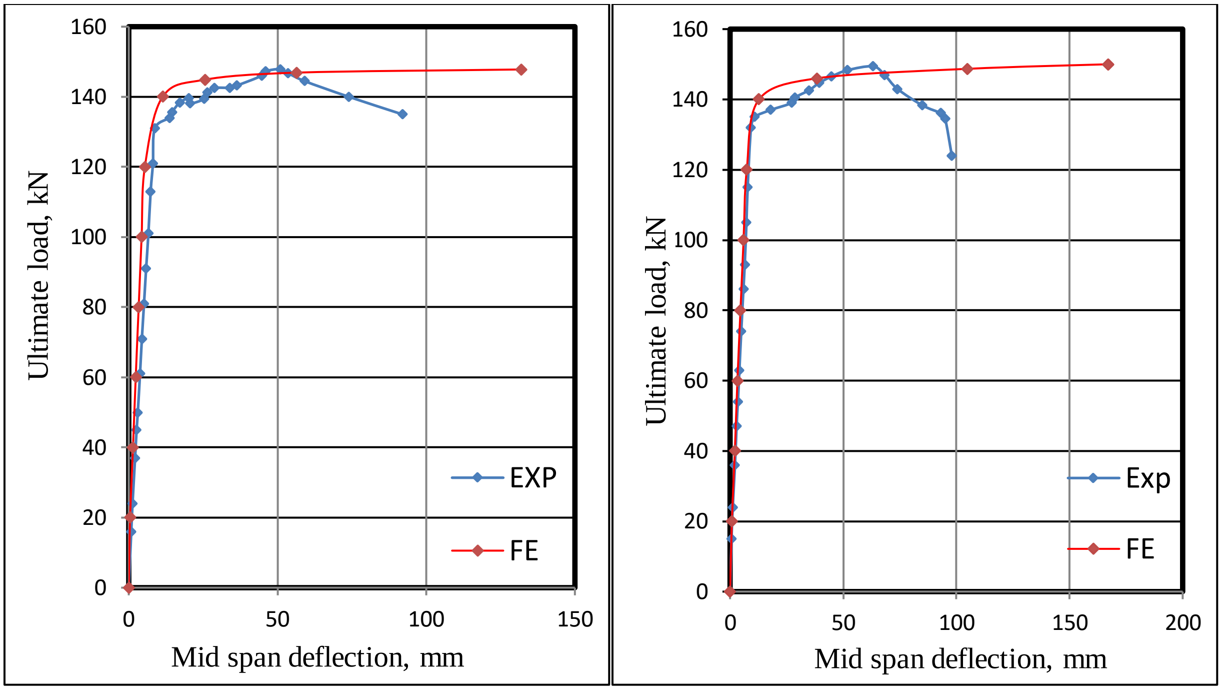

c.(B6) d.(B7)

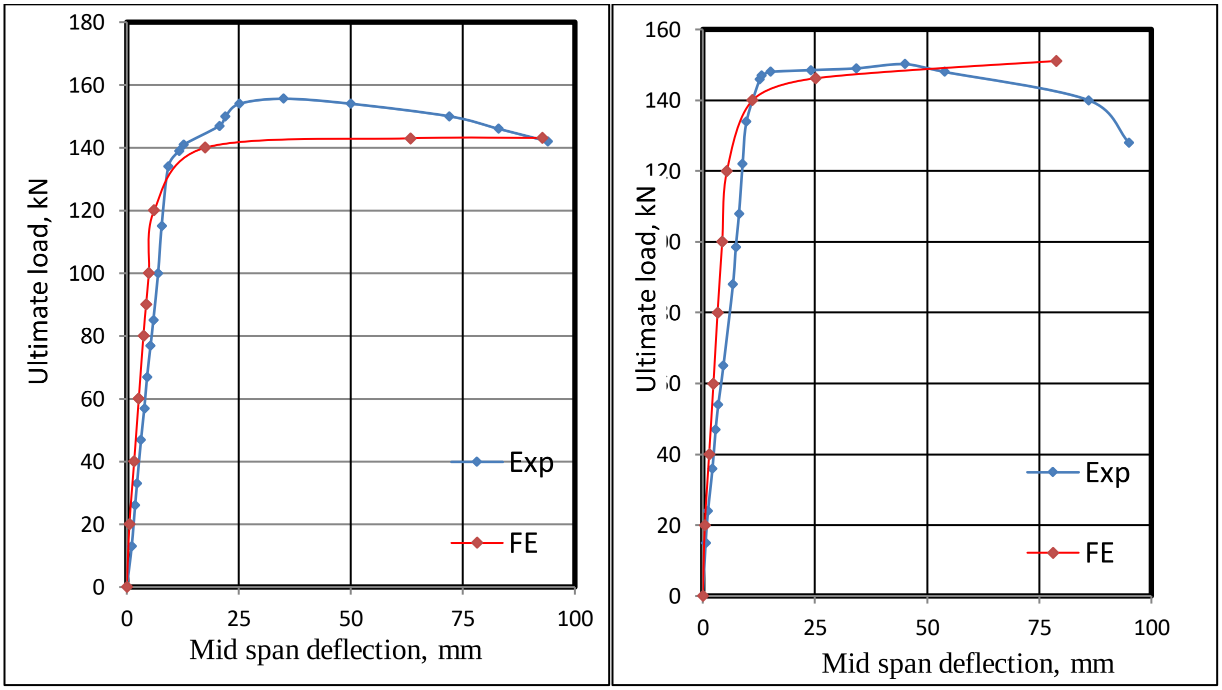

e.(B8) f.(B9)

Figure 4-2: Cont.

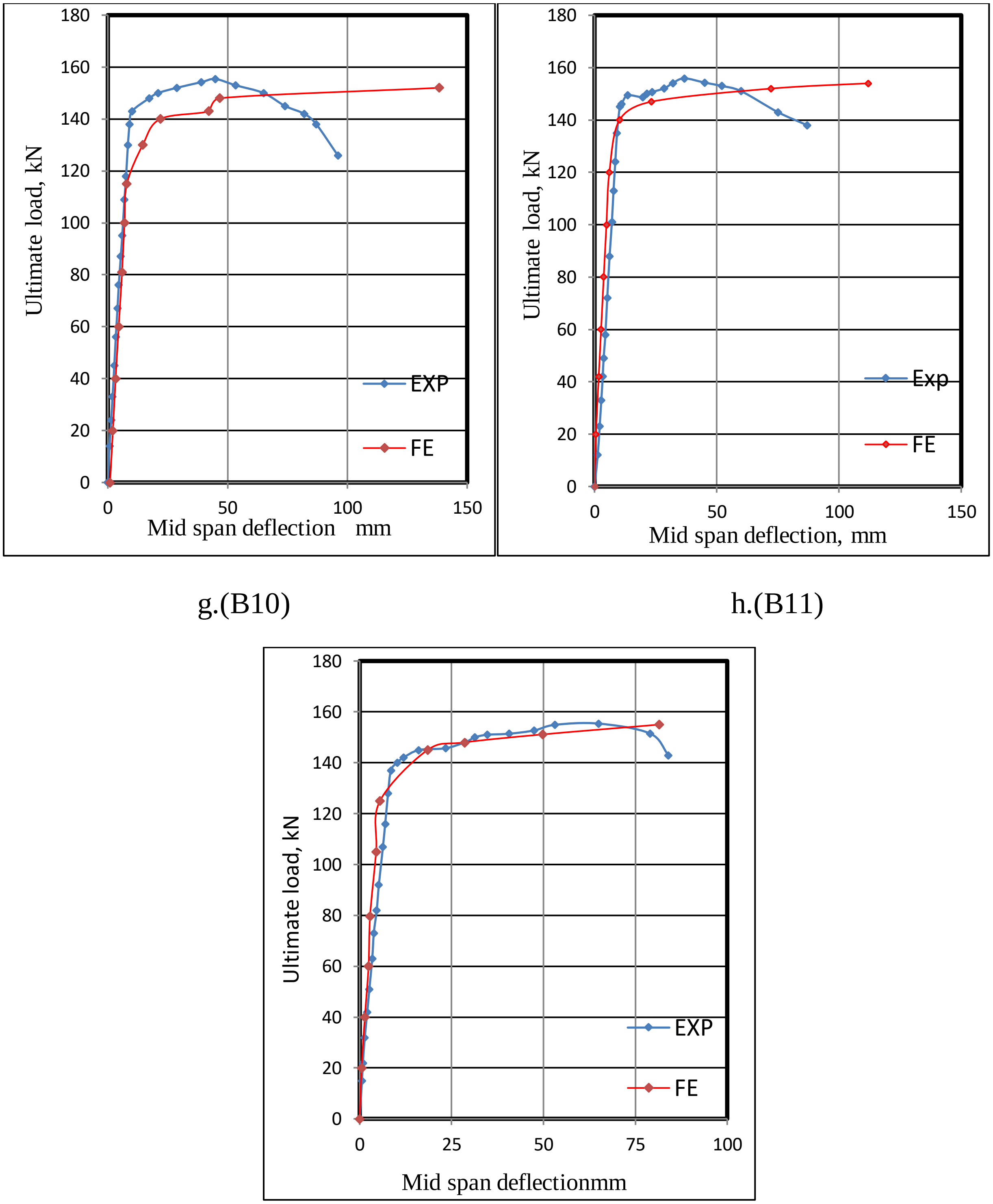

g.(B10) h.(B11)

i.(B12)

Figure 4-2 : Cont.

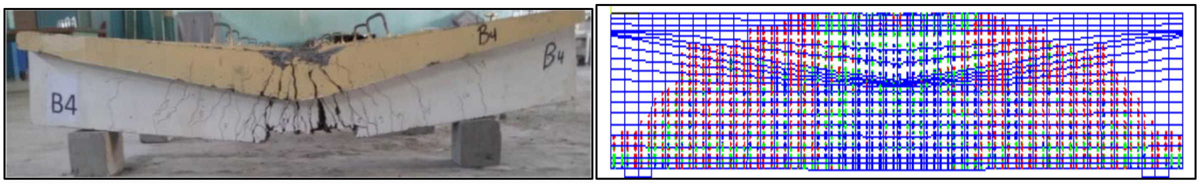

a)B4

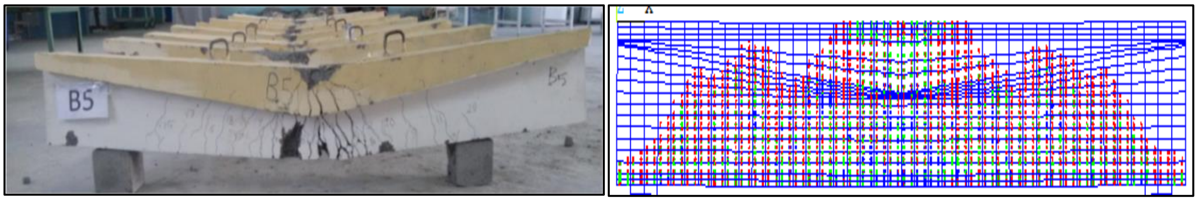

b)B5

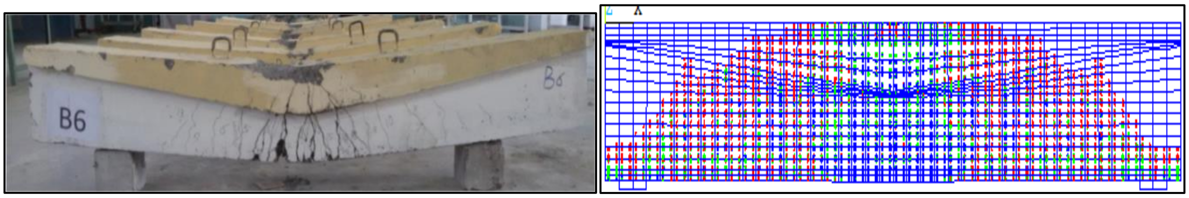

c)B6

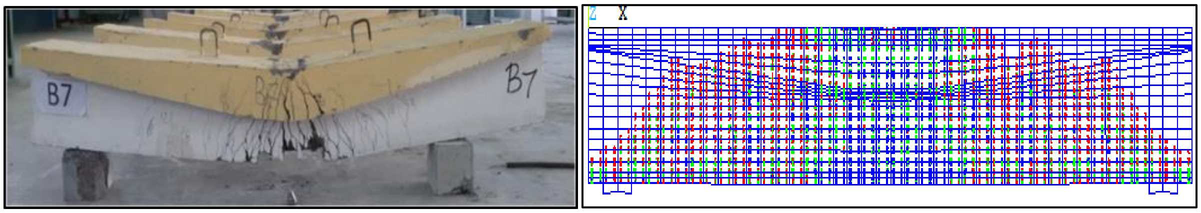

d)B7

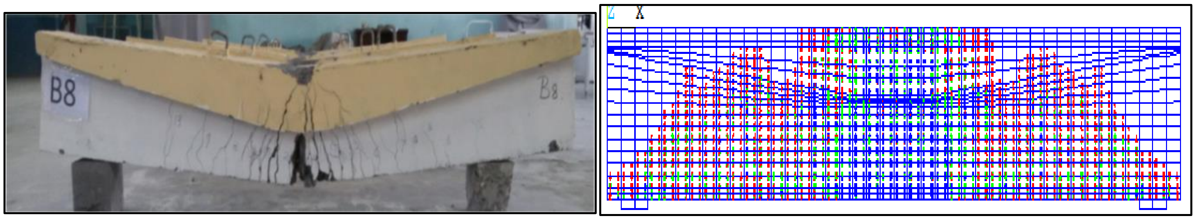

e)B8

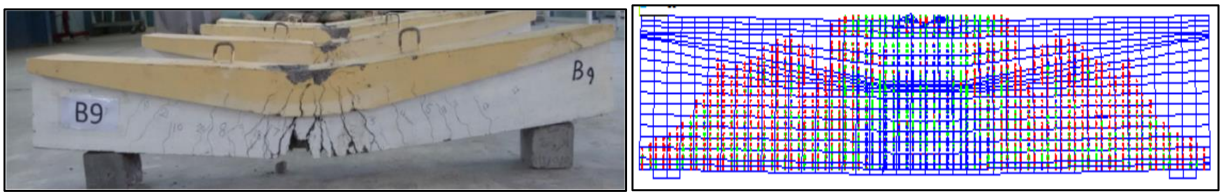

f) B9

Figure 4-3 Failure modes and crack patterns; experimental-Numerical comparative view

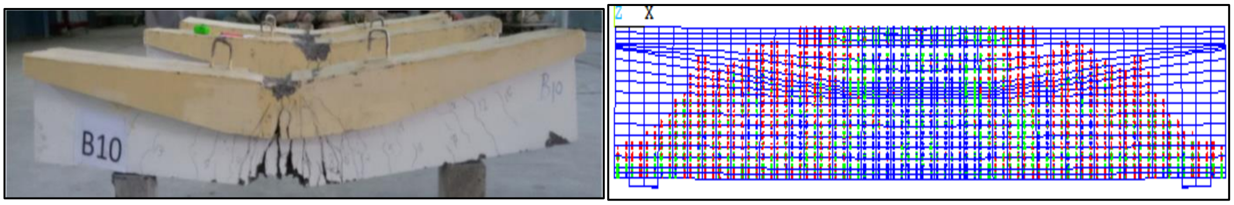

g)B10

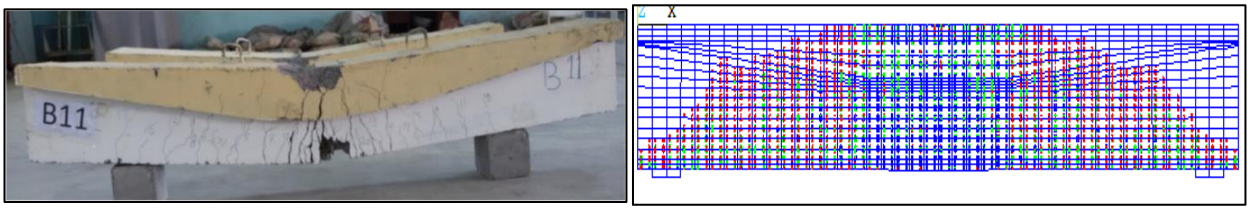

h) B11

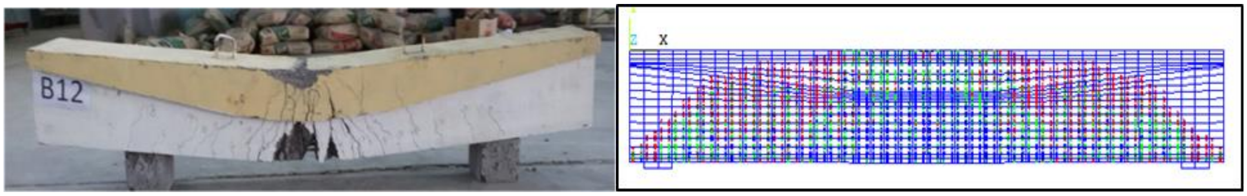

i)B12

Figure 4-3 : Cont.

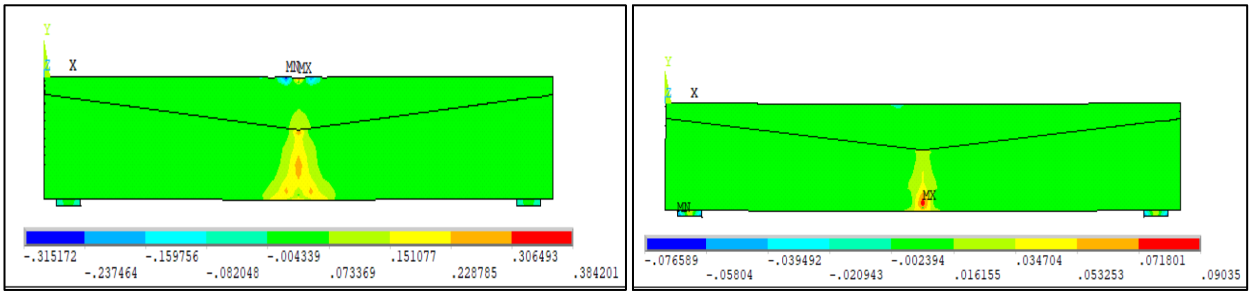

a)B4 b)B5

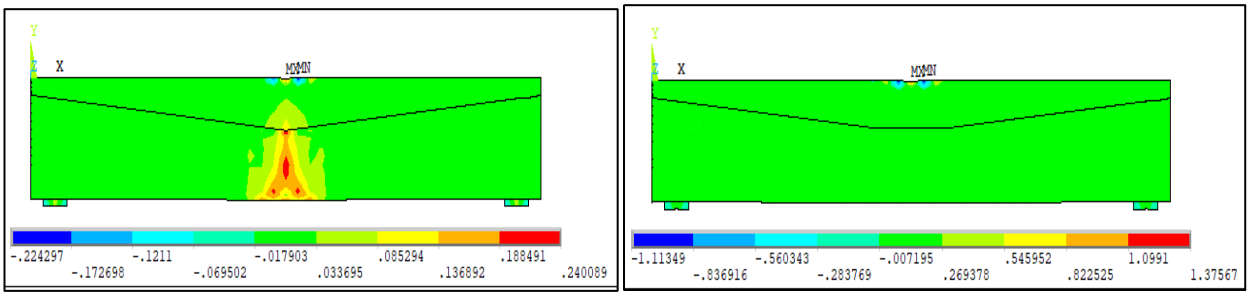

c)B6 d)B7

Figure 4-4 total Strain distribution: experimental-Numerical comparative view

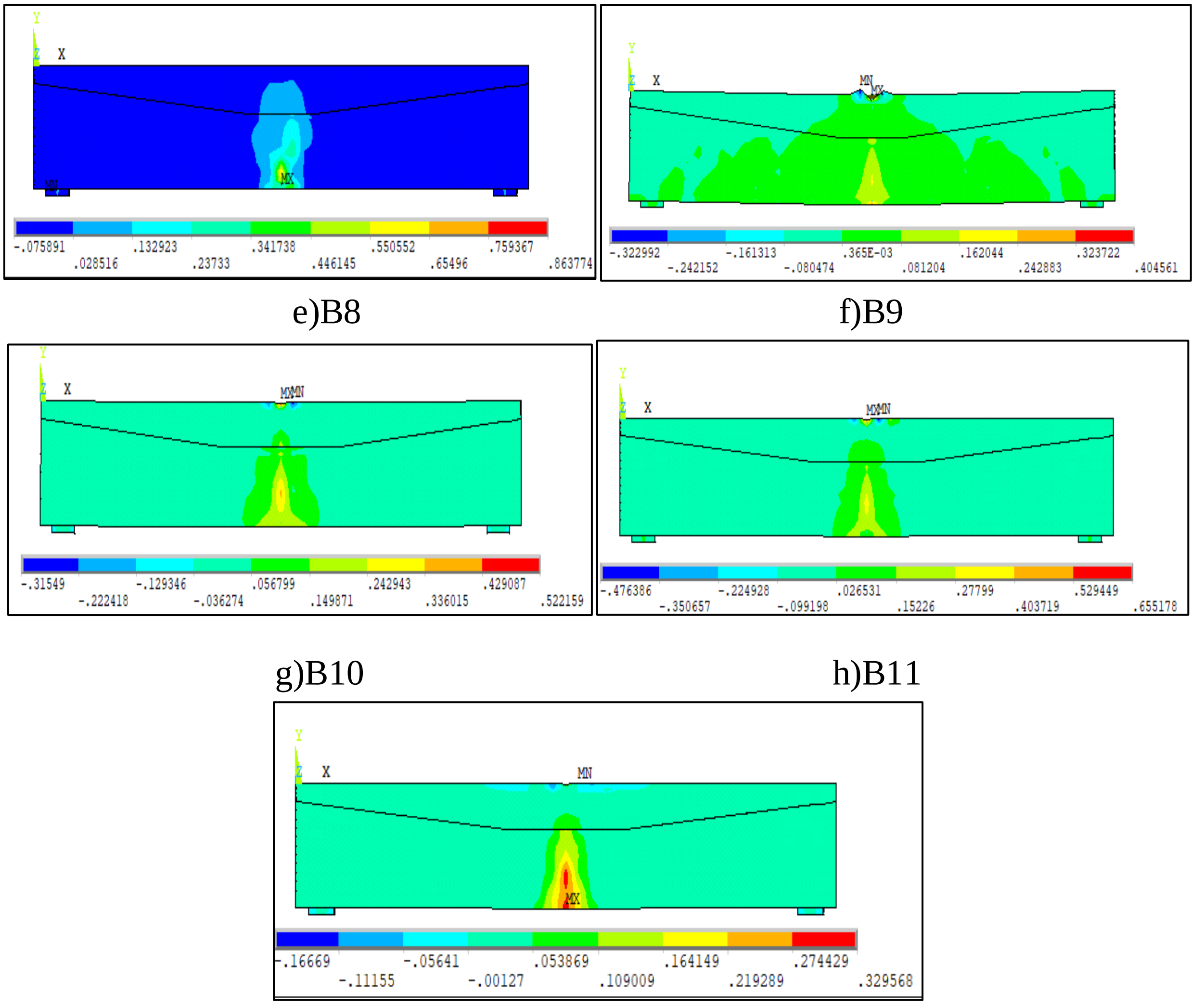

e)B8 f)B9

g)B10 h)B11

i)B12

Figure 4-4: Cont.

4.3 Parametric Study

4.3.1Geometrical Characteristics

4.3.1.1Extended Middle Uniform Region(Lf)

The extended middle uniform region within overall tapered flanged modes is investigated numerically. The middle section of uniformity investigation relates to the inspection of strength rating (ultimate strength / beam overall weight). The maintenance of section strength with uniformity region reduction mean, higher strength rating (ultimate strength / beam overall weight) and mean reduction in the attainted dead load. Wide range of extended regions distance as variable are considered, the adopted numerical modeling details are summarized in Table 4-2. The obtained results show that, as uniformity region increased from 0 to 52 cm, the ultimate strength get improving from 147 kN to 155.3 kN with slightly increment rates 1.02 While the best flexural ductility and the best energy dissipation are predicted in a certain uniformity length (26 cm) which is indicated as an optimum uniformity length that corresponding to ductility improving rate of 1.49 and energy dissipation enhancement rate of 1.53. Table 4-3 exhibits results analysis that relate to middle uniform region investigation. These observation could be clearly monitored by the introduced load -deflection curves that shown in Figure 4-5 and related ultimate strength, ductility indices and energy enhancement rates in Figure 4-7. Figure 4-8 shows the observed failure modes in scope of the crack patterns and total Strain distribution.

The mathematical normalization of the obtained results are shown in Figure 4-6. nonlinear relationship of three degree is succeeded to normalized the result, an optimum value of uniformly region is attained within wide uniformity range, and this observation could be related to the effect of tapered flange to dominate the stress distribution.

Table 4-2 Specimens' modeling details: midspan uniformity

No.	Variable	L cm	d cm	h cm	b_f cm	b_w cm	d_{fe} cm	d_{fm} cm	$L,_{fm}$ cm
1	U0	210	26	30	24	10	5	15	0
2	U13	210	26	30	24	10	5	15	13
3	U26	210	26	30	24	10	5	15	26
4	U39	210	26	30	24	10	5	15	39
5	U52	210	26	30	24	10	5	15	52

Table 4-3 Results analysis: midspan uniformity investigation

No.	Code	The variable parameter	Pu, kN	Pui/Pu1	Δe, mm	Δmax, mm	(Δmax)i/(Δmax)1	D.I.	(D.I)i/(D.I)1	ψ, kN.mm	ψi/ψ1
1	U0	The extension of midspan tapering, Lfm	147	1.00	8.1	112.5	1.00	13.88	1.00	7410	1.00
2	U13		152	1.03	7.97	152.4	1.35	19.12	1.37	10506	1.41
3	U26		150	1.02	8.11	167.9	1.49	20.7	1.49	11393	1.53
4	U39		153	1.04	8.1	106.2	0.94	13.11	0.94	6978	0.94
5	U52		155.3	1.05	7.95	138.3	1.23	17.39	1.25	9446	1.27

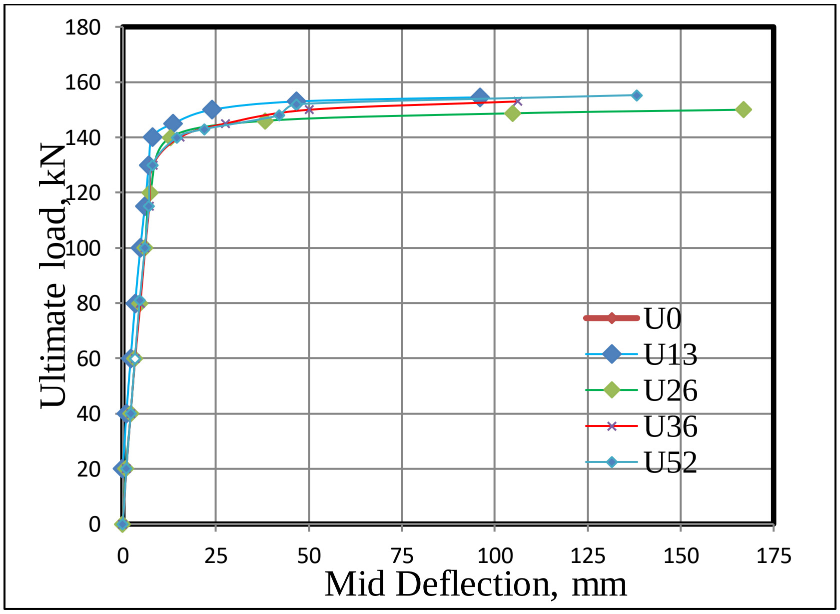

Figure 4-5 load – deflection response : midspan uniformity effect

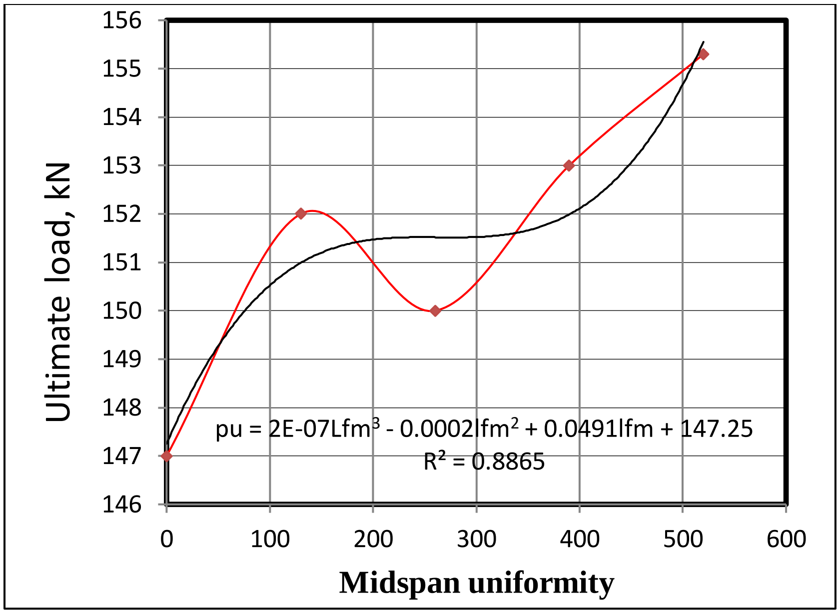

Figure 4-6 Mathematical normalization: midspan uniformity effect

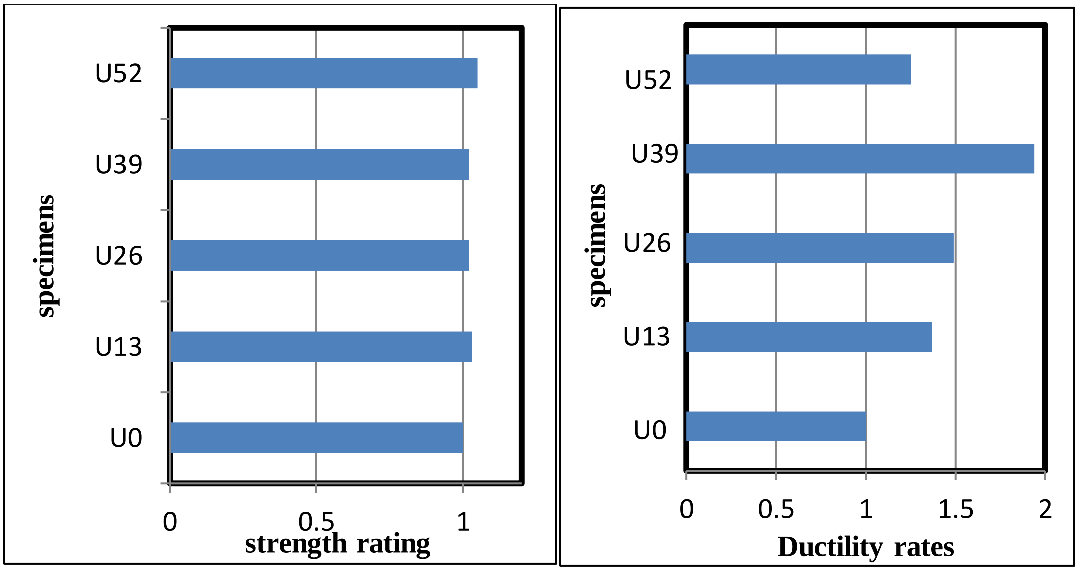

a) b)

Figure 4-7 a) Strength variation rates b) Ductility variation rates c) Energy dissipation variation rates :midspan uniformity effect

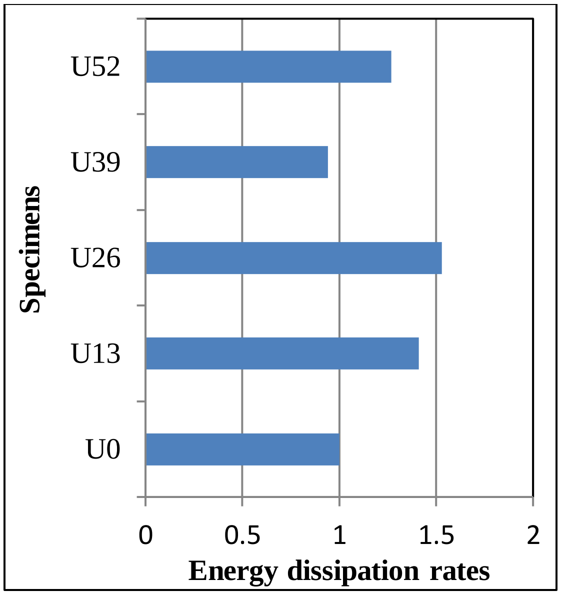

c)

Figure 4-7: Cont.

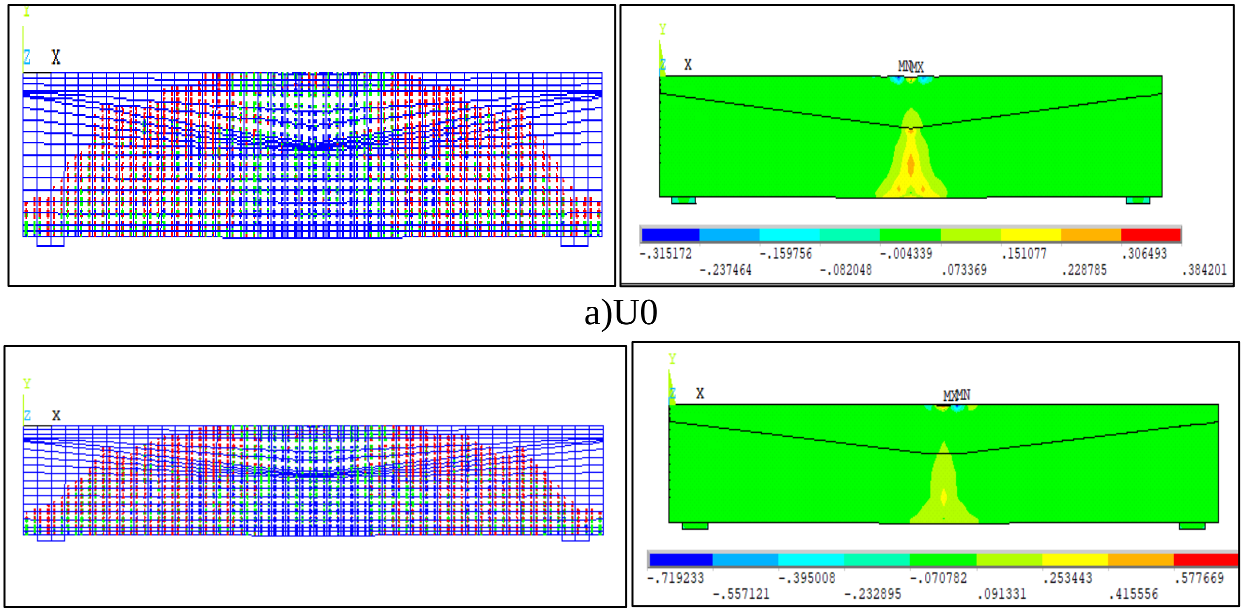

a)U0

b)U13

Figure 4-8 Failure modes(crack patterns) and total Strain distribution of FE model by effect of mid span uniform length

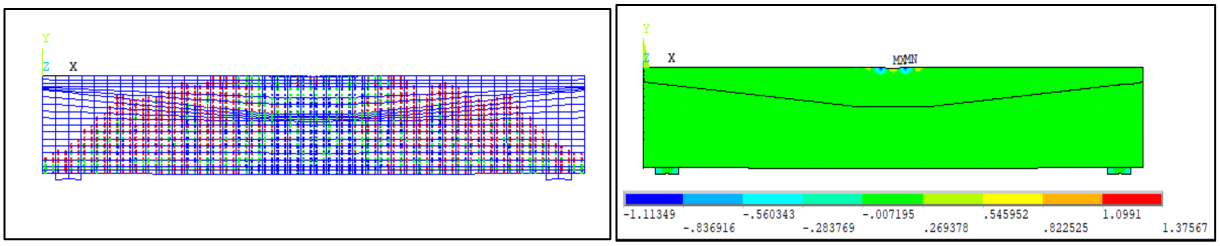

c)U26

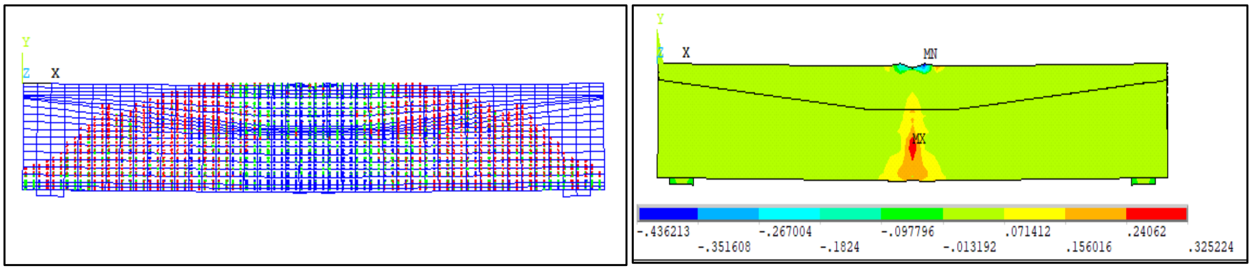

d)U36

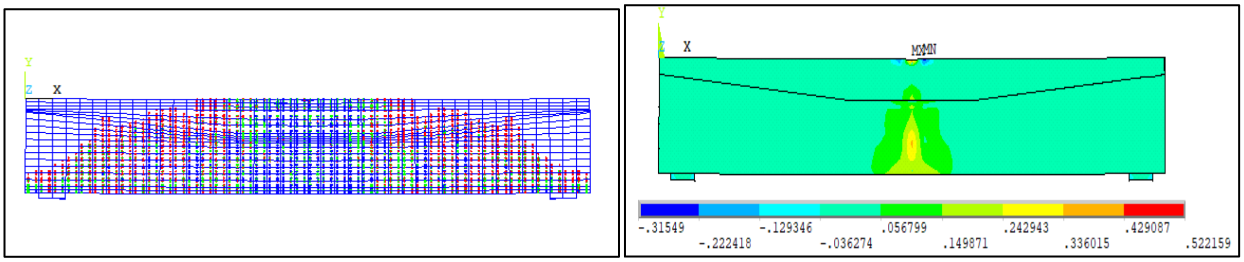

e)U52

Figure 4-8: Cont.

4.3.1.2 The Orient Variation of Tapered Flange

As shown in uniformity region investigation, the tapered effect the stress distribution and so effect the developed strength, ductility and of the structural aspect in this section, the orient variation of tapered region is investigation. Table 4-4, describe the consider specimens of varied (α). slightly variation in strength is assigned, while the significant effect is introduced in ductility and energy dissipation trend. the increasing of (α) from 3.27° to 5.44° correspond by ductility and energy dissipation improving of 5.49 and 4.83

Figure 4-9 show the adopted tapering orientation ,While Figure 4-10 clearly depicts the positive effect of orient increment on load-deflection response and so the correspond in ductility and energy dissipation. the slightly strength improving fixed by the normalized results that approximately constant function $pu = -1.9968\,\alpha^2 + 17.53\,\alpha + 111.53$.

as shown in Figure 4-11. Figure 4-12 show the variation rates of strength , ductility and energy dissipation due to orientation variation. while Figure 4-13 exhibit cracks pattern and the corresponding strain distribution.

Table 4-4 Specimens' modeling details: orientation of tapered flange

	Code	fy Mpa	f'c Mpa	ρ	L cm	d cm	h cm	bf cm	bw cm	dfe cm	dfm cm	α
1	Hf1	490	35	0.0063	210	26	30	24	18	9	15	3.27
2	Hf2	490	35	0.0063	210	26	30	24	18	7	15	4.35
3	Hf3	490	35	0.0063	210	26	30	24	18	5	15	5.44

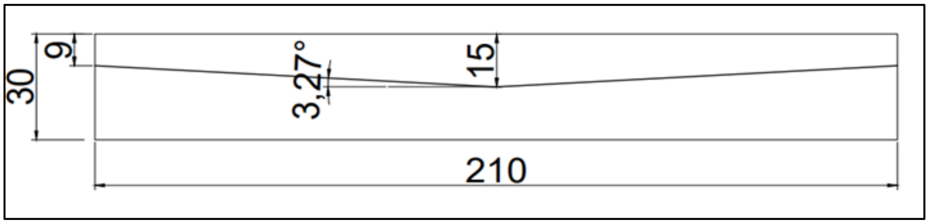

a)Hf1

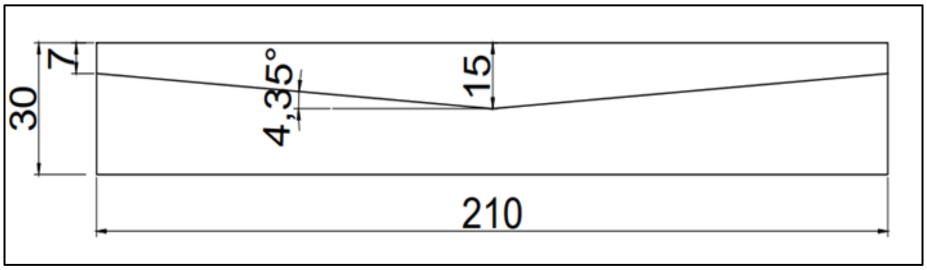

b)Hf2

Figure 4-9 The adopted tapering orientation

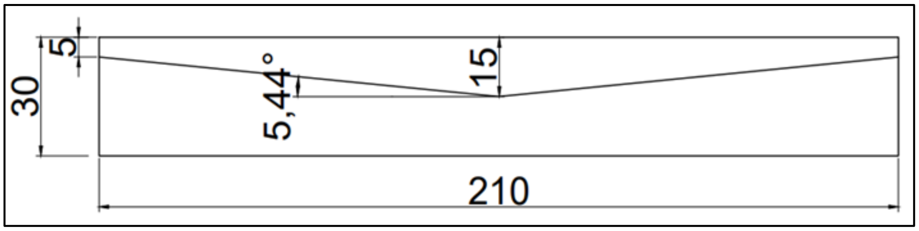

c)Hf3

Figure 4-9: Cont.

Table 4-5 Results analysis: orientation of tapered flange

No	Code	The variable parameter	Pu, kN	Pui/Pu1	Δe, mm	Δmax, mm	(Δmax)i/(Δmax)1	D.I.	(D.I)i/(D.I)1	ψ, kN.mm	ψi/ψi
1	Hf1	orientation of tapered flange	147.5	1.00	5.31	23.7	1.00	4.46	1.00	1174	1.00
2	Hf2		150	1.16	5.681	32.8	1.383	5.77	1.29	1869.0	1.59
3	Hf3		147.8	1.002	5.41	132.8	25	24.5	5.49	9037.1	4.83

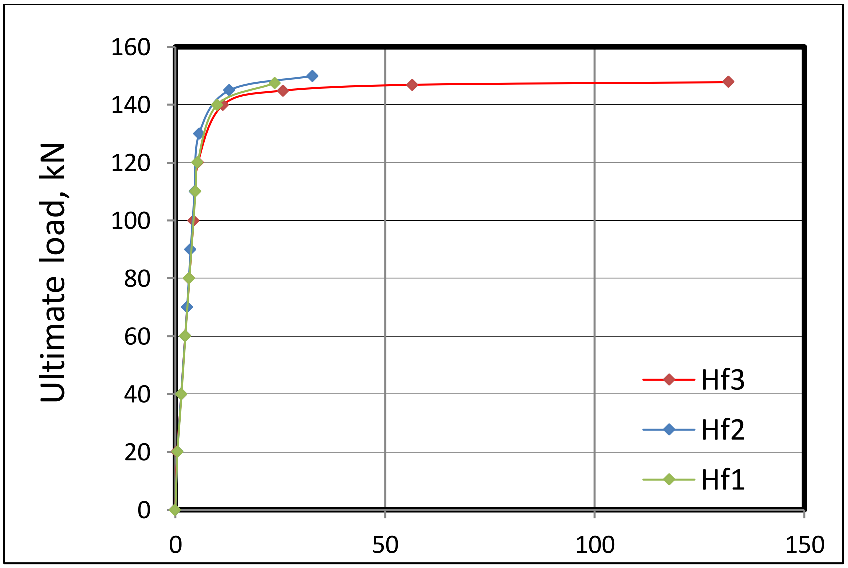

Figure 4-10 load - deflection response: Tapered flange orientation effect

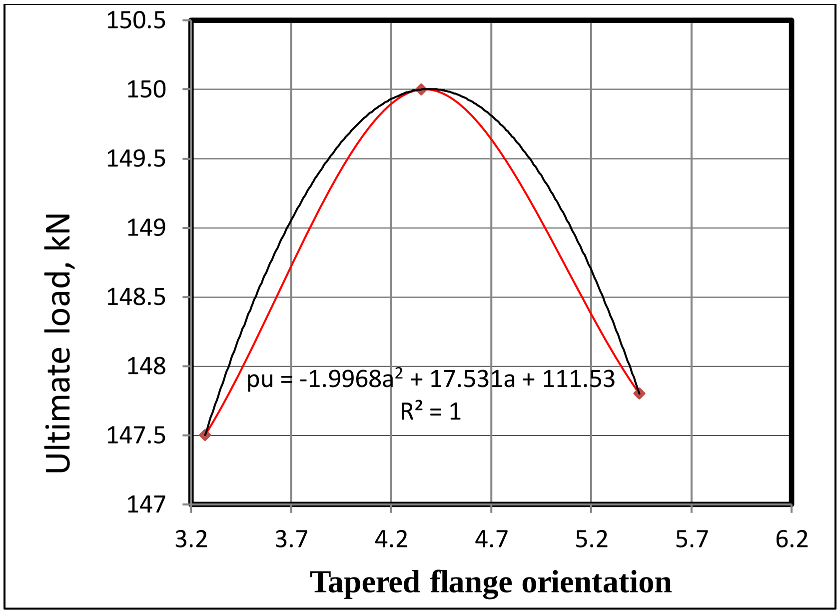

Figure 4-11 Mathematical normalization: Tapered flange orientation effect

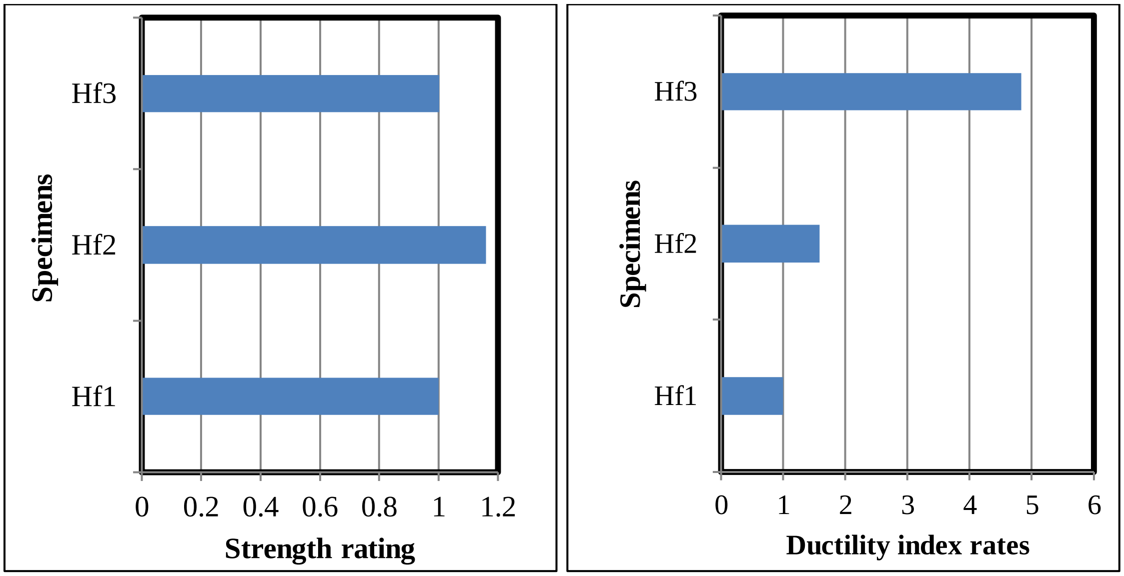

a) b)

Figure 4-12 a)Strength variation rates b) Ductility variation rates c) Energy dissipation :Tapered flange orientation effect

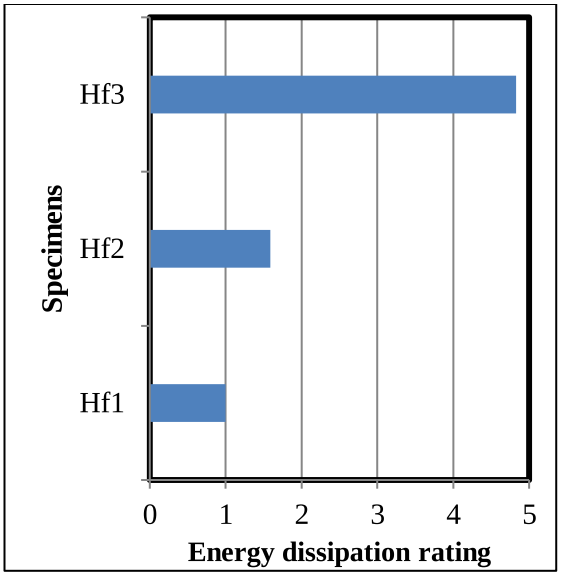

c)

Figure 4-12: Cont.

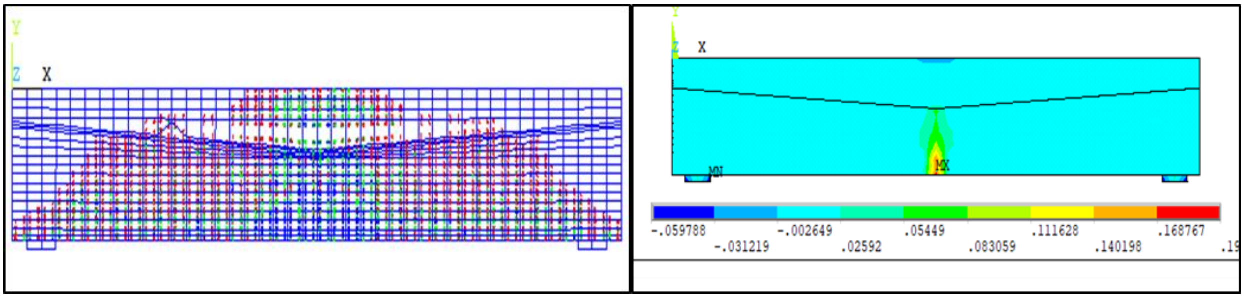

a)Hf1

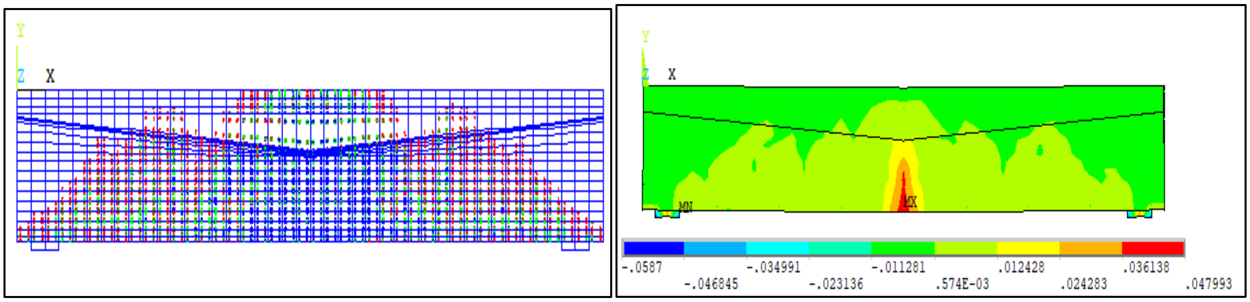

b)Hf2

Figure 4-13 Failure modes(crack patterns) and total Strain distribution of FE model by effect of varies orient angle

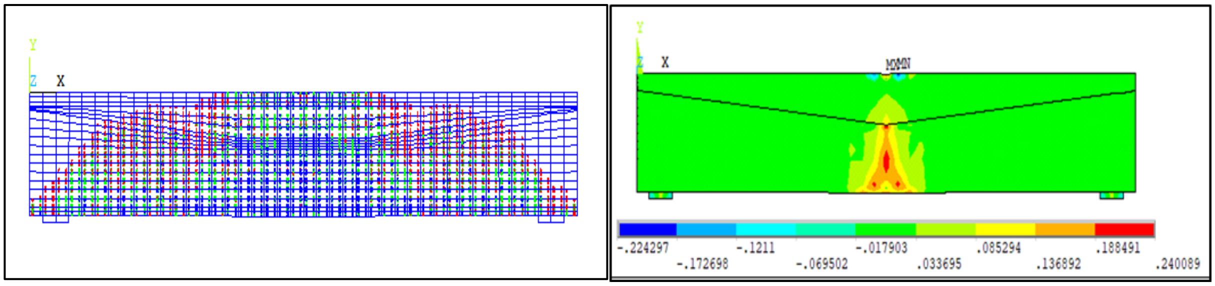

b) Hf3

Figure 4-13: Cont.

4.3.1.3 Boundary Conditions

Different boundary condition and considered to inspect their effect on strength, ductility and energy dissipation of developed tapered flange beam. Hinged, fully fixed and a partial fixed boundary condition states are geometry details of adopted specimens which are indicated in the Table 4-6, where Table 4-7 exhibits the related results. Analysis the partial state concerned with a specified state that constrained the bottom face of section web in support the region only, while the fully fixed state relate to constrain the overall cross section within support region. Figure 4-14 clearly depicts the various aspect of boundary conditions on load deflection response, the fixed state turned the behavior as brittle behavior and the presented of the traditional hinged mode maintained the ductility and energy dissipation. while the specified partial fixing mode exhibit a differed response of relatively less ductility and of a significant strength improving, of strength update rate 1.17.

Figure 4-15 show the strength, ductility, and energy dissipation rates in term of various boundary condition, while the Figure 4-16 illustrates the corresponding crack patterns and strain distribution

Table 4-6 Specimens' modeling details: boundary conditions effect

No.	Code	Description	L, cm	d, cm	h, cm	bf, cm	bw, cm	dfe, cm	dfm, cm	L,fm cm
1	Bs	T-Section of non-prismatic flange with simple support	210	26	30	24	18	5	15	26
2	Bf	T-Section of non-prismatic flange with fixed support	210	26	30	24	18	5	15	26
3	Bp	T-Section of non-prismatic flange with partial support	210	26	30	24	18	5	15	26

Table 4-7 Results analysis: boundary conditions effect

No.	Code	The variable parameter	Pu, kN	Pui/Pu1	Δe, mm	Δmax, mm	(Δmax)i/(Δmax)1	D.I.	(D.I)i/(D.I)1	ψ, kN.m	ψi/ψi
1	Bs	Boundary Conditions	151.1	1.00	5.38	78.8	1.00	14.64	1.00	5131	1.00
2	Bf		143	.0.94	0.47	1.12	0.014	2.38	0.16	16.48	0.0032
3	Bp		177	1.17	4.68	13.2	0.16	2.82	0.19	506.6	0.098

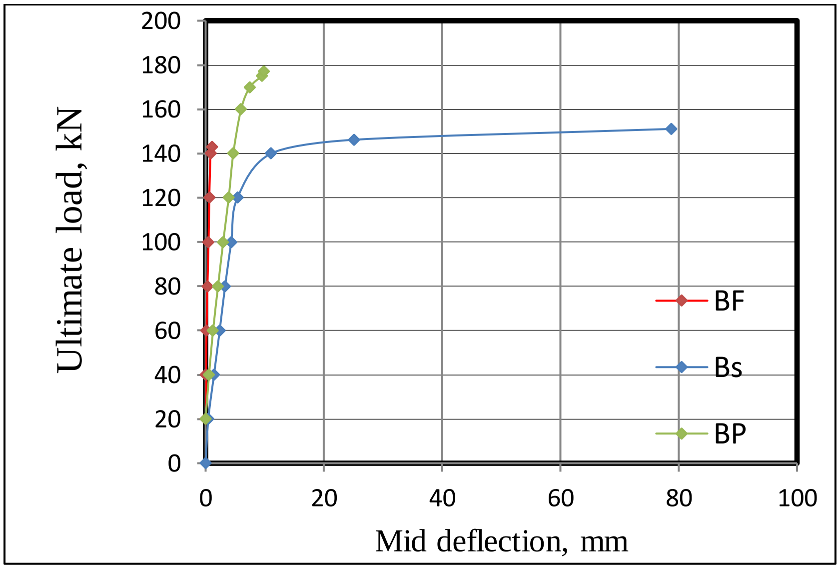

Figure 4-14 Load – deflection response: Boundary Conditions effect

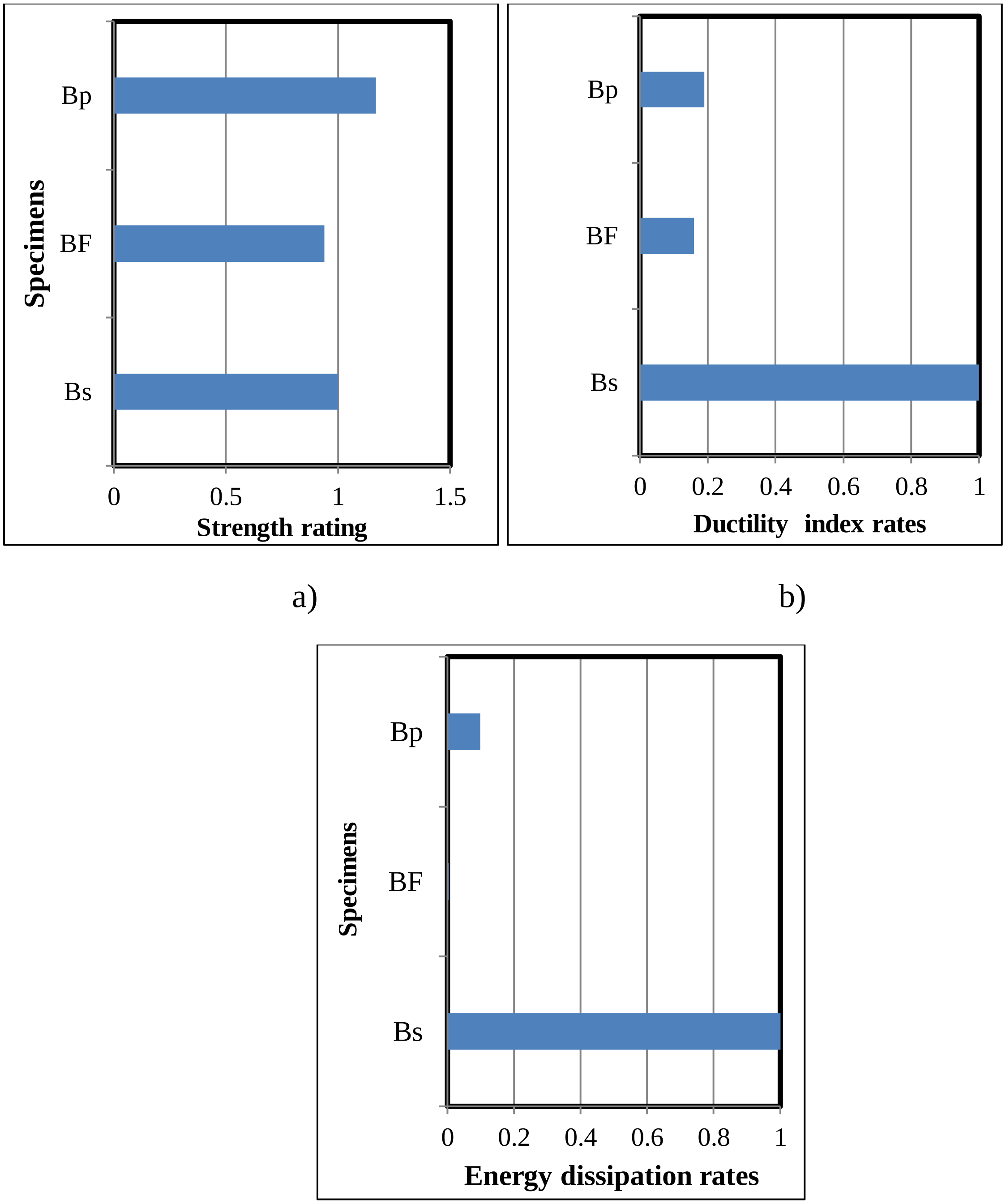

a) b)

c)

Figure 4-15 Strength variation rates Ductility variation rates Energy dissipation variation rates: Boundary Conditions effect

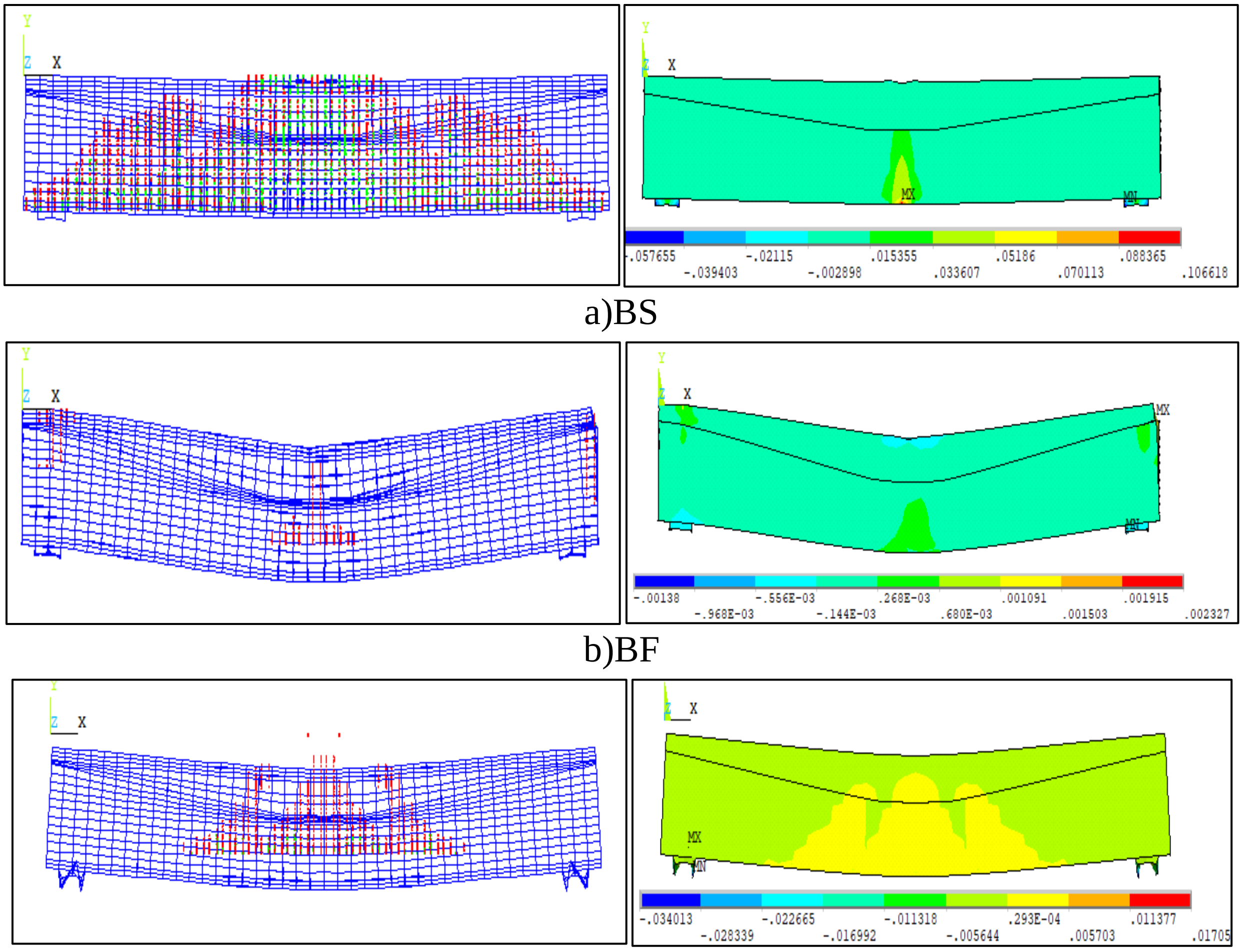

a)BS

b)BF

c)BP

Figure 4-16 Failure modes (crack patterns) and total Strain distribution of FE model by effect boundary condition

4.3.1.4 Concrete Compressive Strength

The effect of concrete compressive strength in various specimens is investigated. The related specimens' modeling details are shown in Table 4-8. Table 4-9. exhibits the related numerical results analysis which depict that, the ultimate strength get improving with concrete compressive strength increasing, the strength improved from 133 kN to 160 kN with improving rate 1.2, as concrete compressive strength changed from 25 to 45 MPa. Besides, the results depict that the optimum flexural ductility of improving rate (6.22) and the optimum energy dissipation of enhancement rate 7.18 are assigned in section of moderated concrete compressive strength of 35 MPa. The effect of provided concrete strength variation could be clearly monitored by the introduced load deflection curves that shown in Figure 4-17 while the related variation of ultimate strength, ductility indices and energy enhancement rate are shown in Figure 4-19. the results indicated that there are optimum enhancement upgrading in ductility and corresponding toughness in specific compressive concrete strength (35 MPa), beyond this value and within equilibrium and compatibility conditions that relate to section reliability within ACI [20] ductility requirement; slightly decreased in ductility is assigned without any sever influence on the overall section structural behavior while the ultimate strength gets improving. Figure 4-20 shows the observed failure modes in scope

of crack patterns and total Strain distribution. The obtained results are normalized in a nonlinear relationship of second degree,

Pu =0.0365 f'c2-1.23 f'c +141.44 as shown in Figure 4-18.

Figure 4-23 clearly depicts the normalizing results of ultimate strength that relate to steel reinforcement yielding strength

Table 4-8 Specimens' modeling details: Concrete Compressive Strength

	Code	Fy Mpa	f'c Mpa	ρ	L cm	d cm	h cm	bf cm	bw cm	dfe cm	dfm cm
1	Bc1	490	25	0.0063	210	26	30	24	18	5	15
2	Bc2	490	35	0.0063	210	26	30	24	18	5	15
3	Bc3	490	45	0.0063	210	26	30	24	18	5	15

Table 4-9 Results analysis: Concrete Compressive Strength

No.	Code	The variable parameter	Pu, kN	Pui/Pu1	Δe, mm	Δmax, mm	(Δmax)i/(Δmax)1	D.I.	(D.I)i/(D.I)1	ψ, kN.mm	ψi/ψi
1	Bc1	Concrete Compressive Strength	133.5	1.00	8.01	19.6	1.00	2.446	1.00	828.2	1.00
2	Bc2		143.1	1.07	6.11	92.8	4.73	15.19	6.21	5943.2	7.18
3	Bc3		160	1.20	6.17	78.14	3.98	12.66	5.18	4843.9	5.85

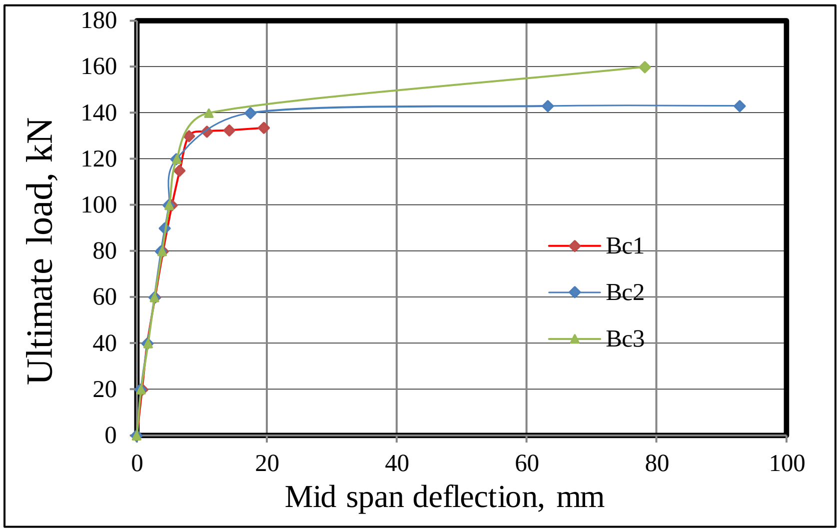

Figure 4-17 load – deflection response : Concrete Compressive Strength effect

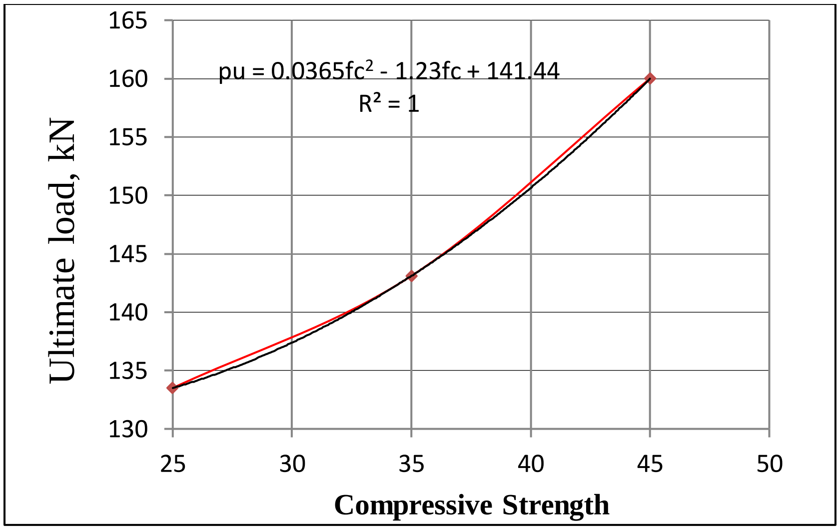

Figure 4-18 Mathematical normalization of obtained results: Concrete Compressive Strength effect

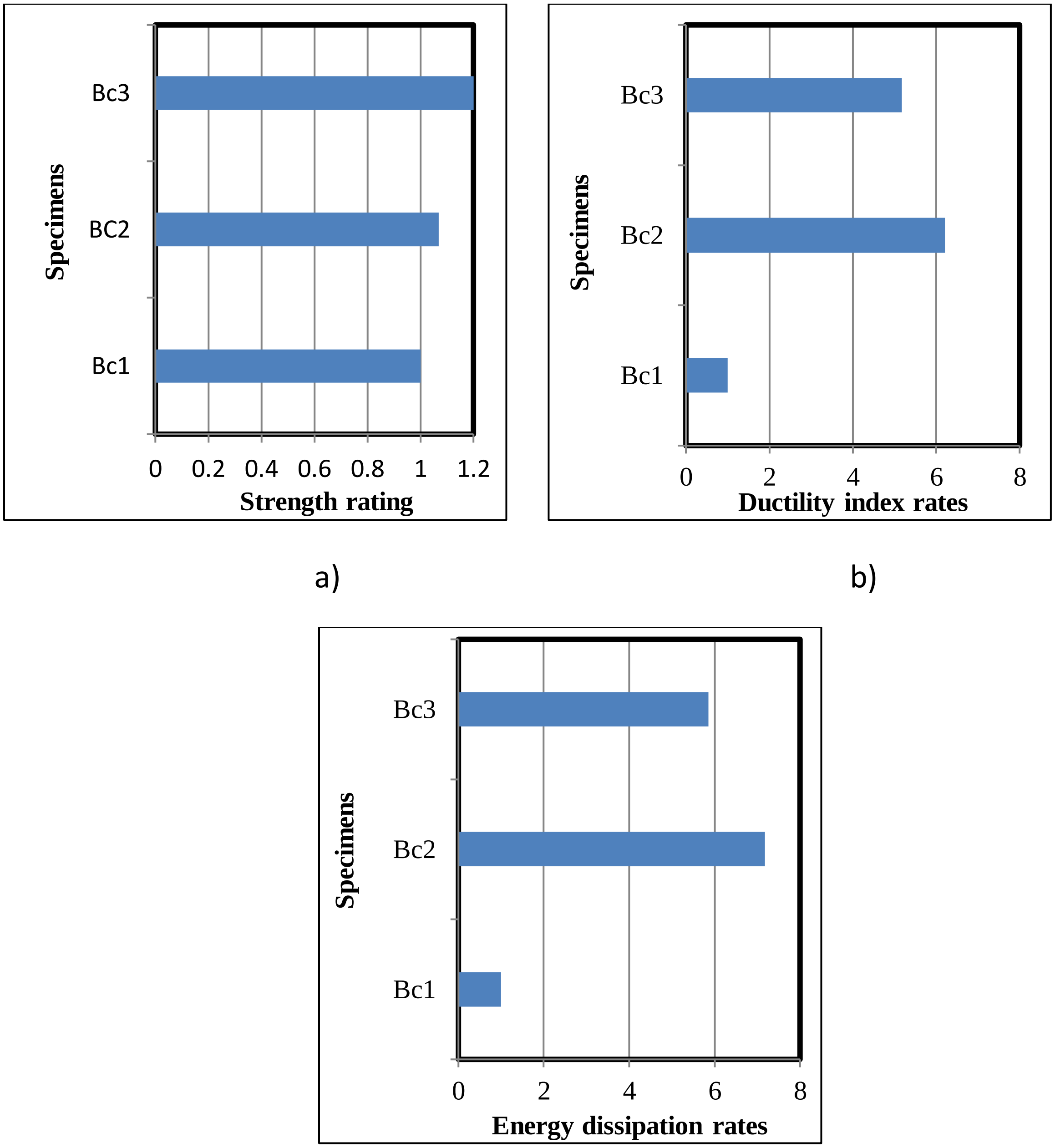

a) b)

c)

Figure 4-19 a)Strength variation rates b) Ductility variation rates c) Energy dissipation variation rates : Concrete Compressive Strength effect

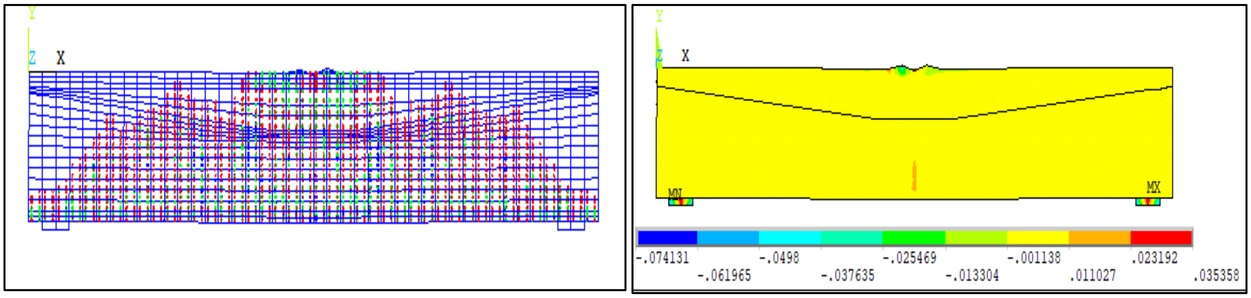

a)BC1

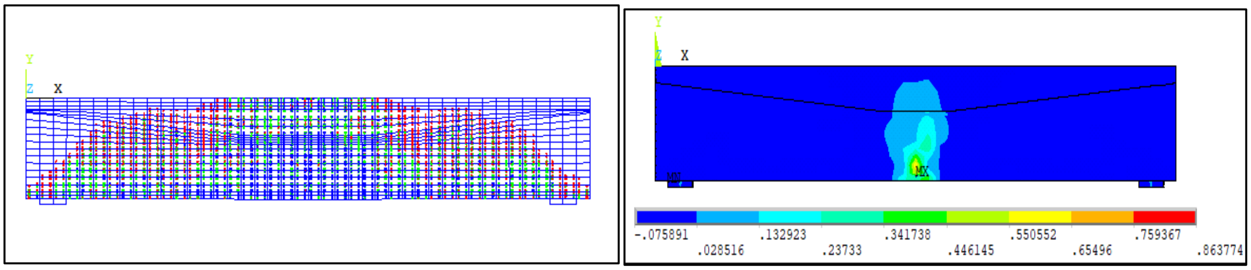

b)BC2

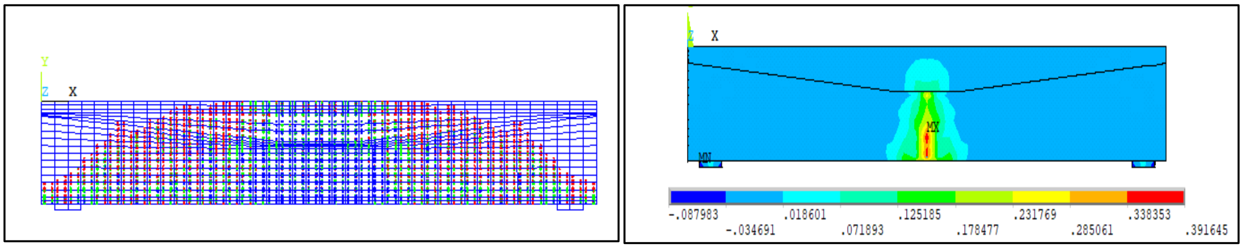

c)BC3

Figure 4-20 Failure modes(crack patterns) and total Strain distribution: Concrete Compressive Strength effect

4.3.2.2 Steel Reinforcement Strength

The effect of steel strength of the provided reinforcement in various specimens of constant area, within and out of ACI [20] ductility limits is investigated. The related specimens' modeling details are shown in Table 4-10. Table 4-11. exhibits the related numerical results analysis which depict that, the ultimate strength get improving with steel strength increasing and the over increment turn the section to be over reinforcement section. Besides, the results depicts that the best flexural ductility (D.I.=23.3) compatible with the humble steel strength (*fy* =325 MPa) and the optimum energy dissipation (7410 kN.mm) are assigned in section of moderated provided steel strength (*fy* =490 MPa). The independence of the flexural stiffness regarding provided steel strength variation could be clearly monitored by the introduced load deflection curves that are shown in Figure 4-21. While the variation of related ultimate strength , ductility indices and energy enhancement rate are shown in Figure 4-23. The results depict that with increasing of yield strength, the ductility and the corresponding toughness decreased in the linear approach, The extreme yield strength value leads to significant sever dropping and could be used as limit state in design while the best results are assigned in specific yield strength (490 MPa). Figure 4-24 shows the observed failure modes in scope of crack patterns and strain distribution.

The obtained results are normalized in a nonlinear relationship of second degree, Pu =7E-05 fy2+0.1337fy +63.668 as shown in Figure 4-22 .

Figure 4-30 clearly illustrates the normalizing results of ultimate strength that relate to steel reinforcement yielding strength.

Table 4-10 Specimens' modeling details of Steel reinforcement strength

No	Code	fy Mpa	f'c Mpa	ρ	L cm	d cm	h cm	bf cm	bw cm	dfe cm	dfm cm
1	BS1	325	35	0.0063	210	26	30	24	10	5	15
2	BS2	490	35	0.0063	210	26	30	24	10	5	15
3	BS3	610	35	0.0063	210	26	30	24	10	5	15

Table 4-11 Results analysis of Steel reinforcement strength

No.	Code	The variable parameter	Pu, kN	Pui/Pu1	Δe, mm	Δmax, mm	(Δmax)i/(Δmax)1	D.I.	(D.I)i/(D.I)1	ψ, kN.mm	ψi/ψi
1	B_{S1}	Steel yield strength	115	1.00	4.8	112	1.00	23.3	1.00	5096.15	1.00
2	B_{S2}		147.1	1.27	8.1	112.5	1.004	13.88	0.59	7410.23	1.45
3	B_{S3}		173	1.50	8.7	10.2	0.09	1.17	0.05	872.9	0.171

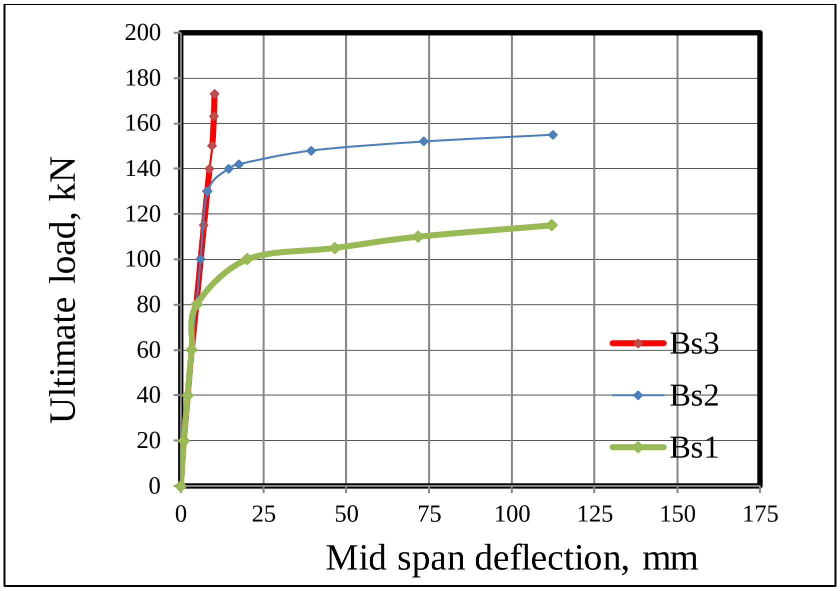

Figure 4-21 load – deflection response : Steel reinforcement strength effect

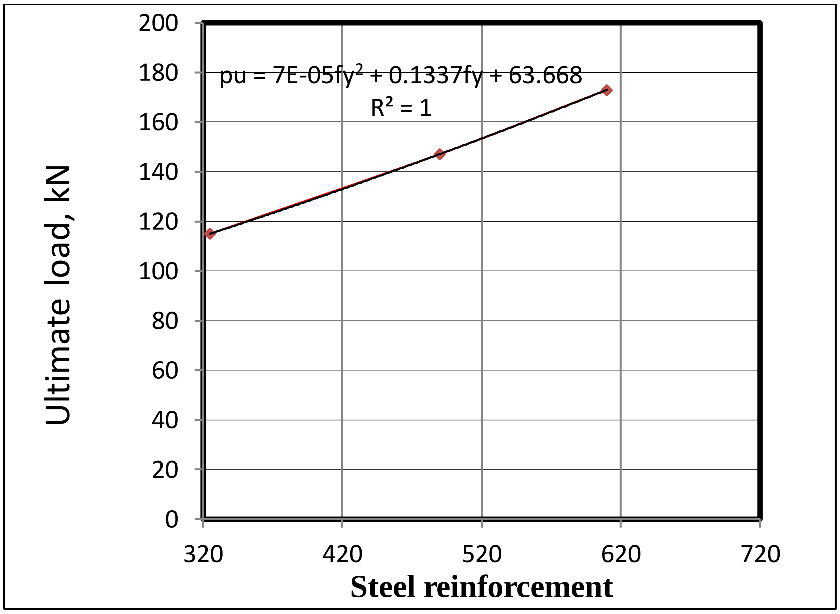

Figure 4-22 Mathematical normalization of obtained results: Steel reinforcement strength effect

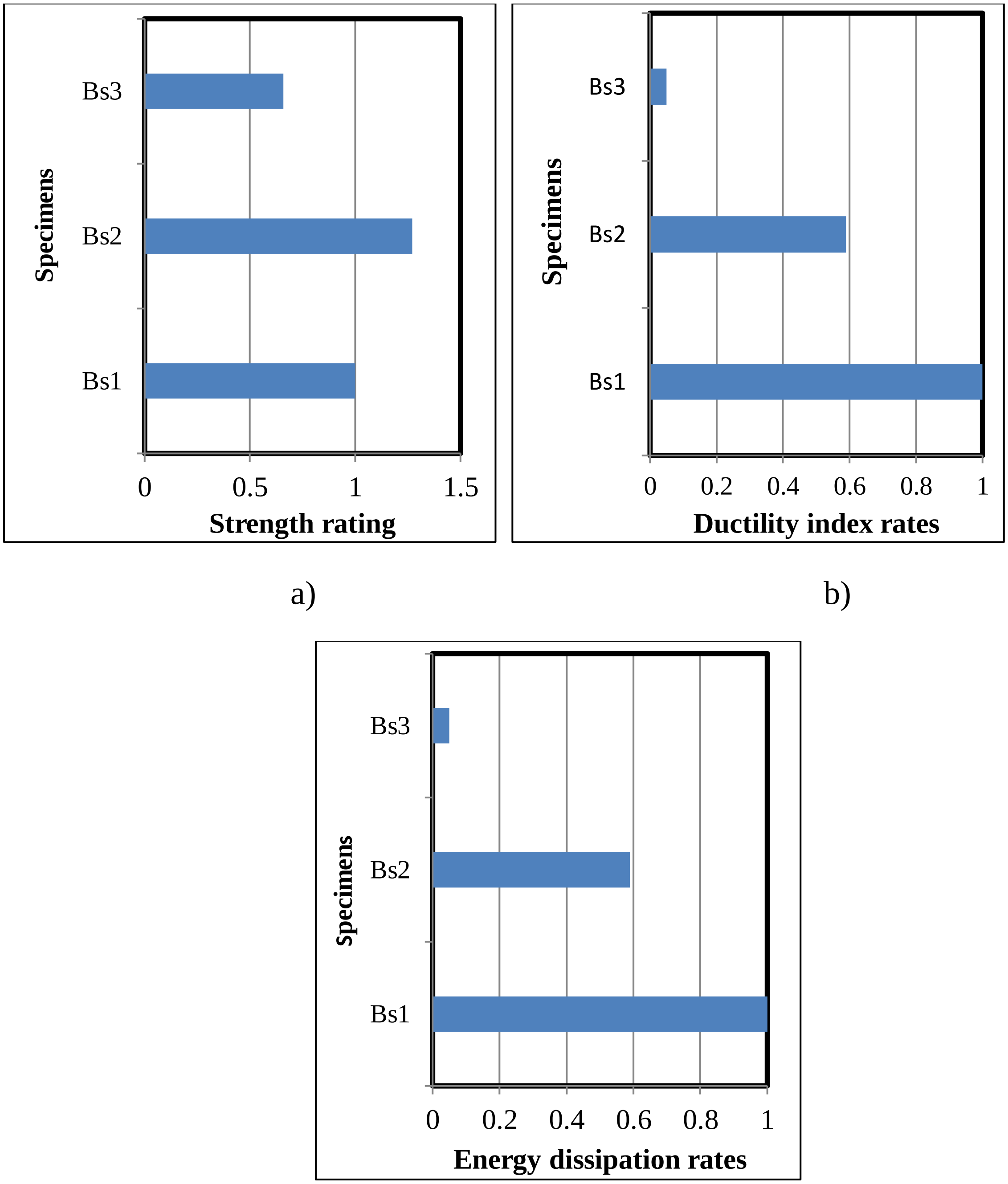

a) b)

c)

Figure 4-23 a)Strength variation rates b) Ductility variation rates c) Energy dissipation variation rates :Steel reinforcement strength effect

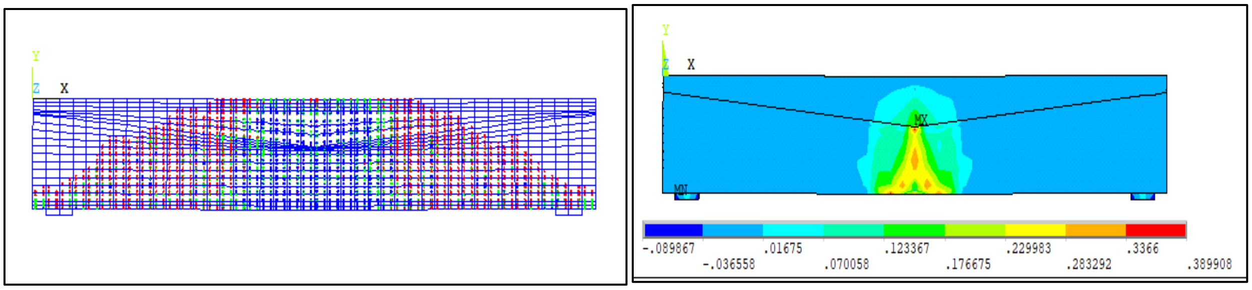

a)BS1

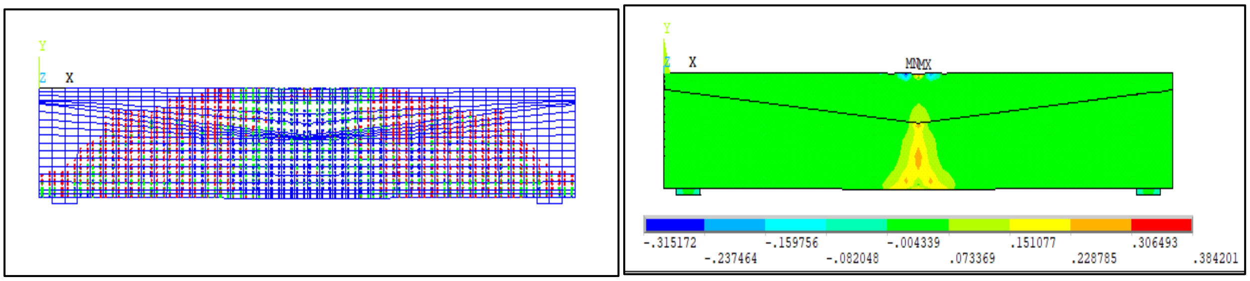

b)BS2

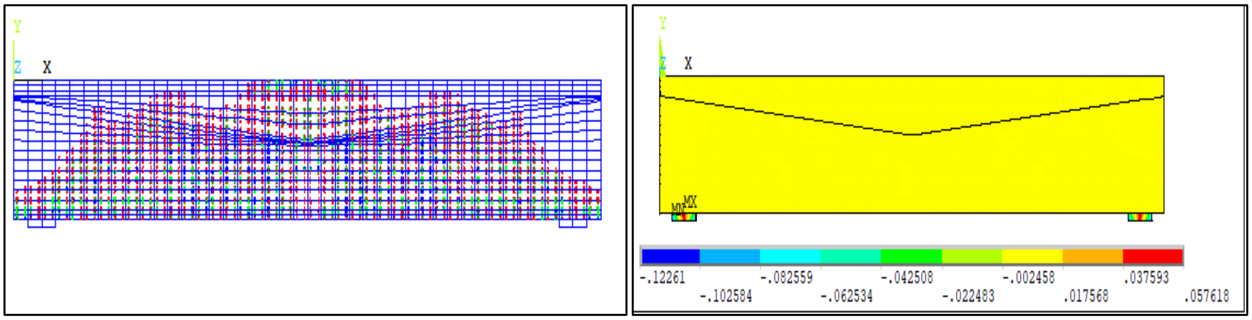

c)BS3

Figure 4-24 Failure modes(crack patterns) and total Strain distribution : Steel yield strength effect

4.3.2.3Provided Reinforcement Steel Ratio, ρ

The effect of steel ratio within ACI [20] ductility limits, on section flexural response is considered and attainted in specimens (Bw1, Bw2) while the comparative analysis of them with section of over reinforcement (B_{ove}) also presented. The related specimens' modeling details are shown in Table 4.12. The numerical results are summarized in Table 4-13, the section strength is improved from 147.1 kN to 215kN with improving rate of 1.46 as steel ratio change from ρ=0.0063 to ρ= 0.0091 which are within ductility limit, the over reinforcement section (ρ= 0.039), turns the section to be over reinforcement with brittle failure mode. Also, the results depict that the increasing of reinforcement out of ACI [20] ductility limit, negatively affected flexural ductility and energy dissipation. These observation could be clearly monitored by the introduced load deflection curves that shown in Figure 4-25, While the related ultimate strength, ductility indices and energy enhancement rates are shown in Figure 4-27. the results depicts that the increasing of reinforcement steel ratio companied with nonlinear sever dropping trend in ductility and its corresponding toughness values and should be assigned carefully in the design purpose. The inspection of over reinforcement section (B_{ove}), exhibits unacceptable response before failure limits likewise that knows in the customary reinforcement concrete sections. Figure 4-28 shows the observed failure modes in scope of crack patterns total Strain distribution.

The obtained results are normalized in a nonlinear relationship of second degree Pu =-61.42p2+252.1p -43.52 .

Figure 4-26 clearly illustrates the normalizing results of ultimate strength that relate of steel ratios.

Table 4-12 Specimens' modeling details: provided material properties

No.	Code	fy Mpa	f'c Mpa	ρ	L cm	d cm	h cm	b_f cm	b_w cm	d_{fe} cm	d_{fm} cm
1	BW1	490	35	0.0063	210	26	30	24	10	5	15
2	BW2	490	35	0.0091	210	26	30	24	10	5	15
3	Bove	490	35	0.039	210	26	30	24	10	5	15

Table 4-13 Results analysis: provided material properties

No.	Code	The variable parameter	Pu, kN	Pui/Pu1	Δe, mm	Δmax, mm	(Δmax)i/(Δmax)1	D.I.	(D.I)i/(D.I)1	ψ, kN.mm	ψi/ψi
1	BW1	Ductility limits in scope of provided steel ratio	147.1	1.00	8.1	112.5	1.00	13.88	1.00	7410.23	1.00
2	BW2		215	1.46	10	32	0.28	3.2	0.23	2164.32	0.29
4	Bove		160	1.08	7.4	7.8	0.069	1.05	0.07	572.84	0.077

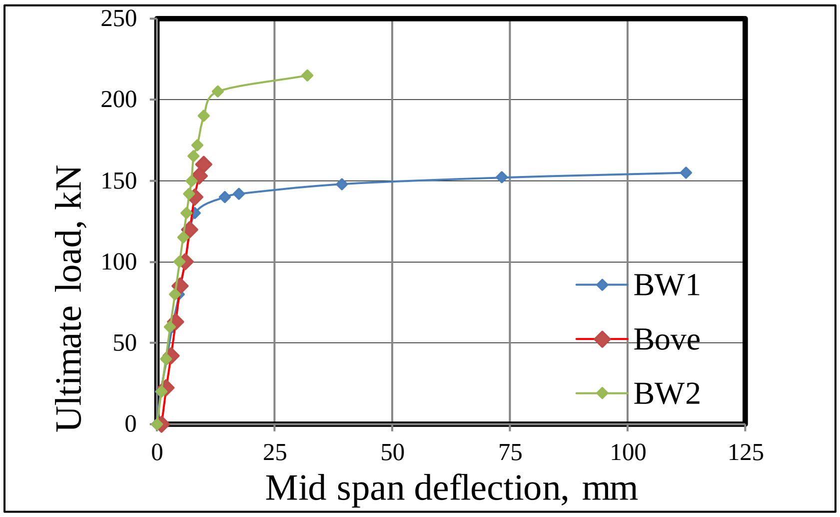

Figure 4-25 load – deflection response : Provided Reinforcement Steel Ratio(ρ)

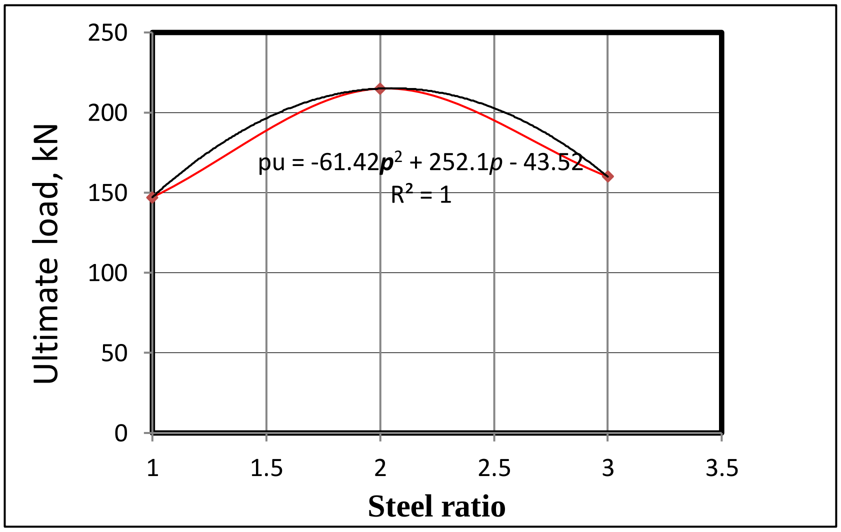

Figure 4-26 Mathematical normalization of steel ratio effect

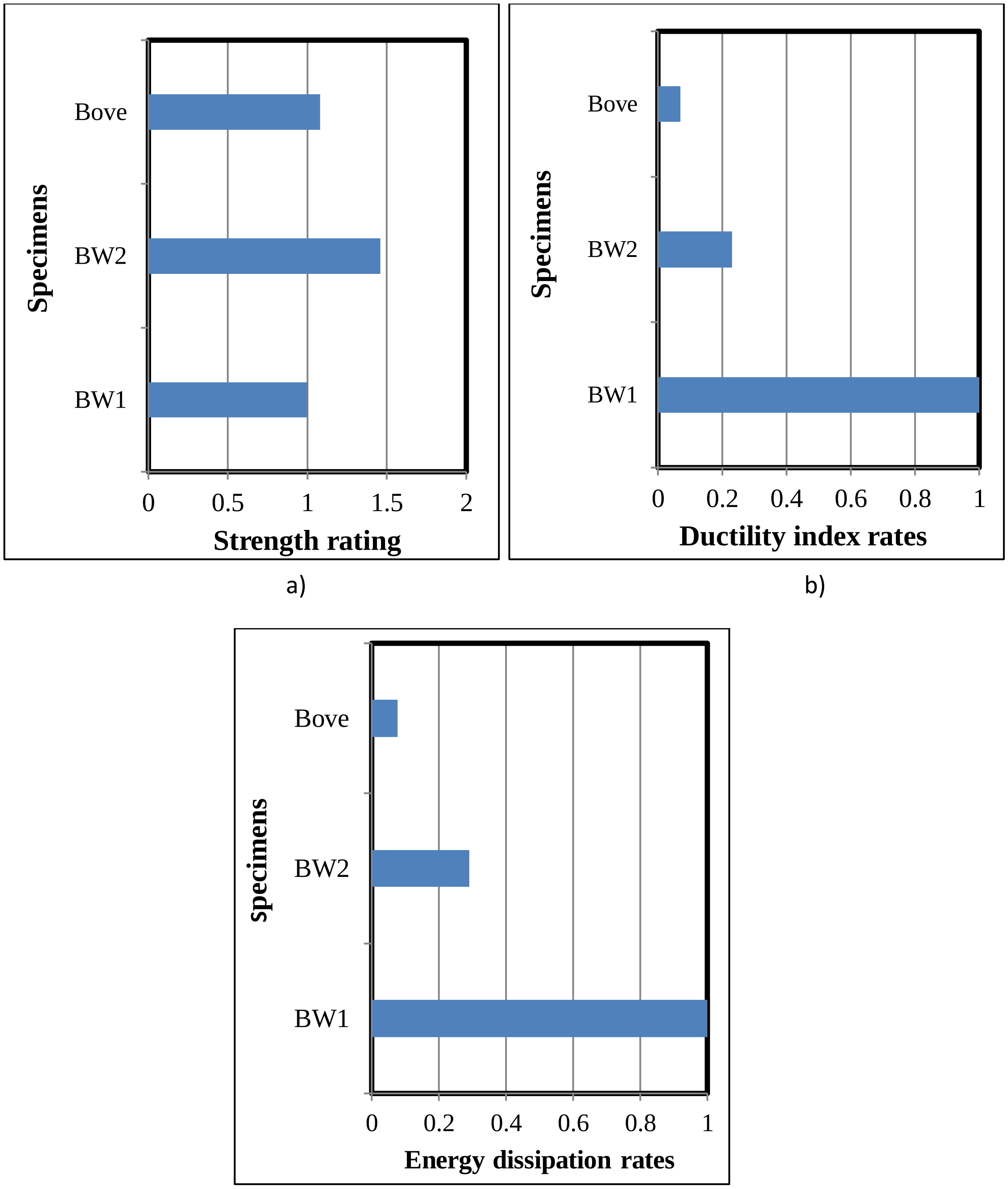

a)

b)

c)

Figure 4-27 a)Strength variation rates b) Ductility variation rates c)Energy dissipation : Provided Reinforcement Steel Ratio(ρ) effect

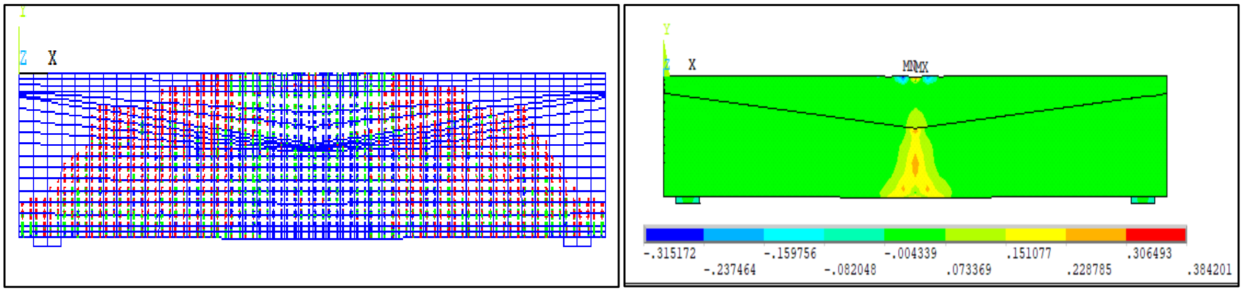

a)BW1

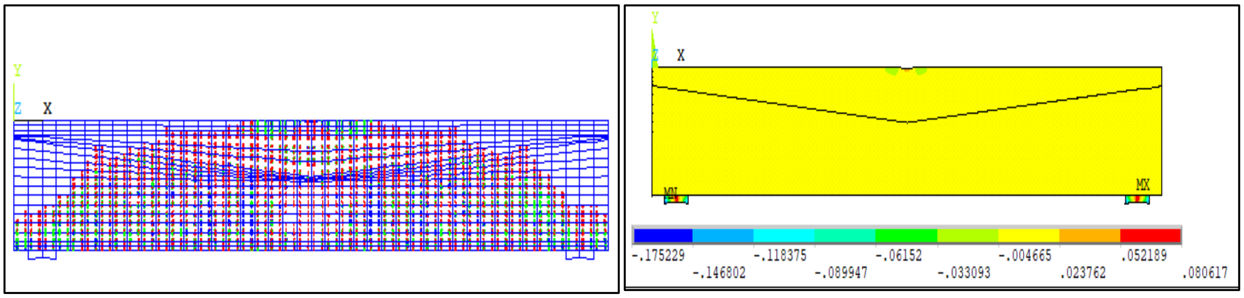

b)BW2

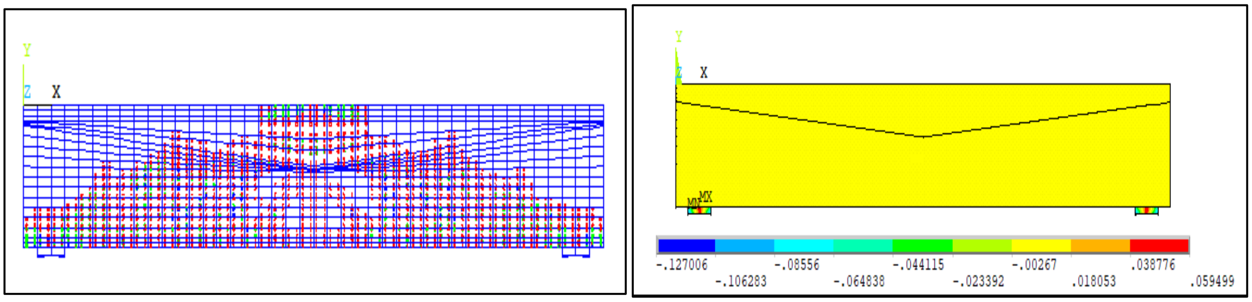

C) Bove

Figure 4-28 Failure modes(crack patterns) and total Strain distribution :Provided Reinforcement Steel Ratio(ρ)

4.4 Serviceability investigation

The tapered flange mode compatible with varying of section moment of inertia along the beam. Hence, the serviceability limit in scope of deflection could be effected. full scale specimens are introduced to check acceptance of getting deformation to be with ACI [20] limitations. Besides, a comparative analysis is achieve by considering T-section specimens of uniform flange. Table 4-14 lists the geometrical details of adopted specimens sets of uniformed tapered flanges while Table 4-15 depicts the related results analysis. Figure 4-29 illustrates the load-deflection response of tapered flange specimens for various length, the obtained deflection that correspond to service load which is considered as 2/3 p_u, are approximately the same while the max deflection that corresponding to ultimate load have got slightly variation are compared with ACI limit, By comparing all specimens with ACI limits, it was found that allowable value of deflection are greater than the actual deflection except for the specimens (T3,N3) whose the length span is 910 cm where the elastic deflection exceeded the deflection limits.

The obtained results are normalized in relationships of second degree

pu= 0.0002l2 -0.3067l+176 for uniform section

Pu= 0.0002l2 -0.3067l+186 for tapered section

Figure 4-30 exhibits the normalizing. Figure 4-31 depict strength, ductility and energy dissipation respectively while Figure 4-32 , illustrates the related crack patterns and strain distribution.

Table 4-14 Specimens' modeling details: length span

No.	Code	fy Mpa	f'c Mpa	ρ	L cm	d cm	h cm	bf cm	bw cm	dfe cm	dfm cm
1	T1	490	35	0.0063	310	26	30	24	10	5	5
2	T2	490	35	0.0063	610	26	30	24	10	5	5
3	T3	490	35	0.0063	910	26	30	24	10	5	5
4	N1	490	35	0.0063	310	26	30	24	10	5	15
5	N2	490	35	0.0063	610	26	30	24	10	5	15
6	N3	490	35	0.0063	910	26	30	24	10	5	15

Table 4-15 Results analysis: length span

No.	Code	The variable parameter	Pu, kN	Pui/Pu1	Δe, mm	Δmax, mm	(Δmax)i/(Δmax)1	D.I.	(D.I)i/(D.I)1	ψ, kN.mm	ψi/ψi	ACI limit L/250
1	T1	length span of beam	99	1	11	51	1	4.63	1	1917.9	1.00	12.4
2	T2		52	0.525	23	280	5.49	12.17	2.61	5448.2	2.84	24.4
3	T3		35	0.53	46	132	2.58	2.86	0.61	1081.8	0.56	36.4
4	N1		104	1	8.41	107.5	1	12.7	1	4496	1.00	12.4
5	N2		54	0.519	23	300	2.79	13	1.03	6214.2	1.38	24.4
6	N3		36	0.346	51.5	220	2.05	4.27	0.336	2346.5	0.521	36.4

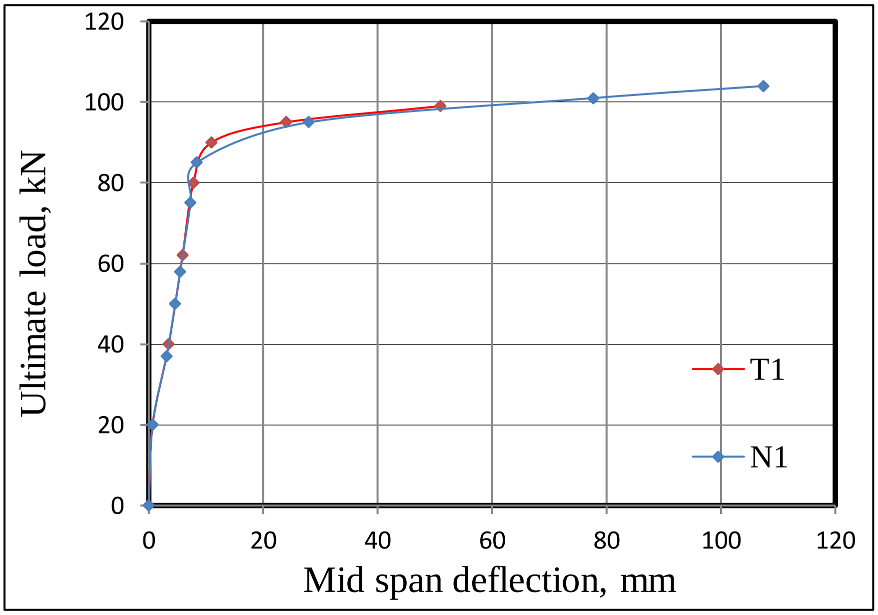

Figure 4-29 load – deflection response : Serviceability investigation

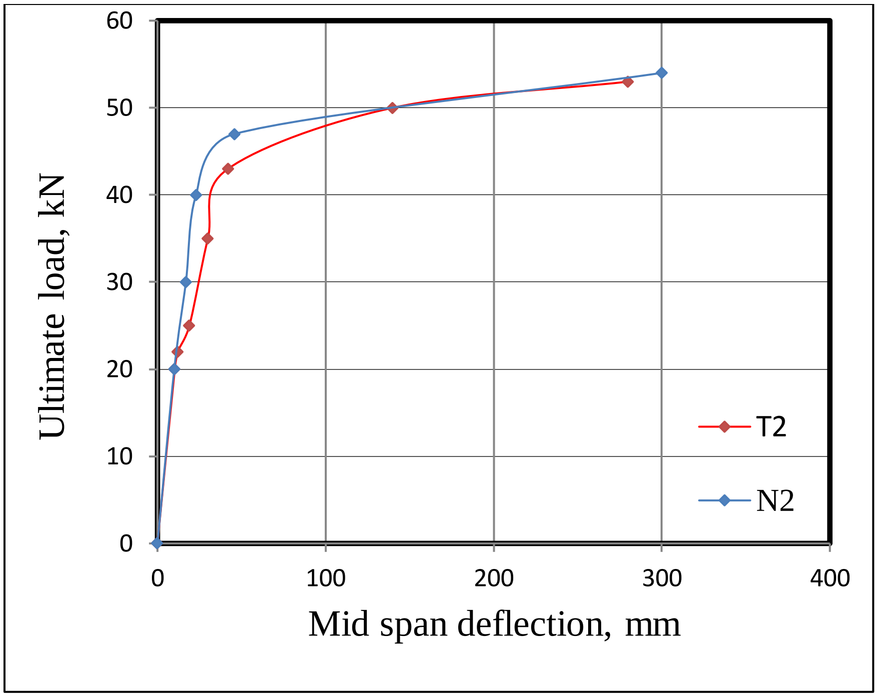

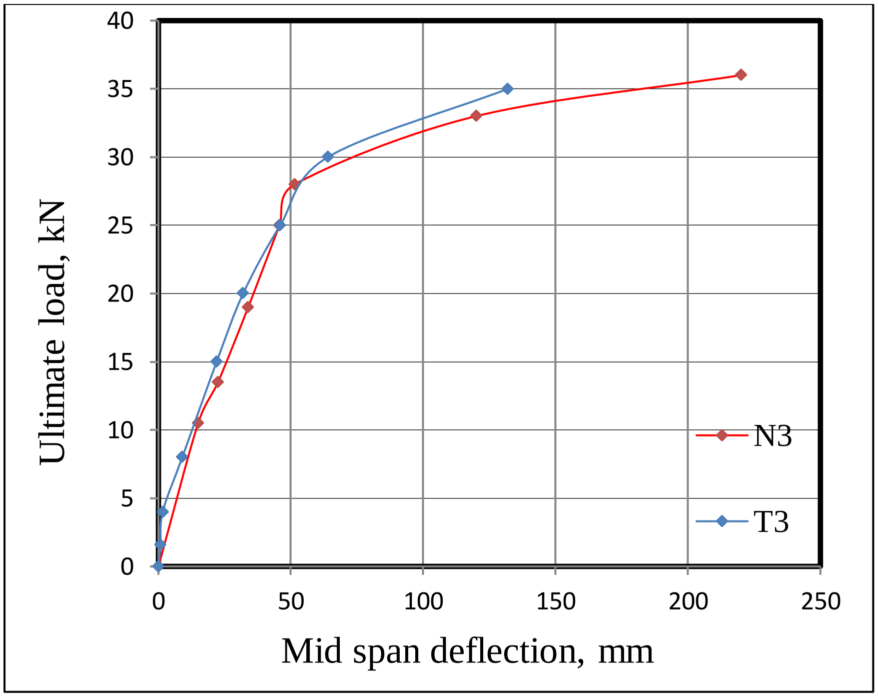

Figure 4-29: Cont.

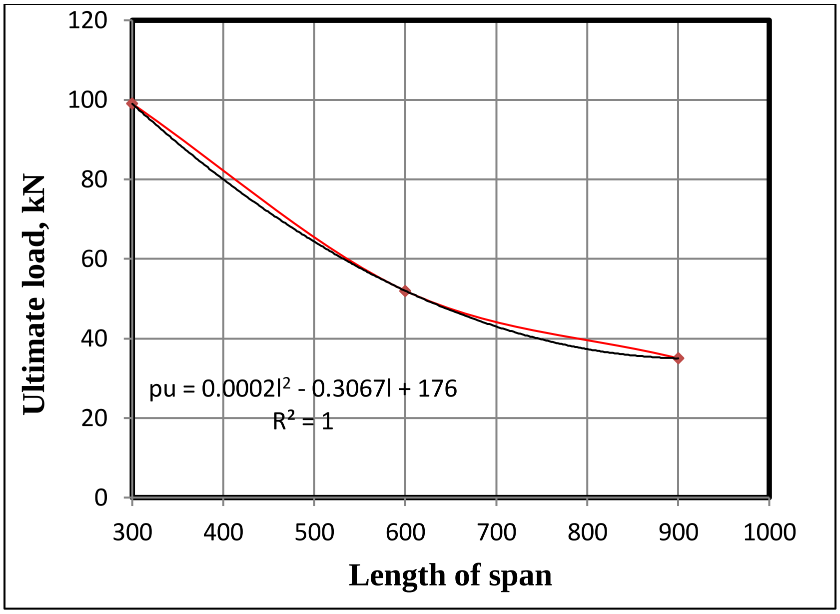

a) Uniform flange section

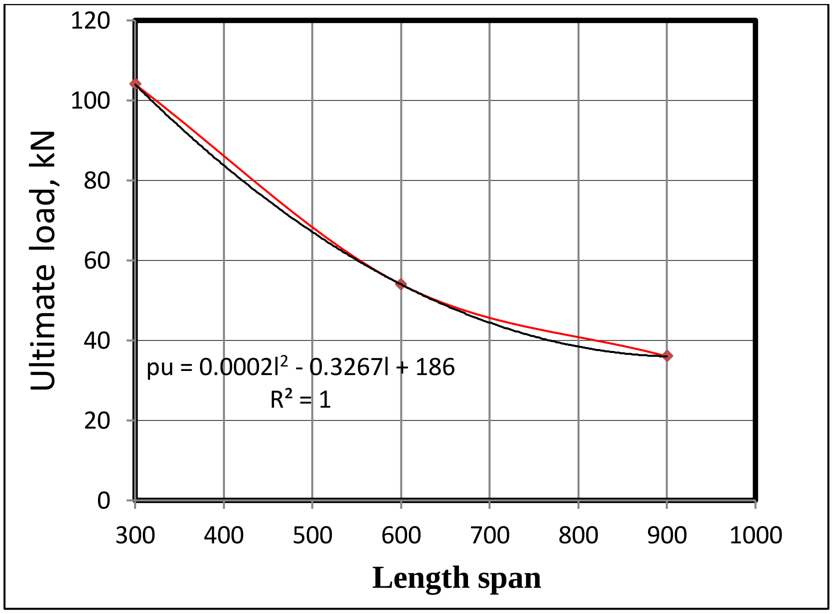

(b) Tapered flange section

Figure 4-30 Mathematical normalization: Serviceability investigation

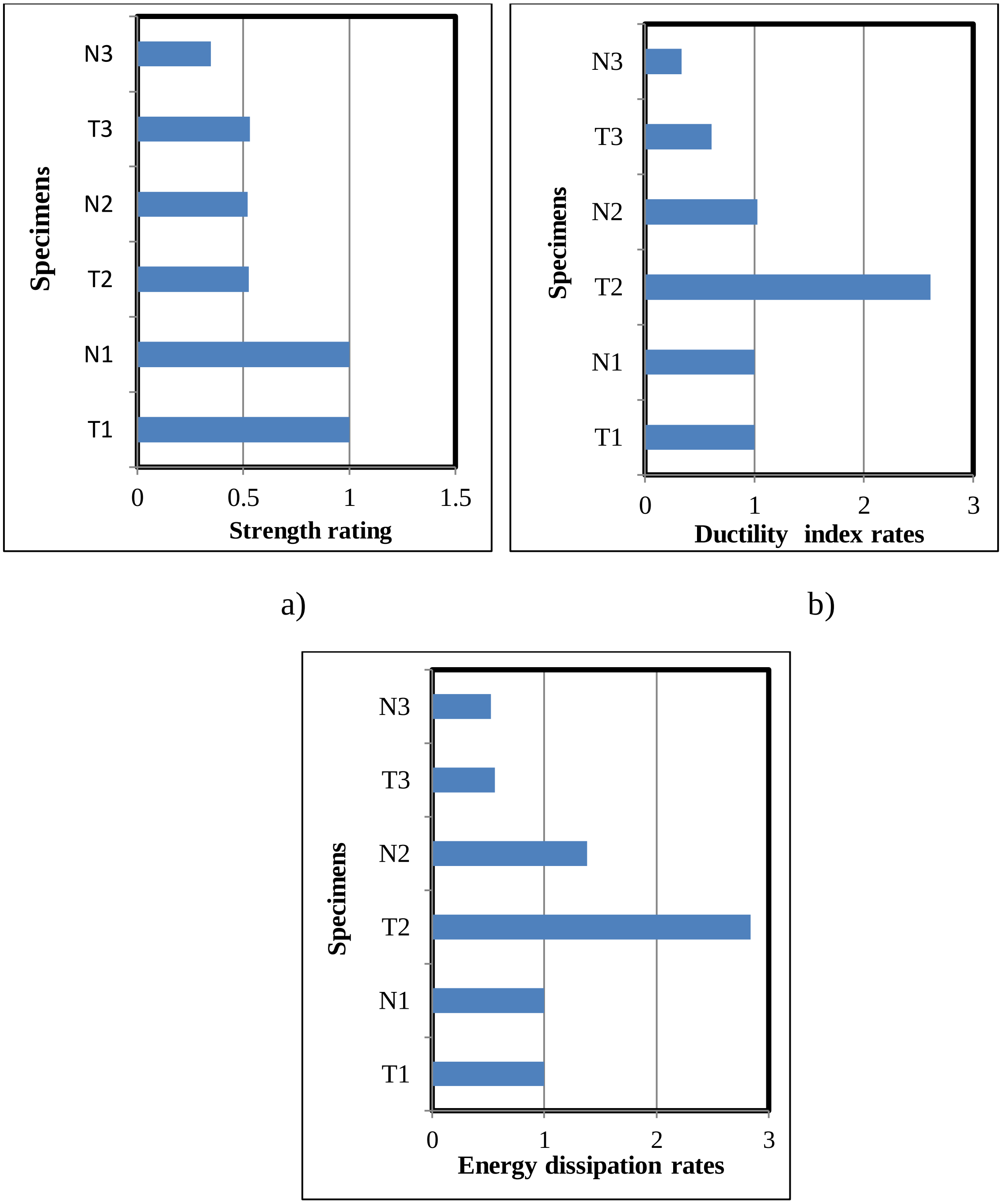

a)

b)

c)

Figure 4-31 a)Strength variation rates b) Ductility variation rates c) Energy dissipation variation rates: Serviceability investigation

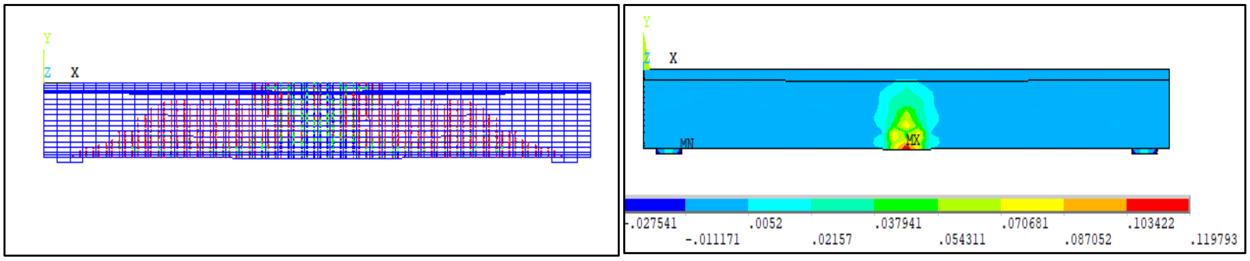

a)T1

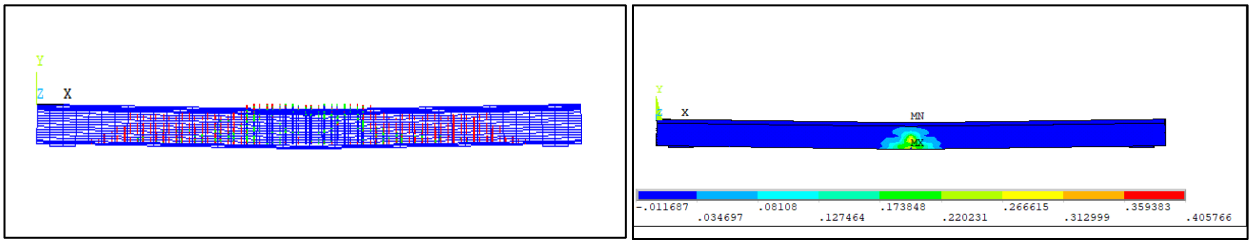

b)T2

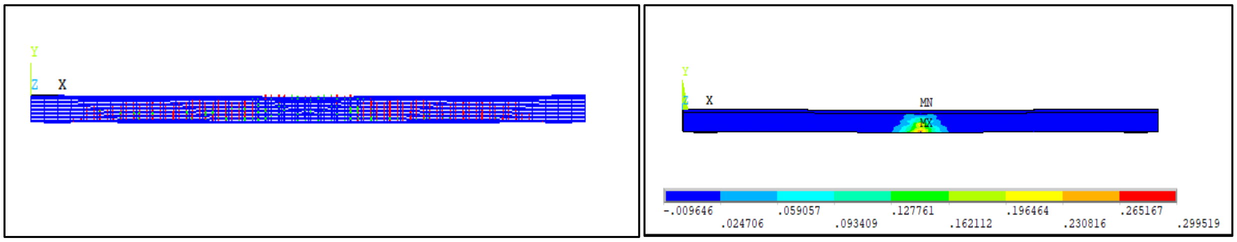

C)T3

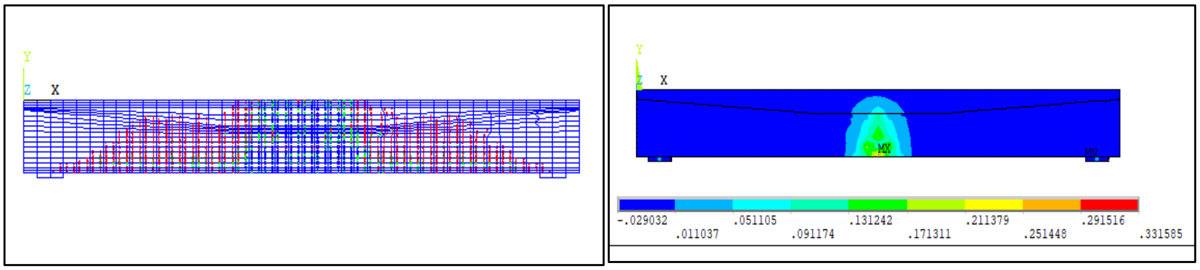

d)N1

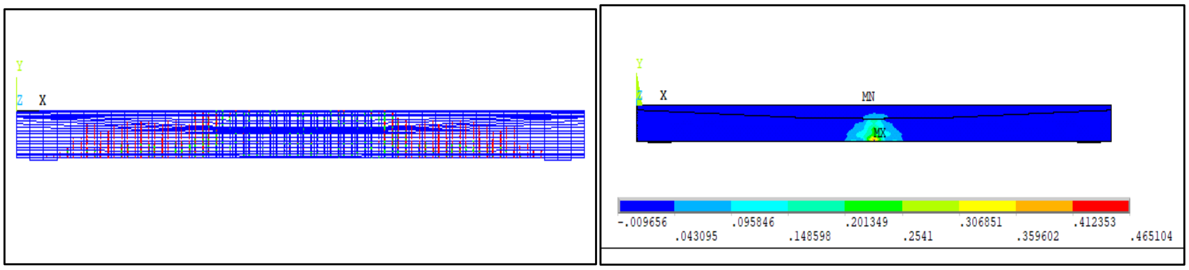

e) N2

Figure 4-32 Failure modes(crack patterns) and total Strain distribution : Serviceability investigation

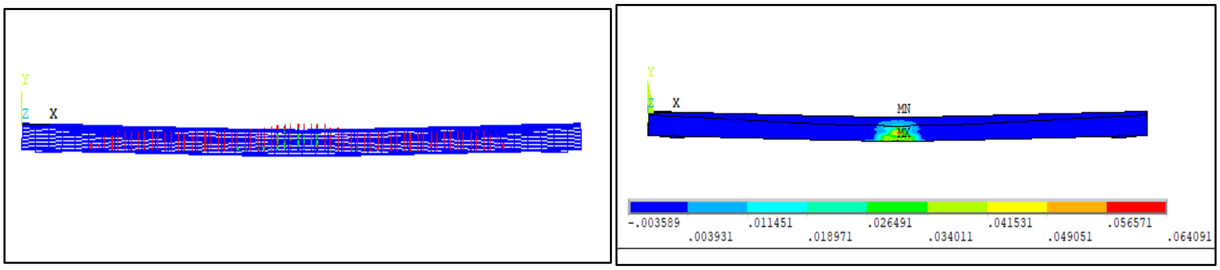

f) N3

Figure 4-32: Cont.

4.5 Flange Effective width

The ACI-318 [20] code specified a certain limits of the effective width of flanged section for slab-beam concrete system of mono. Concrete costing this section intends to check the reliability of tapered flange section for a spectrum range of flange width, besides, comparing analysis with the corresponding specimens of uniform flanges. Figure 4-33 shown that the adopted cross section of various flange width.

Table 4-16 lists the geometrical details of uniformed tapered flange section specimens sets, While Table 4-17 summarized the related results analysis.

As the flange width changed from 65cm to 85cm in both uniform and tapered section specimens, the strength, ductility and energy dissipation rates are approximately the same .for strength improving, an optimum rates is assigned for specimens of 75cm flange width for both sets. The strength improve rate is 1.18 for uniform flange section verse 1.012 for tapered flange section, while, the analysis in term of ductility show the ductility tends to get more improving as flange effective width increased.

The normalizing of results are shown in Figure 4-35, the same relationship degree are success and to normalized results of both configuration.

$pu = 0.0013Bf2 -2Bf+ 851.88$ for uniform section

$pu = 0.0013Bf^2 - 2Bf + 851.88$ for tapered section

Figure 4-34 show the strength, ductility and energy dissipation rate for both section configuration. while Figure 4-36 illustrate the related crack patterns and strain distribution.

Table 4-16 Specimens' modeling details: Effective flange width

No.	Code	fy Mpa	f'c Mpa	ρ	L cm	d cm	h cm	bf cm	bw cm	dfe cm	dfm cm
1	Ts1	490	35	0.0063	600	26	30	65	18	5	5
2	Ts2	490	35	0.0063	600	26	30	75	18	5	5
3	Ts3	490	35	0.0063	600	26	30	85	18	5	5
4	Ns1	490	35	0.0063	600	26	30	65	18	5	15
5	Ns2	490	35	0.0063	600	26	30	75	18	5	15
6	Ns3	490	35	0.0063	600	26	30	85	18	5	15

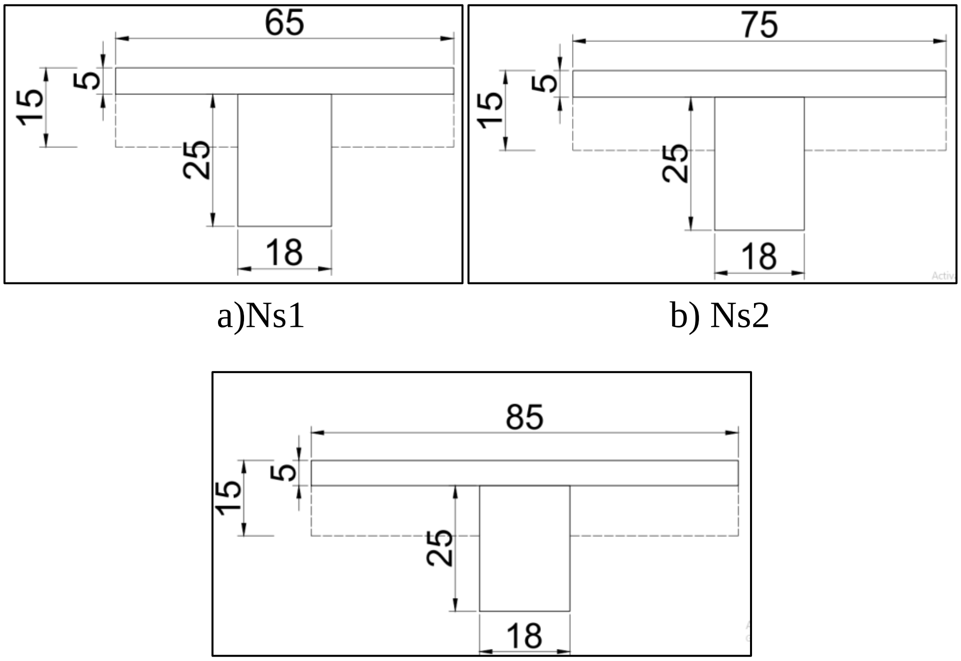

a)Ns1

b) Ns2

C) Ns3

Figure 4-33 adopted cross section of various flange width

Table 4-17 Results analysis: Effective flange width

No	Code	The variable parameter	Pu, kN	Pui/Pu1	Δe, mm	Δmax, mm	(Δmax)i/(Δmax)1	D.I.	(D.I)i/(D.I)1	ψ, kN.mm	ψi/ψi
1	Ts1	Effective flange width	80	1.00	2.36	31.6	1.00	13.38	1.00	469.99	1.00
2	Ts2		55	0.68	1.7	32.2	1.18	18.93	1.414	100.35	0.213
3	Ts3		55	0.68	1.1	29.32	0.927	26.65	1.99	154.4	0.328
4	Ns1		80	1.00	2.4	30	1.00	12.5	1.00	470.24	1.00
5	Ns2		55	0.68	1.6	32	1.012	20	1.6	88.49	0.188
6	Ns3		56	0.7	1	29.5	0.933	29.5	2.36	183.71	0.390

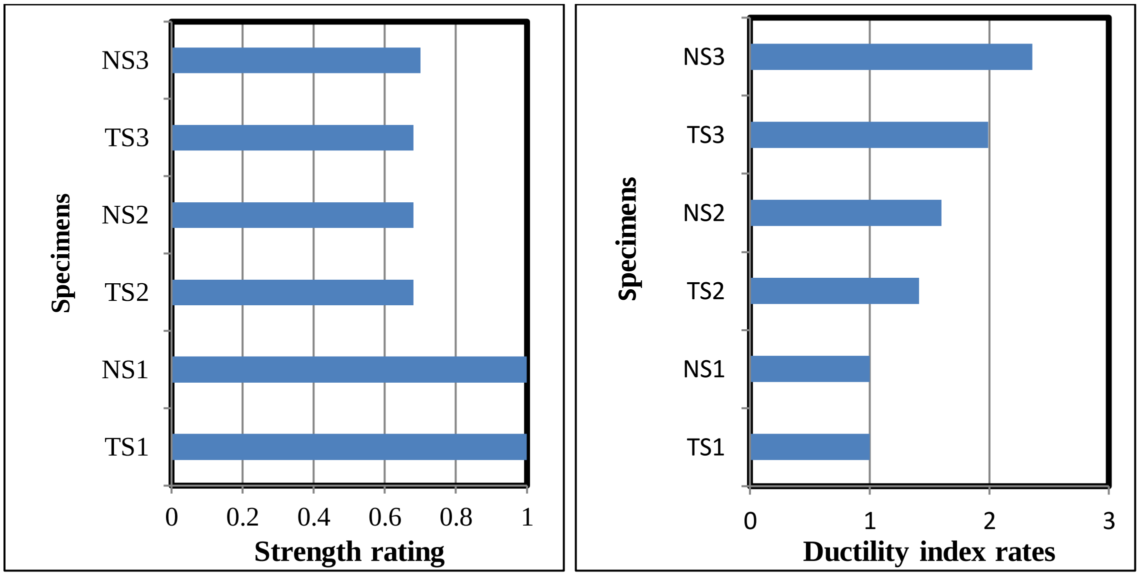

a) b)

Figure 4-34 a)Strength variation rates b) Ductility variation rates c) Energy dissipation variation: Effective flange width

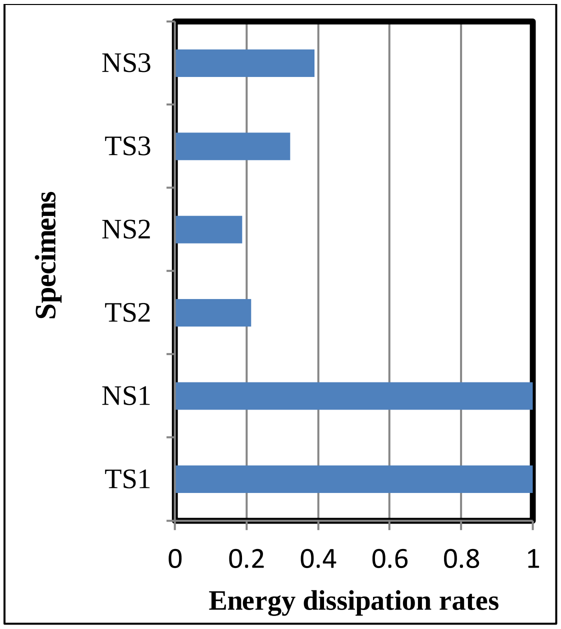

c)

Figure 4-34: Cont.

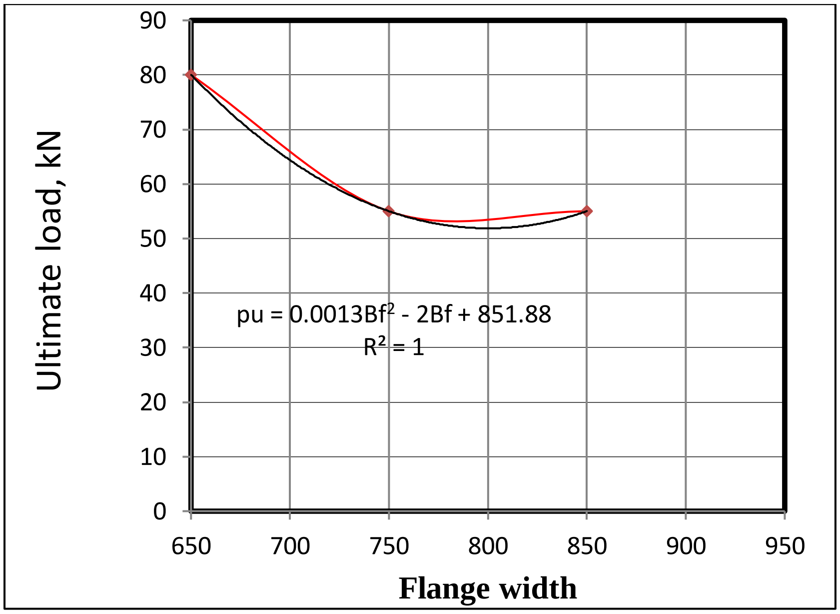

a) Uniform flange section

Figure 4-35 Mathematical normalization: Effective flange width

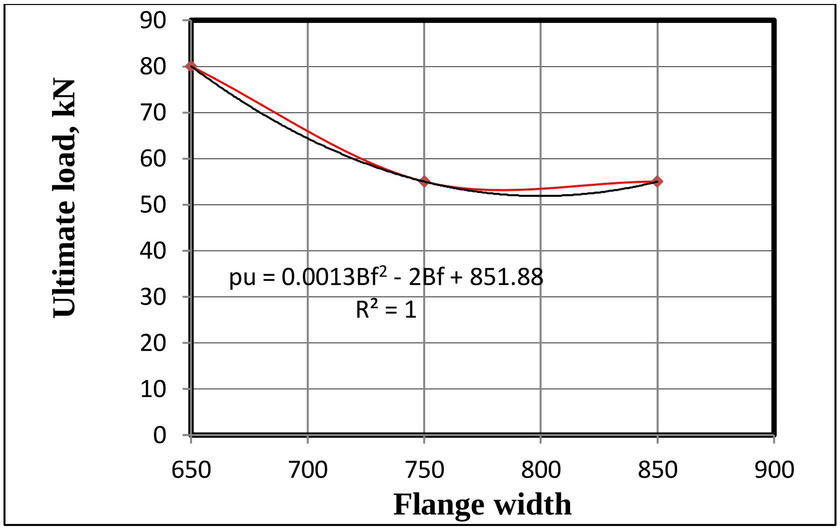

(b) Tapered flange section

Figure 4-35: Cont.

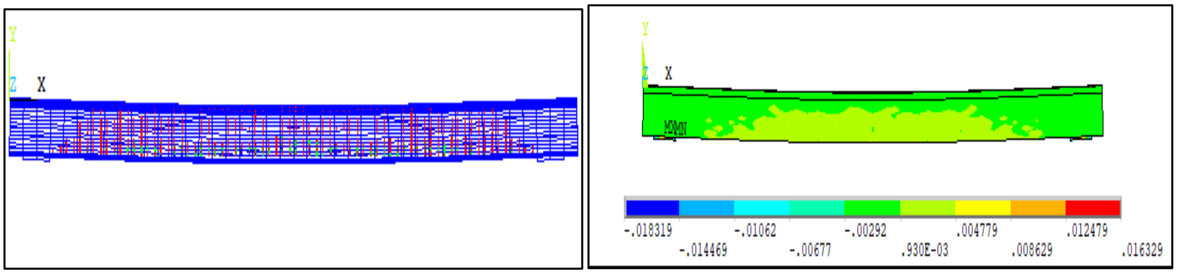

a)Ts1

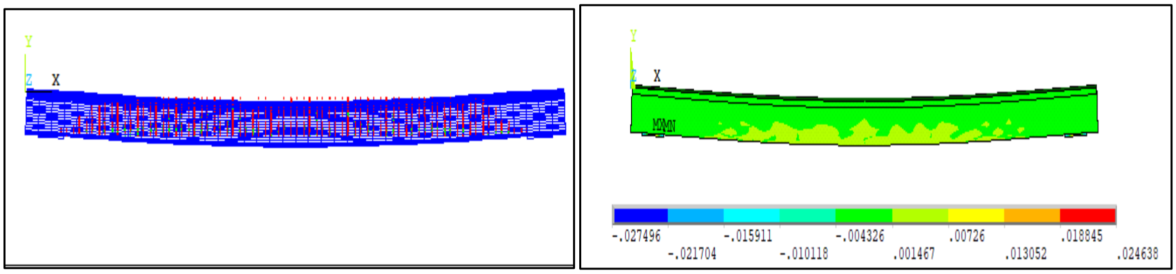

b)Ts2

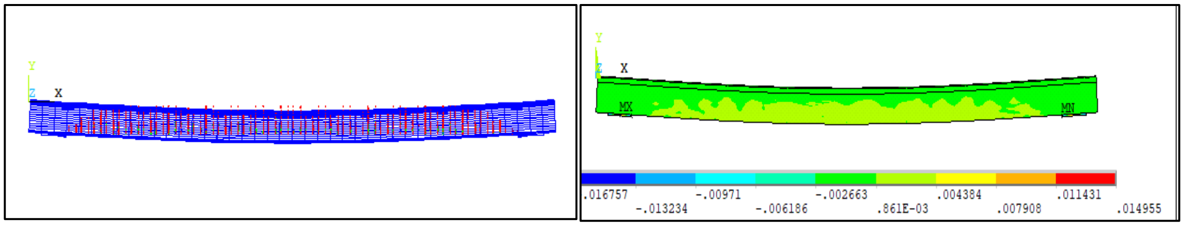

c)Ts3

Figure 4-36 Failure modes(crack patterns) and total Strain distribution: Effective flange width

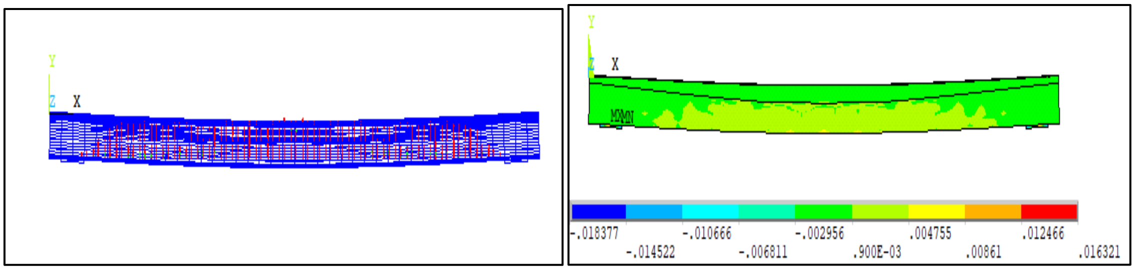

d)Ns1

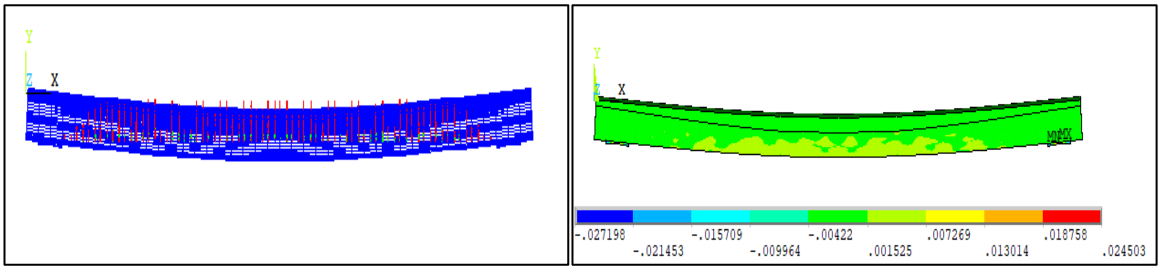

e)Ns2

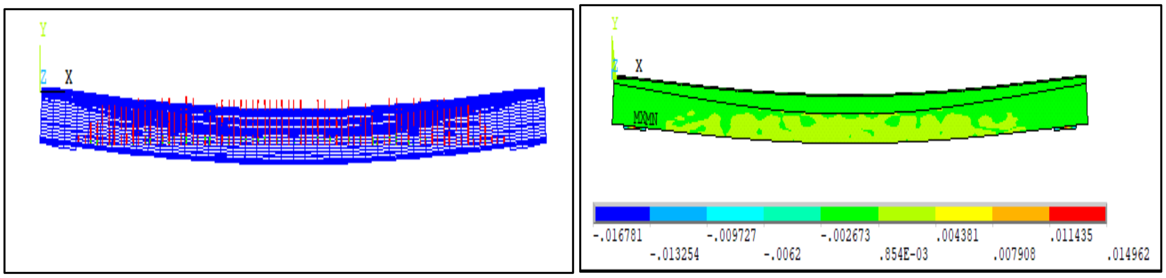

f)NS3

Figure 4-36: Cont.

4.6 Continues Beam and Moment Redistribution

Continuity of tapered flange beam are investigation, besides the moment redistribution that expected due to the highly ductility of tapered section. Two span beam under the effect of concentrated mid span loads are consider, the numerical modeling utilizing the benefit of symmetrical numerical approach. The geometrical details are listed in Table 4-18 While Table 4-19 involve the results analysis. The reduction of reinforcement in negative region which is companied with enchainment provided reinforcement in mid span, tends to upgrade strength capacity by 1.19 while the over design that introduced in C_{ove} specimens turns the behavior to brittleness response as depicts in Figure 4-38 without moment redistribution. While the significant moment redistribution in specimens C_{w1} is assigned the change of p from 0.0063 to 0.0094 companied by strength improving due to moment redistribution of (β= 0.889). Figure 4-39 indicate the strength, ductility and energy dissipation improving rates in term of provided steel reinforcement while Figure 4-40 depicts the related crack patterns and strain distribution.

Table 4-18 Specimens' modeling details: continuous beams

No.	Code	*Fy Mpa*	*f'c Mpa*	ρ	L cm	d cm	h cm	b_f cm	b_w cm	d_{fe} cm	d_{fm} cm
1	CW1	490	35	0.0063	420	26	30	24	18	5	15
2	CW2	490	35	0.0094	420	26	30	24	18	5	15
3	Cove	490	35	0.023	420	26	30	24	18	5	15

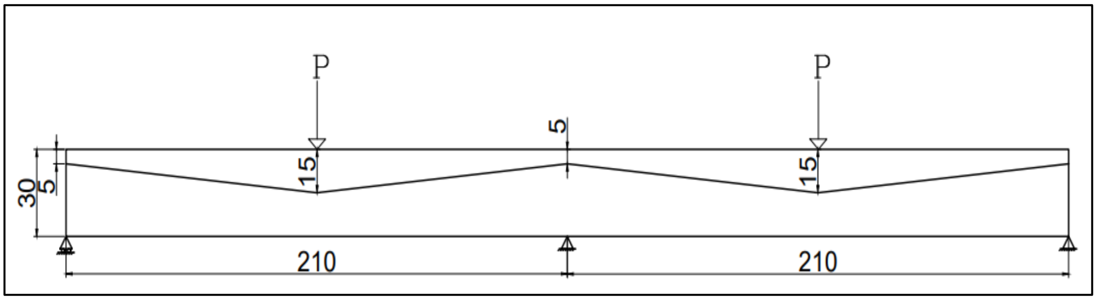

Figure 4-37 continuous tapered flange beam

Table 4-19 Result analysis : continuous beams

No.	Code	The variable parameter	Pu, kN	Pui/Pu1	Δe, mm	Δmax, mm	(Δmax)i/(Δmax)1	D.I.	(D.I)i/(D.I)1	ψ, kN.mm	ψi/ψi	M_e KN.m	M_p KN.m	β
1	CW1	Ductility limits in scope of provided steel ratio	168	1.00	4.36	20	1.00	1185.6	1.00	4.58	1.00	66.2	58.8	0.889
2	CW2		200	1.19	5.67	13.5	0.675	659.6	0.553	2.38	0.519	78.8	60.2	0.764
4	Cove		140	0.83	2.64	4.5	0.225	57.3	0.048	0.196	0.042	55.1	36.8	0.66

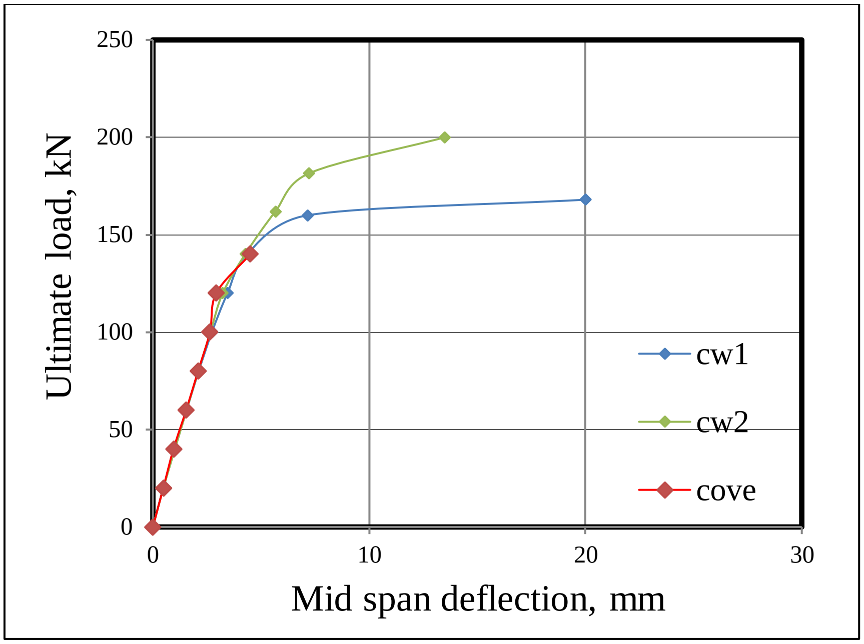

Figure 4-38 load – deflection response: continuous beam

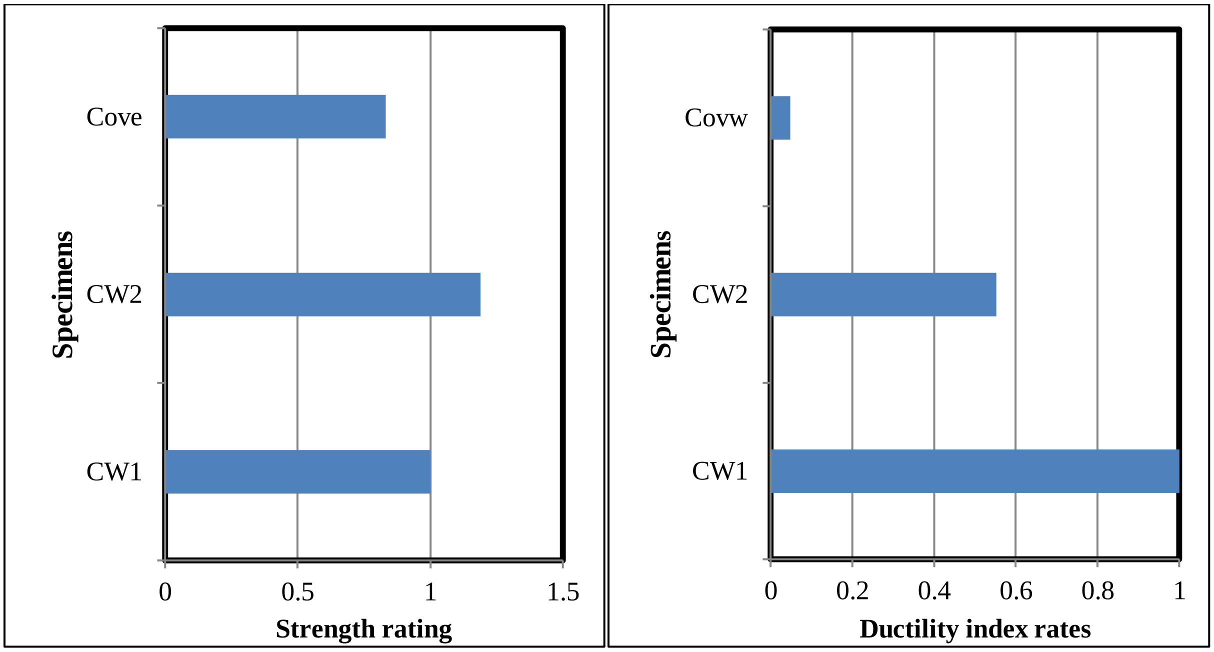

a) b)

Figure 4-39 a)Strength variation rates b) Ductility variation rates c) Energy dissipation variation rates: continuous beams

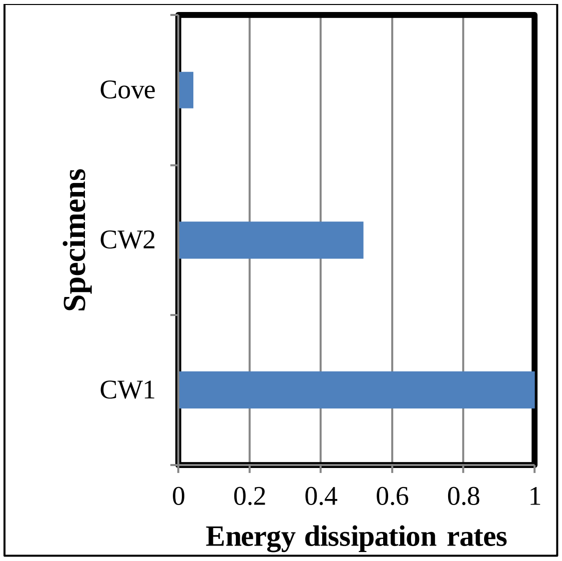

c)

Figure 4-39: Cont.

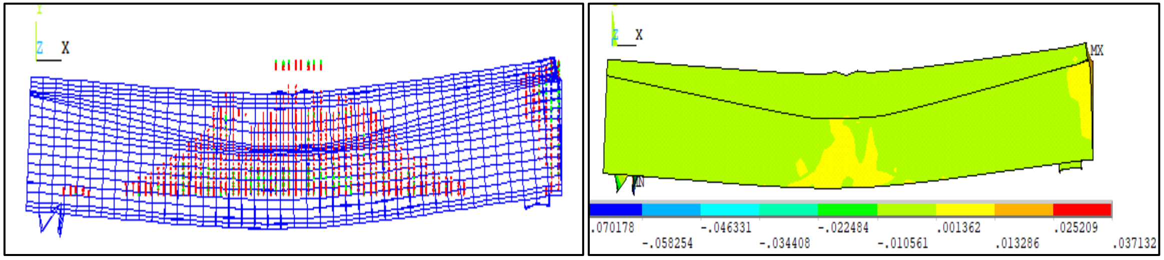

a) CW1

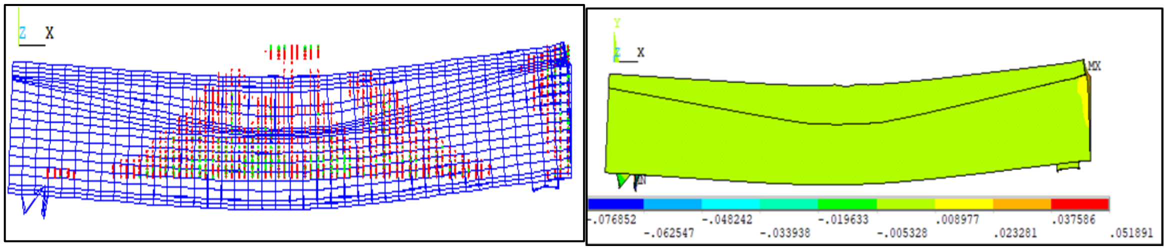

b)CW2

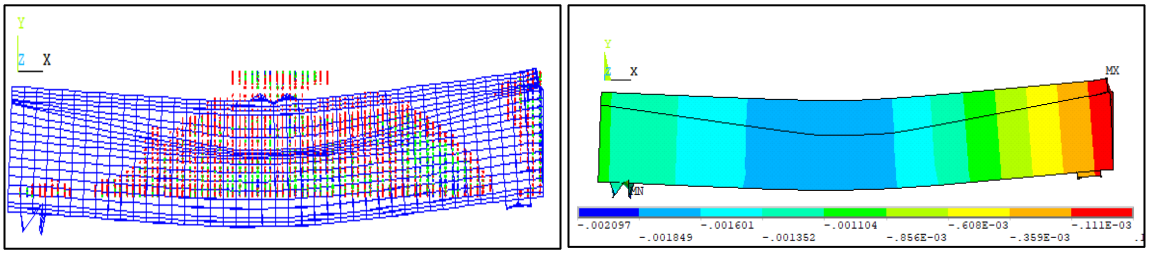

C) Cove

Figure 4-40 Failure modes(crack patterns) and total Strain distribution in term of (ρ) : continuous beams

4.7Shear Span Effect

Although the web part within section is traditionally utilized to resist shear stress, the present of flange affects shear section resistance due to its role in resisting normal compression stress that interaction with shear effect. Various shear spans (a/d) are considered (1.5, 2.5, 3.5) to inspect section shear resistance under by producing various stress distribution modes. Disturbed stress distribution D region which compatible with a/d more than 2 (specimens Av2 and Av3 of a/d =2.5 and 3.5) and Bernoulli stress distribution B region which compatible with a/d less than 2 (specimens Av1 of a/d= 1.5).

Table 4-20 lists the geometry description of adopted specimens sets while table 4-21 exhibit the related results analysis which depict that, the changing of shear span that correspond to turn stress distribution modes, compatible with failure mode turning to flexural, flexural-shear, and shear failure mode respectively as a/d have varying range 1.5, 2.5, 3.5 respectively. Figure 4-41show the adopted tapered flange beams under various concentrated load, While the Figure 4-42 exhibit strength, ductility, and energy dissipation rate that corresponding to shear span effect. The Figure 4-43 depicts the load-deflection response for specimens of various shear spans. The specimens Av3 which it dominate by flexural failure mode exhibits ductility response and this finding relate to the absence of strut-tie reinforcing mode due to disturbed stress within assigned D-region while the specimens Av2 exhibits acceptable ductile response that characteristics by flexural-shear failure mode. The strength in term of shear span are normalized by second degree relationship, Pu = -26.25(a/d)2+132.5(a/d) +7.8125.

As illustrated in Figure 4-44., while Figure 4-45 show the related crack patterns and strain distribution.

Table 4-20 Specimens' modeling details: shear span effect

No.	Code	*Fy* *Mpa*	*f'c* *Mpa*	ρ	a/d	L cm	d cm	h cm	b_f cm	b_w cm	d_{fe} cm	d_{fm} cm
1	Av1	490	35	0.0063	1.5	210	26	30	24	18	5	15
2	Av2	490	35	0.0063	2.5	210	26	30	24	18	5	15
3	Av3	490	35	0.0063	3.5	210	26	30	24	18	5	15

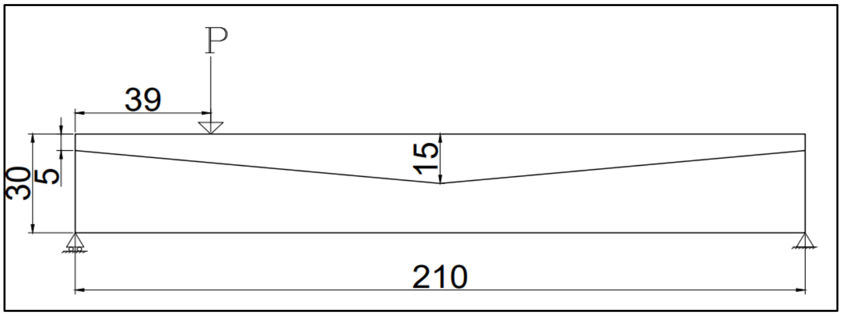

a) Av1

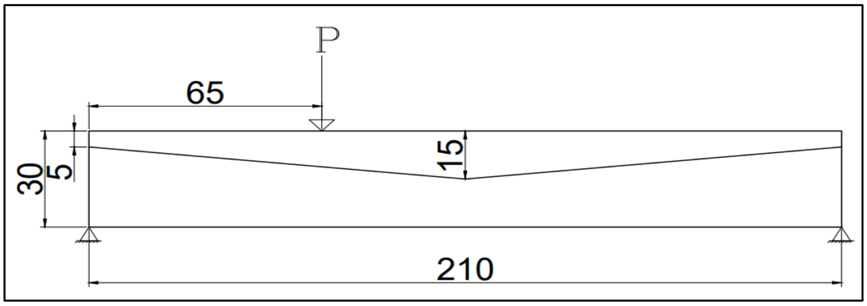

b) Av2

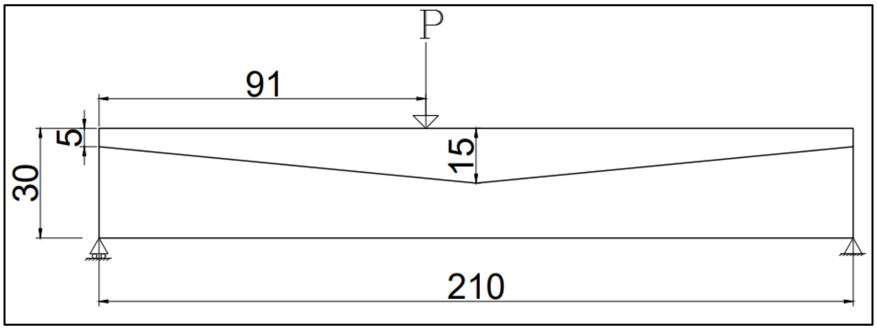

a)Av3

Figure 4-41 the adopted tapered flange beams under various concentrated load

Table 4-21 Results analysis: shear span effect

No.	Code	The variable parameter	Pu, kN	Pui/Pu1	Δe, mm	Δmax, mm	(Δmax)i /(Δmax)1	D.I.	(D.I)i/(D.I)1	ψ, kN.mm	ψi/ψi
1	Av1	Effect of shear span	147.5	1.00	12.38	12.38	1.00	213.65	1.00	1.00	1.00
2	Av2		175	1.186	11.4	25.2	2.03	1032.25	4.83	2.21	2.21
4	Av3		150	1.016	5.95	33.21	2.683	1656.6	7.75	5.58	5.58

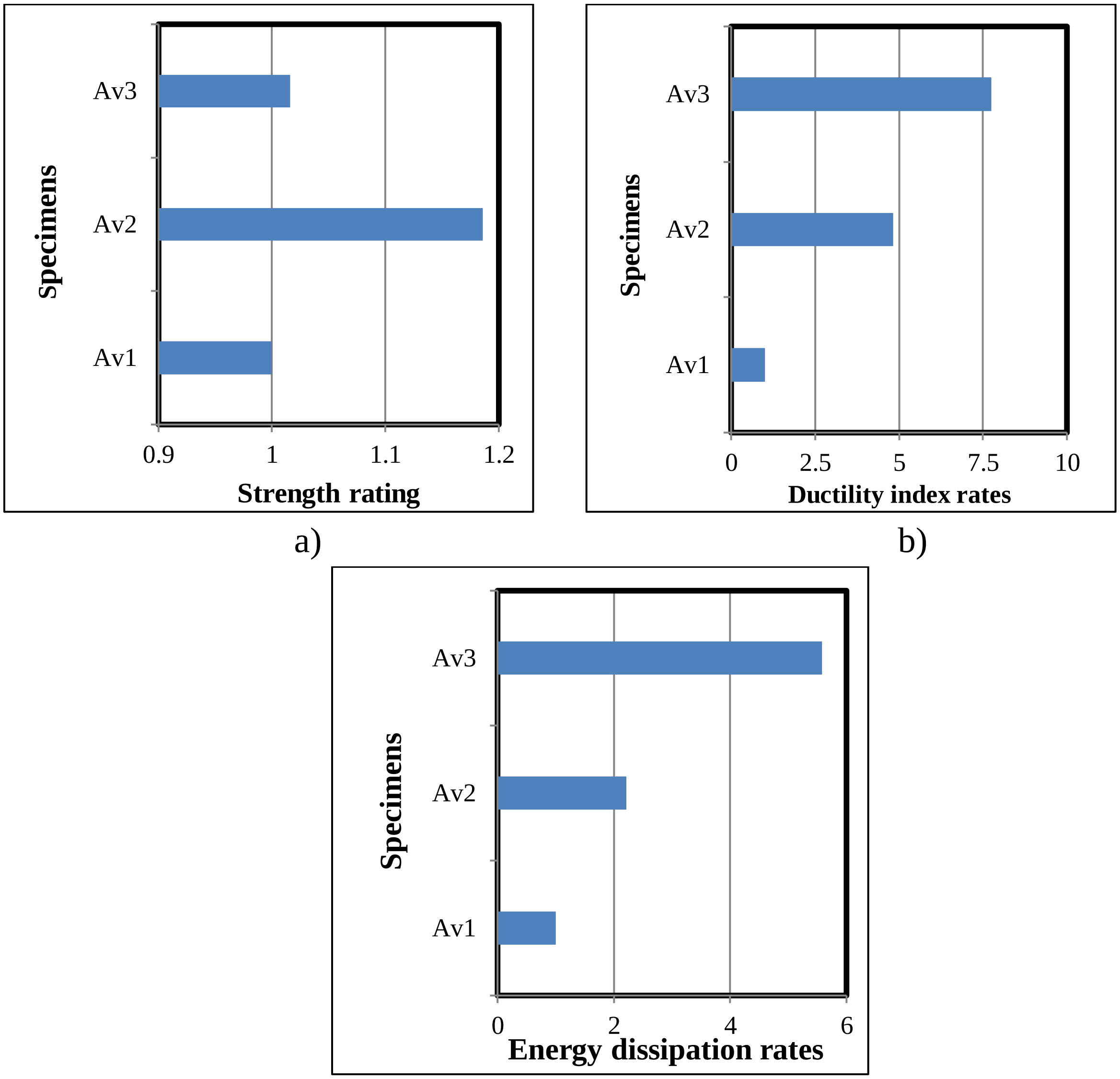

a) b)

c)

Figure 4-42 (a) Strength variation rates (b) Ductility variation rates (c)Energy dissipation rates: shear span effect

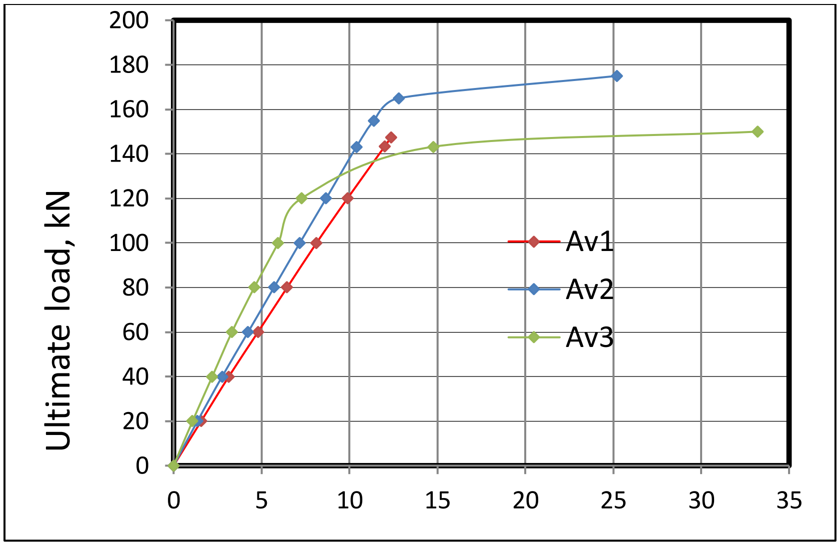

Figure 4-43 load – deflection response : shear span effect

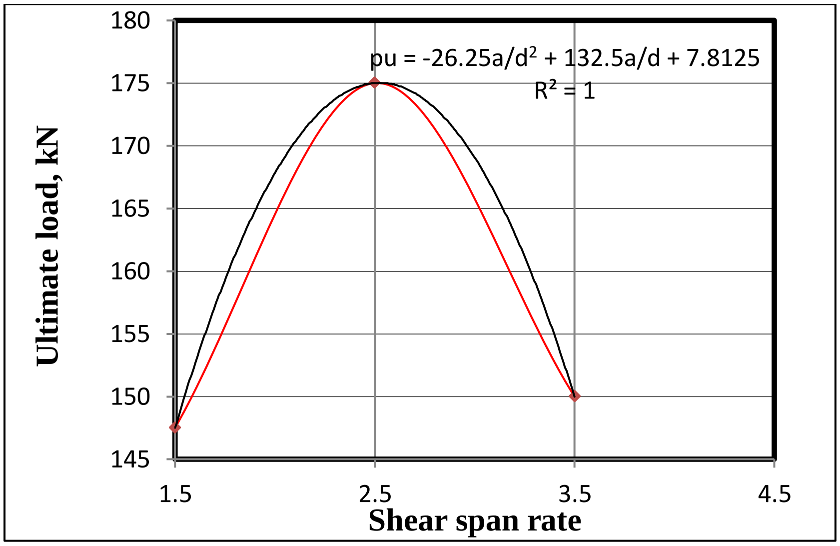

Figure 4-44 Mathematical normalization: shear span effect

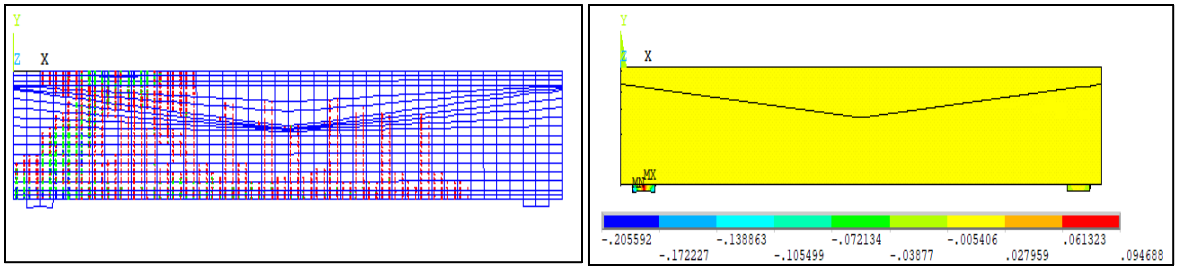

(Av1) Shear failure mode

Figure 4-45 Failure modes(crack patterns) and total Strain distribution: shear span effect

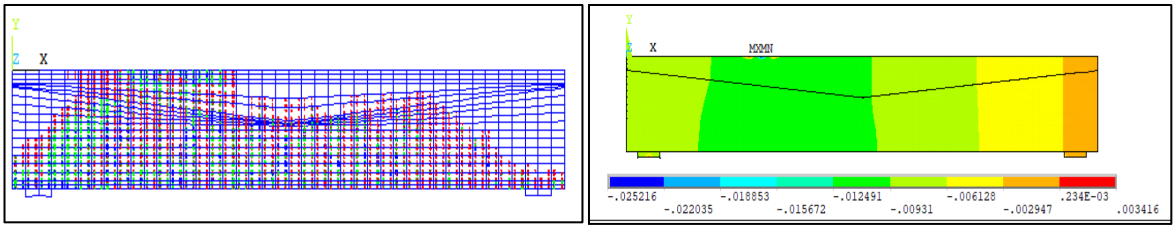

(Av2) flexural-shear failure mode

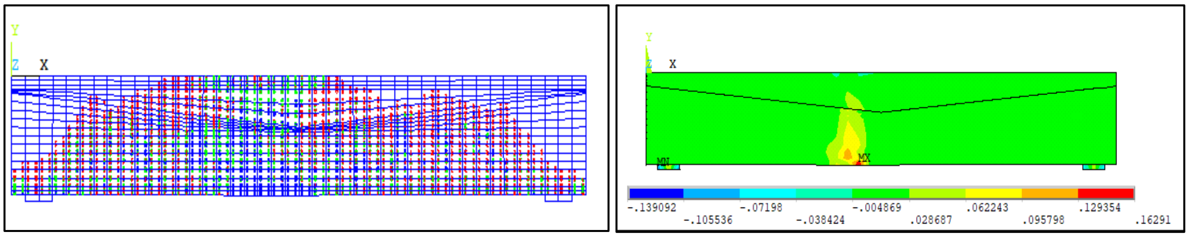

(Av3) flexural failure mode

Figure 4-45: Cont.

CHAPTER FIVE:CONCLUSION AND RECOMMENDATIONS

5.1 Conclusion

The present numerical study is focused on the behavior of reinforced concrete Tapered beams. Based on the results obtained from the FEM by using NSYS (15.0) program. Many factors have significant effect on the general behavior of beam at failure and these effects can be summarized as follows:

1. The predicated results verified the reliability of the developed numerical model that adopted in current study and deals with various spectrum of variable (extended middle length, web thickness), the predicted rates are varied between 0.964 to 1.08.
2. The middle region uniformity within tapered domain, assigned slightly effect on ultimate strength, the increasing from 0 to 52 cm, the ultimate strength get improving from 147 kN to 155.3 kN with slightly increment rates 1.02 while the best flexural ductility and the best energy dissipation are predicted in a certain uniformity length (26 cm) which is indicated as optimum uniformity length that corresponding to ductility improving rate of 1.49 and energy dissipation enhancement rate of 1.53.
3. The orient variation of tapered region, assigned slightly effect on ultimate strength, the ductility and energy dissipation improving with increment rate 5.49 and 4.83, when the orient variation of tapered region changed from 3.27^o to 5.44^o.

4. The fixed B.Cs. state turned the behavior as brittle behavior and the presented of the traditional hinged mode maintained the ductility and energy dissipation. while the specified partial fixing mode exhibit a differed response of relatively less ductility and of a significant strength improving, of strength update rate 1.17 .
5. The concrete compressive strength affected the strength capacity positively, the ultimate strength improved from 133 kN to 160 kN with improving rate 1.2, as concrete compressive strength changed from 25 to 45 MPa. Besides, the results depict that the optimum flexural ductility of improving rate (6.21) and the optimum energy dissipation of enhancement rate 7.18 are assigned in section of moderated concrete compressive strength of 35 MPa.
6. The ultimate strength get improving with steel strength increasing and the over increment turns the section to be over reinforcement section. Also, the results depicts that the flexural ductility get improving (D.I.=23.3) compatible with the humble steel strength (fy =325 MPa) and the optimum energy dissipation (7410 kN.m) are assigned in section of moderated provided steel strength (fy =490 MPa).
7. The section strength is improved from 147.1 kN to 215 kN with improving rate of 1.46 as steel ratio change from ρ=6.3*10-3 to ρ= 9.06*10-3 which are within ductility limit, the over reinforcement section (ρ= 0.039), turns the section to be over reinforcement with brittle failure mode. Also, the results depict that the increasing of reinforcement out of ACI ductility limit, negatively affected flexural ductility and energy dissipation.
8. The tapered flange mode compatible with varying of section moment of inertia along the beam the obtained deflection that correspond to service load which is considered as 2/3 pu, are approximately the same while the max deflection that corresponding to ultimate load have got slightly variation was compared with

ACI limit, By comparing all specimens with ACI limits, it was found that allowable value of deflection are greater than the actual deflection.

9. When changing the flange width from 65cm to 85cm in both uniform and tapered section specimens, the strength, ductility and energy dissipation rates are approximately the same. strength improves at a rate is 1.18 for uniform flange section verse 1.012 for tapered flange section for specimens of 75cm flange width, while, the analysis in term of ductility show the ductility tends to get more improving as flange effective width increased.
10. The reduction of reinforcement in negative region which is companied with enchainment provided reinforcement in mid span, tends to upgrade strength capacity by 1.19 while the over design that introduced in Cove specimens turns the behavior to brittleness response without moment redistribution. While the significant moment redistribution in specimensCw1 is assigned the change of p from 0.0063 to 0.0094 companied by strength improving due to moment redistribution of (β=0.889).
11. It is observed that the change of the shear span effect corresponds to the stress distribution modes (D region which compatible with a/d more than 2 and B region which compatible with a/d less than 2) corresponding to the failure mode which turns into bending, flexural shear, and failure shear mode respectively as a/d having varying range 1.5, 2.5, 3.5 respectively. the specimens Av3 which it dominate by flexural failure mode exhibits ductility response and this finding relate to the absence of strut-tie reinforcing mode due to disturbed stress within assigned D-region while the specimens Av2 exhibits acceptable ductile response that characteristics by flexural-shear failure mode.

5.2 Recommendations for Future Works

Extra investigation to understand the basic behavior of RC beams is required. The following suggestions are recommended:

1. Investigation of the non-prismatic behavior when strengthened with CFRP bar and GFRP sheet.
2. Investigation of behavior in hybrid strength reinforced concrete beams of non-prismatic section.
3. Detailed study of behavior in RC non-prismatic deep beams.

REFERENCES

[1] Bentz, D. P., Garboczi, E. J., & Schlangen, E. (1994). Computer Simulation of Interfacial Zone Microstructure and Its Effect on the Properties of Cement-Based Composites.

[2] Howard C S 1923 Formulas tables and graphs for trapezoidal reinforced concrete beams Bachelor's thesis California Institute of Technology.

[3] Ali, A. H., Mohamed, H. M., & Benmokrane, B. (2017). Shear Strength of Circular Concrete Beams Reinforced with Glass Fiber-Reinforced Polymer Bars and Spirals. ACI Structural Journal, 114(1).

[4] Teixeira, P. W. G., Maffei, C. E. M., & Guazzelli, M. C. (2012). Shear strength of reinforced concrete circular cross-section beams. Revista IBRACON de Estruturas e Materiais, 5, 781-797.

[5] Sada, M. J. (2021, February). Shear Performance of Hybrid Concrete Deep Beams of Trapezoidal Section. In IOP Conference Series: Materials Science and Engineering (Vol. 1067, No. 1, p. 012015). IOP Publishing.

[6] El-Azab, I. A. Nonlinear Analysis of Reinforced Concrete T-Beam.

[7] Darwin, D., Dolan, C.W. and Nilson, A.H., 2016. Design of concrete structures. New York, NY, USA:: McGraw-Hill Education.

[8] Ghailan, D. B. (2010). T-Beam behavior in flexure with different layers of concrete in web and flange. Kufa Journal of Engineering, 2(1).

[9] Abbas, R. M., & Fadala, W. A. (2021). Behavioral Investigation of Reinforced Concrete T-Beams with Distributed Reinforcement in the Tension Flange. In E3S Web of Conferences (Vol. 318, p. 03010). EDP Sciences.

[10] Kalluri, R. K. (1999). Bending behavior of concrete T-beams reinforced with glass fiber-reinforced polymer (GFRP) bars. West Virginia University.

[11] Nawy, E.G.(1990) Reinforced Concrete: Fundamental Approach. Prentice Hall Publications.99 70-300.

[12] ACI Committee. (2008). Building code requirements for structural concrete (ACI 318-08) and commentary. American Concrete Institute.

[13] Cladera, A., Marí, A., Ribas, C., Bairán, J., & Oller, E. (2015). Predicting the shear–flexural strength of slender reinforced concrete T and I shaped beams. Engineering Structures, 101, 386-398.

[14] Zararis, P. D., & Papadakis, G. C. (2001). Diagonal shear failure and size effect in RC beams without web reinforcement. Journal of structural engineering, 127(7), 733-742.

[15] Nampalli, P., & Sangave, P. (2015). Linear and Non-Linear Analysis of Reinforced Concrete Frames with Members of Varying Inertia. IOSR Journal of Mechanical and Civil Engineering.

[16] Ibrahim, S. K., & Rad, M. M. (2020). Numerical Plastic Analysis of Non-Prismatic Reinforced Concrete Beams Strengthened by Carbon Fiber Reinforced Polymers. In Proc. of the 13th fib International PhD Symposium in Civil Engineering (pp. 208-215). Paris France: Marne-la-Vallée.

[17] Toshniwal, S. (2019). Shear Analysis of Non-Prismatic Concrete Beams.

[18] Tena-Colunga, A., Archundia-Aranda, H. I., & González-Cuevas, Ó. M. (2008). Behavior of reinforced concrete haunched beams subjected to static shear loading. Engineering Structures, 30(2), 478-492.

[19] Jaafer, A. A., & Abdulghani, A. W. (2018, December). Nonlinear finite element analysis for reinforced concrete haunched beams with opening. In IOP Conference Series: Materials Science and Engineering (Vol. 454, No. 1, p. 012152). IOP Publishing.

[20] ACI (American Concrete Institute). 2014. Building code requirements for structural concrete and commentary. ACI 318-14. Farmington Hills,MI: ACI

[21] BSI (British Standards Institute). 1988. Steel, concrete and composite bridges. General statement. BS 5400-1. London: BSI.

[22] Shooshtari, A., & Khajavi, R. (2010). An efficient procedure to find shape functions and stiffness matrices of nonprismatic Euler–Bernoulli and Timoshenko beam elements. European Journal of Mechanics-A/Solids, 29(5), 826-836.

[23] Ozay, G., & Topcu, A. (2000). Analysis of frames with non-prismatic members. Canadian Journal of Civil Engineering, 27(1), 17-25.

[24] Tan, K. H. (2004). Design of non-prismatic RC beams using strut-and-tie models. Journal of Advanced Concrete Technology, 2(2), 249-256.

[25] El-Mezaini, N., Balkaya, C., & Çitipitio g ˇ lu, E. (1991). Analysis of frames with nonprismatic members. Journal of Structural Engineering, 117(6), 1573-1592.

[26] Stefanou, G. D. (1983). Shear resistance of reinforced concrete beams with non-prismatic sections. Engineering Fracture Mechanics, 18(3), 643-666.

[27] El-Niema, E. I. (1988). Investigation of concrete haunched T-beams under shear. Journal of Structural Engineering, 114(4), 917-930.

[28] Orr, J., Darby, A. P., Ibell, T., Evernden, M., Lava, P., & Debruyne, D. (2013). The shear behaviour of non-prismatic reinforced concrete beams determined using digital image correlation.

[29] Park, R., Paulay, T.(1975). Reinforced concrete structures (John Wiley and Sons.

[30] Release, A. M. A. (2013). 15, ANSYS Mechanical APDL element reference.

[31]Vodenitcharova, T., & Zhang, L. C. (2006). Bending and local buckling of a nanocomposite beam reinforced by a single-walled carbon nanotube. International journal of solids and structures, 43(10), 3006-3024.

[32] Mahzuz, H. M. A. (2011). Performance evaluation of triangular singly reinforced concrete beam. International Journal of Structural Engineering, 2(4), 303-314.

[33] Concrete, 19(6), 1633-1648. Al-Ansari, M. S. (2015). Reliability and flexural behavior of triangular and T-reinforced concrete beams. International Journal of Advanced Structural Engineering (IJASE), 7(4), 377-386. Ali, A. H., Mohamed, H. M., &

[34] Concrete, 19(6), 1633-1648. Al-Ansari, M. S. (2015). Reliability and flexural behavior of triangular and T-reinforced concrete beams. International Journal of Advanced Structural Engineering (IJASE), 7(4), 377-386. Ali, A. H., Mohamed, H. M., &

[35] Khalil, A. H., Nabil, M., & Mohamed, M. (2017). Shear Behavior of Trapezoidal Beams. Journal of Al-Azhar University Engineering Sector, 12(42), 37-53.

[36] Européen, C. (2004). Eurocode 2: Design of concrete structures—Part 1-1: General rules and rules for buildings. *London: British Standard Institution*.

[37] Hussnawi, M. (2018, November). Effects of trapezoidal cross-section dimensions on the behaviours of CFRP SCC beams. In IOP Conference Series: Materials Science and Engineering (Vol. 433, No. 1, p. 012012). IOP Publishing.

[38] Al-Ansari, M. S., & Afzal, M. S. (2019). Simplified Irregular Beam Analysis and Design. Civil Engineering Journal, 5(7), 1577-1589.

[39] Mousa, S., Mohamed, H. M., & Benmokrane, B. (2019). Deflection prediction methodology for circular concrete members reinforced with fiber-reinforced polymer bars. ACI Structural Journal, 116(2), 279-293.

[40] Johnson, R. P., Oehlers, D. J., & BS 5400. (1981). Analysis and design for longitudinal shear in composite T-beams. Proceedings of the Institution of Civil Engineers, 71(4), 989-1021.

[41] Khalifa, A., & Nanni, A. (2000). Improving shear capacity of existing RC T-section beams using CFRP composites. Cement and Concrete Composites, 22(3), 165-174.

[42] ACI Committee. (1995). ACI 318-95: Building code requirements for structural concrete and commentary. Farmington Hills.

[43] European Committee for Standardization. (1994). Eurocode 2: Design of concrete structures. Central Secretariat, CEN.

[44] Deniaud, C., & Roger Cheng, J. J. (2003). Reinforced concrete T-beams strengthened in shear with fiber reinforced polymer sheets. Journal of Composites for Construction, 7(4), 302-310.

[45] Kwan, A. K. H., & Au, F. T. K. (2004). Flexural strength–ductility performance of flanged beam sections cast of high-strength concrete. The structural design of tall and special buildings, 13(1), 29-43.

[46] Hawileh, R. A., Abdalla, J. A., & Tanarslan, M. H. (2012). Modeling of nonlinear response of r/c shear deficient t-beam subjected to cyclic loading. Computers &Concrete,10(4),419-434.tions. Journal of structural engineering, 127(8), 940-946.

[47] Santos, P., Laranja, G., França, P. M., & Correia, J. R. (2013). Ductility and moment redistribution capacity of multi-span T-section concrete beams reinforced with GFRP bars. Construction and Building Materials, 49, 949-961.

[48] Demir, A., Caglar, N., Ozturk, H., & Sumer, Y. (2016). Nonlinear finite element study on the improvement of shear capacity in reinforced concrete T-Section beams by an alternative diagonal shear reinforcement. Engineering Structures, 120, 158-165.

[49] ABAQUS/Standard v. 6.12 SE. Providence (RI, USA): Dassault Systemes Simulia Corp.

[50] Subramani, T., Ali, A. M., Karthikeyan, R., Selvan, E. P., & Periyasamy, K. (2017). Analytical Study Of T-Beam Using ANSYS.

[51] Panggabean, H., & Pakpahan, N. (2018). Experimental analysis of T-beam reinforced concrete with holes. In MATEC Web of Conferences (Vol. 195, p. 02006). EDP Sciences.

[52] Ghaziyani, S. Z. H., Mostafavian, S., & Chirani, M. A. (2018). Analytical Study of Bending Behavior for Concrete Beams with T-Shaped Cross Section using Composite and Steel Bars. American Journal of Engineering and Applied Sciences, 11(2), 979-985.

[53] Fang, Z., Jiang, H., Liu, A., Feng, J., & Chen, Y. (2018). Horizontal shear behaviors of normal weight and lightweight concrete composite T-beams. International Journal of Concrete Structures and Materials, 12(1), 1-21.

[54] Al-Rousan, R., & Abo-Msamh, I. (2019). Bending and torsion behaviour of CFRP strengthened RC beams. Magazine of Civil Engineering, (8 (92)), 48-62.

[55] To, C. W. S. (1981). A linearly tapered beam finite element incorporating shear deformation and rotary inertia for vibration analysis. Journal of Sound and Vibration, 78(4), 475-484.

[56] BLCP 80, British Standard Code (1969). Practice for the structural use of concrete, British Standards Institute p. 241

[57] Principles and Recommendations: June 1970, FIP Sixth Congress, Prague. Cement & Concrete Association of Great Britain.

[58] Balkaya, C. (2001). Behavior and modeling of non-prismatic members having T-sec

[59] Tena-Colunga, A., Archundia-Aranda, H. I., Grande-Vega, A., & González-Cuevas, O. M. (2007, June). Cyclic shear behavior of reinforced concrete

haunched beams. In Memorias, Ninth Canadian Conference on Earthquake Engineering (9CCEE).

[60] Al-Maliki, H. N. G. M. (2013). Experimental behavior of hollow non-prismatic reinforced concrete beams retrofit with CFRP sheets. Journal of Engineering and Sustainable Development, 17(5), 224-237.

[61] Tena-Colunga, A., Urbina-Californias, L. A., & Archundia-Aranda, H. I. (2017). Shear behavior of continuous reinforced concrete haunched beams subjected to cyclic loading. In Memorias, 16th World Conference on Earthquake Engineering.

[62] Al-Attar, T. S., Abdulqader, S. S., & Ibrahim, S. K. (2017). Behavior of Tapered Self-Compacting Reinforced Concrete Beams Strengthened by CFRP. Engineering and Technology Journal, 35(3 Part A).

[63] Qissab, M. A., & Salman, M. M. (2018). Shear strength of non-prismatic steel fiber reinforced concrete beams without stirrups. Struct. Eng. Mech, 67(4), 347-358.

[64] Siswantoro, E. P., & Pradana, P. (2021, May). Finite element analysis on flexural behavior of nonprismatic longitudinal section reinforced concrete deep beam. In IOP Conference Series: Materials Science and Engineering (Vol. 1144, No. 1, p. 012038). IOP Publishing

[65] Zamel, J. K. (2021). Flexural behavior of developed reinforced concrete beams of non -prismatic flanges. Materials Today: Proceedings, 42, 2974-2983.

[66] Zienkiewicz, O. C. (1977). The Finite Element Method, 3rd edn, Loiadon.

[67] ANSYS, 2011, "ANSYS Help", Release 11.0

[68] Kachlakev, D. I., Miller, T. H., Potisuk, T., Yim, S. C., & Chansawat, K. (2001). Finite element modeling of reinforced concrete structures strengthened with FRP laminates (No. FHWA-OR-RD-01-XX). Oregon. Dept. of Transportation. Research Group.

[69] Al-Shaarbaf, I. A. S. (1990). Three-dimensional non-linear finite element analysis of reinforced concrete beams in torsion (Doctoral dissertation, University of Bradford).

[70] Cotsovos, D. M., Zeris, C. A., & Abbas, A. A. (2009, June). Finite element modeling of structural concrete. In Proceedings of the 2nd International Conference on Computational Methods in Structural Dynamics & Earthquake Engineering.

[71] Dwight, J. (1999). Aluminum design and construction. CRC Press..

[72] Willam, K. J. (1975). Constitutive model for the triaxial behavior of concrete. Proc. Intl. Assoc. Bridge Structl. Engrs, 19, 1-30..

[73] Kachlakev, D.I. (2002), “Finite element analysis and model validation of shear deficient reinforced concrete beams strengthened with GFRP laminates”, Proceedings of the Third International Conference on Composites in Infrastructure, Paper 002, San Francisco, California, USA

[74] Desayi, P., & Krishnan, S. (1964, March). Equation for the stress-strain curve of concrete. In Journal Proceedings (Vol. 61, No. 3, pp. 345-350).

[75] ACI (American Concrete Institute). (2011). Building code requirements for structural concrete and commentary.

[76] Kachlakev, D. I., Miller, T. H., Potisuk, T., Yim, S. C., & Chansawat, K. (2001). Finite element modeling of reinforced concrete structures strengthened with FRP laminates (No. FHWA-OR-RD-01-XX). Oregon. Dept. of Transportation. Research Group.

[77] ACI-ASCE Committee 445 (1999) Recent Approaches to Shear Design of Structural Concrete.

الخلاصة

العتبات الخرسانية المسلحة ذات الشفاه هي العتبات الامثل ولديها اهمية خاصة حيث ان شكلها الغير موشوري (المدبب) يمثل الية خاصة يمكن استخدامها في الهندسة الانشائية للحصول على الاستثمار الامثل للمواد .

هذه الدراسة مقدمة للتحقق من الثقة الهيكلية للعتبات ذات الشفاه المطورة حديثا للاتجاه الجديد في استخدام الشفاه الغير موشورية باستخدام التحليل العددي بواسطة حزمة برنامج الانسز والتي تضمنت مجموعة واسعة من المتغيرات التي تتعلق بالجوانب الهيكلية المختلفة .

تم تقسيم هذا العمل الى ستة مراحل حيث تم اجراء عملية التحقق على تسعة عتبات غير موشورية تم تحليلها بواسطة طريقة العناصر المحددة اللاخطية. للتأكد من صحة ودقة طريقة العناصر المحددة تم الحصول على العتبات بواسطة دراسة تجريبية تمت في سنة 2020 واظهرت نتائج التحقق ان هناك تطابقا جيدا بين نماذج طريقة العناصر المحددة والاختبار التجريبي المتضمن معدل المقاومة, مخطط (الحمل-الانحراف) ونمط الشقوق .

الى جانب ذلك تهتم الدراسة البارومترية المتعلقة بالعتبات الخرسانية المسلحة المتطورة بالعديد من المعاملات الهيكلية مثل توحيد الطول المتوسط داخل الطول المدبب (غير منتظم). ,إختلاف اتجاه الشفاه الغير منتظمة (α),المساند ,مقاومة حديد التسليح ,مقاومة الانضغاط للخرسانة ونسبة حديد التسليح .

بالإضافة الى دراسة تأثير القص والتحقق من قابلية الخدمة ,العرض الفعال للشفة ,العتبات المستمرة واعادة توزيع العزوم .

اظهرت النتائج ان انتظام المنطقة الوسطية ضمن الطول الغير موشوري تحدث تأثيرا طفيفا على المقاومة القصوى عندما تزداد من 0 الى 52 سم ويتوقع افضل ليونة للثني وافضل تبديد للطاقة بطول وسطي منتظم (26 سم).

والتي تشير الى ان الطول المنتظم الامثل يتوافق مع معدل تحسين ليونة يبلغ 1.49 ومعدل تبدد للطاقة يبلغ 1.53. إلى جانب ذلك ، تتحسن المقاومة النهائية مع مقاومة حديد التسليح ، و تؤدي زيادة حديد التسليح الى تحويل المقطع لمقطع مسلح بصورة زائده ضمن حدود معينة. من ناحية أخرى ، عند زيادة قيمة (α) من 3.27 درجة إلى 5.44 درجة ، يحدث اختلاف طفيف في المقاومة. تم التحقق من موثوقية الشفاه المدببة عند عرض (65،75،85 سم) وتمت مقارنة التحليل مع العينات المقابلة من الشفاه المنتظمة للمقاطع. معدلات القوة والليونة وتبديد الطاقة هي نفسها تقريبًا في كل من المقاطع المنتظمة والغير موشورية. علاوة على ذلك

، فإن وضع الشفة المدببة تتوافق مع تغير عزم القصور الذاتي على طول العتبة. ومن ثم ، يمكن أن يتأثر حد الخدمة في نطاق الانحراف. يتم تقديم عينات كاملة الحجم للتحقق من قبول الحصول على تشوه مع محددات الكود الامريكي ويتم إجراء تحليل مقارن من خلال النظر في العينات ذات الشفاه المنتظمة . بالإضافة إلى ذلك ، تم التحقيق في استمرارية العتبات ذات الشفاه الغير موشورية وإعادة توزيع اللحظي . يميل تقليل التسليح في المنطقة العليا من العتبات مع زيادة مقدار التسليح في منتصف طول العتبات الى زيادة في سعة المقاومة بمقدار 1.19 بينما يحول التصميم الزائد الذي تم تقديمه في عينة Cove السلوك إلى تصرف هش دون إعادة التوزيع اللحظي. تم اعادة التوزيع اللحظي في العينة Cw1 عند تغيير نسبة حديد التسليح من 0.0063 إلى 0.0094 وهذا ساهم في تحسين المقاومة بسبب إعادة التوزيع اللحظي ($\beta = 0.889$) أخيرًا ،تم تغيير مدى القص الذي يتوافق مع أوضاع توزيع الاجهادات ، متوافق مع وضع الفشل الذي يتحول إلى وضع الانحناء ، والقص و الانحناء ، والقص على التوالي ، حيث أن a / d لها قيم متفاوتة (1.5 ، 2.5 ، 3.5) على التوالي.

جمهورية العراق
وزارة التعليم العالي والبحث العلمي
كلية الهندسة/ جامعة ميسان
قسم الهندسة المدنية

تحري عددي للعتبات الخرسانية المسلحة ذات الشفاه متغيرة المقطع

من قبل
غفران جبار رحيم

رسالة
مقدمة الى كلية الهندسة في جامعة ميسان
كجزء من متطلبات الحصول على درجة الماجستير في علوم الهندسة المدنية / الانشاءات

تموز 2022
بأشراف
الاستاذ الدكتور: سعد فهد رسن